2018

REVERSIBLY SWITCHING ADHESION OF SMART ADHESIVES INSPIRED BY MUSSEL ADHESIVE CHEMISTRY

Ameya R. Narkar
Michigan Technological University, arnarkar@mtu.edu

REVERSIBLY SWITCHING ADHESION OF SMART ADHESIVES INSPIRED BY

MUSSEL ADHESIVE CHEMISTRY

By

Ameya R. Narkar

A DISSERTATION

Submitted in partial fulfillment of the requirements for the degree of

DOCTOR OF PHILOSOPHY

In Biomedical Engineering

MICHIGAN TECHNOLOGICAL UNIVERSITY

2018

This dissertation has been approved in partial fulfillment of the requirements for the

Degree of DOCTOR OF PHILOSOPHY in Biomedical Engineering.

Department of Biomedical Engineering

Dissertation Advisor: *Bruce P. Lee*

Committee Member: *Megan C. Frost*

Committee Member: *Smitha Rao*

Committee Member: *Patricia A. Heiden*

Committee Member: *Kenneth R. Shull*

Department Chair: *Sean J. Kirkpatrick*

Dedicated to my loving grandmother,

Ms. Pushpa Chandrahas Shetty

Table of Contents

iv

vii

viii

ix

List of figures

xii

xiii

xvi

xix

List of tables

Preface

The material used in Chapter 1 of this dissertation was previously published in *Chemistry of Materials* 2016, 10.1021/acs.chemmater.6b01851. This article was republished in its entirety with permission from ACS Publications. The material used in Chapter 2 of this dissertation was previously published in *Biomacromolecules* 2017, 10.1021/acs.biomac.7b01311. This article was reproduced in its entirety with permission from ACS Publications. The material used in Chapter 3 of this dissertation was previously published in *Langmuir 2018,* 10.1021/acs.langmuir.8b00373. This article was reproduced in its entirety with permission from ACS Publications.

I have collected and analyzed the data, as well as written the manuscripts for first authored publications that are a part of this dissertation. Dr. Bruce P. Lee has guided me through my research and also supported my work with this grants. The custom-built adhesion setup was built with the help of Brett Barker and Matthew Clisch from Dr. Jingfeng Jiang's lab group in the Biomedical Engineering department. Jonathan D. Kelley helped with the adhesion testing shown in Chapter 2 and Rattapol Pinnaratip helped with the FOX assay experiments.

The data presented in Chapter 4 of this dissertation is a manuscript in preparation to be submitted to *Soft Matter* (ACS Publications). The research was conducted mainly in Dr. Bruce P. Lee's lab, Microfabrication Facility and Applied Chemical and Morphological Analysis Laboratory (ACMAL) at Michigan Technological University. Dr. Chito

Kendrick fabricated the master mold (Si wafer), Dr. Timothy Leftwich conducted the XPS data acquisition, and Jerry Anzalone helped with the ESEM imaging. Dr. Kishan Bellur conducted the CA experiments in Dr. Jeffrey S. Allen's laboratory in the Mechanical Engineering-Engineering Mechanics department.

The abstract, summary and future outlook sections were specifically written exclusively for this dissertation.

Acknowledgements

I remember the day when I transitioned from Dr. Ong's lab to Dr. Bruce P. Lee's lab in early Spring 2014. My background was in Instrumentation Engineering with some experience in Biomedical Instrumentation. As such, I had a lot to catch up in terms of Biomedical Engineering knowledge. While I reminisce the past, I still sometimes wonder what Dr. Lee saw in me that made him accept me into his lab group as a graduate researcher. However, what I am very confident about is that from that day onward until today, he has been a constant support to me in achieving all my academic goals. Dr. Lee has always guided me in the right direction and his advice has proved to be of utmost value in my pursuit to learn and grow as an independent scientist. I would always like to remember Dr. Lee's strict work ethic and how he trained me to see the silver lining in every dark cloud (what I generally considered bad data that was of no use). He usually smiles and says that it is his job to make sure that I remain optimistic even after several failed experiments and what I considered wasted hours. Dr. Lee has also generously funded all my research with his grants. I was also supported by the Kenneth L. Stevenson Fellowship in Summer 2014. I would like to thank my committee members including Dr. Frost, Dr. Heiden, Dr. Smitha Rao and Dr. Kenneth Shull, who have shared their valuable knowledge to further my research. My sincere gratitude goes to Nick Hendrickson and his team in the machine shop. Their timely assistance with my projects helped me translate my ideas into reality.

Next, I would like to thank my elder sister, Tanvi Bhise who has been the calming voice for all my lengthy, frustration-filled calls. Without your backing, it would not have been possible to sail through my time at grad school. My immediate family including my grandparents (Chandrahas Shetty and grandma mentioned earlier), parents (Dr. Ravindra Kamala-Mahadev Narkar and mother mentioned later), uncle (Dr. Prasad Deshpande) and younger sisters (Anjali and Riddhi) - all combined have been a source of motivation, inspiration and support. In particular, my mother, Dr. Chandralekha Narkar and my aunt, Dr. Chandrika Deshpande have both played pivotal roles not only during my time at Tech, but also in steering me through my 20+ years of education. My proximity to other family members- Harsha, Deepti, baby Arya, Nikhil, Deepa, Kuwar and Ranvir here in the US has meant a lot to me.

Further, I would like to mention Rick Stanitis, Becky the Dog and Kai the Pup, all of who have provided me with plenty of crucial non-academic, personality building expertise. I have a few indispensable friends who also deserve a special mention - Khushboo, Uthara, Vinayak, Varun, Amogh, Manoj, Jay, Chiahsin, Kelsey, Kamlesh, Neel, Nupur and Kishan and also several others who have been with me through thick and thin. Last but certainly not the least, it gives me immense pride to mention all the help and assistance that the office and administration staff including Nancy, Cory and Stacey have provided me with. I wonder if I will ever find such supportive office people again, really!

xxx

Abstract

Catecholic groups in mussel adhesive proteins transition from being strongly adhesive in a reduced state under acidic conditions to being weakly adhesive in an oxidized state under basic conditions. Here, we exploit this pH responsive behavior of catechol and demonstrate that its oxidation state can be manipulated by incorporation of boronic acid to facilitate reversible transitions between strong and weak adhesion. Our first approach involved the addition of 3- acrylamido phenylboronic acid (APBA) to dopamine methacrylamide (DMA) containing adhesives. The synthesized adhesives showed strong adhesion to quartz surface in an acidic medium (pH 3), while weak adhesion was observed on raising the pH to a basic value (pH 9), due to unavailability of catechol and boronic acid because of the formation of a reversible catechol-boronate complex. Boronic acid not only contributed to adhesion at an acidic pH, but also allowed the catechol to reversibly interact with the surface in response to changing pH. In our second study, we demonstrated that addition of an anionic monomer, acrylic acid (AAc), preserved the reduced and adhesive state of catechol even at a neutral to mildly basic pH, while the addition of a cationic monomer, N-(aminopropyl) methacrylamide hydrochloride, led to the oxidized and weak adhesive state at higher basic pH values. This was due to the buffering of local pH offered by the incorporation of the ionic species, which affected the oxidation state of catechol. Although the ideal pH for formation of the complex is 9, it readily forms at neutral to mildly basic pH, leading to decreased adhesion and limiting the adhesive's application in physiological and marine pH environments. In our third

approach, adding elevated amounts of AAc to smart adhesives consisting of DMA and APBA led to strong adhesion to quartz substrate at neutral to mildly basic pH. Moreover, the complex formed at pH 9 remained reversible and the interfacial binding could be tuned by changing the pH during successive contact cycles. pH 3 was required to break the complex and recover the strong adhesive property. Bulk adhesives analyzed in our first three approaches needed extended periods of incubation (up to 30 min) to switch between their adhesive and non-adhesive states. This is because infiltration of the pH media into the bulk polymer is limited by the slow process of diffusion. Finally, we fabricated a hybrid adhesive which was composed of gecko-inspired microstructured PDMS pillars (aspect ratios of 0.4-2) coated with the smart adhesive that we developed in our first approach. By tuning the aspect ratio of the bare templates, hybrid structures that showed strong, elevated adhesion at pH 3, were obtained. The increased adhesion was attributed to contact-splitting effects due to the micropatterning combined with the interfacial binding of the smart adhesive. On the other hand, formation of the complex, and the associated swelling of the adhesive together contributed to a significant decrease in adhesion at pH 9. Additionally, the adhesive properties could be recovered appreciably at pH 3. Further, we also demonstrated that the hybrid structures could rapidly and repeatedly switch adhesion states in response to alternating the pH value between 3 and 9 at 1 min intervals. This dissertation describes various strategies used to tune the oxidation state of catechol to control its reversibly switching adhesion to different substrates under varying pH conditions

1   pH Responsive and Oxidation Resistant Wet Adhesive based on Reversible Catechol-Boronate Complexation[1]

1.1   Abstract

A smart adhesive capable of binding to a wetted surface was prepared by copolymerizing dopamine methacrylamide (DMA) and 3-acrylamido phenylboronic acid (AAPBA). pH was used to control the oxidation state and the adhesive property of the catechol side chain of DMA and to trigger the catechol–boronate complexation. FTIR spectroscopy confirmed the formation of the complex at pH 9, which was not present at pH 3. The formation of the catechol–boronate complex increased the cross-linking density of the adhesive network. Most notably, the loss modulus values of the adhesive were more than an order of magnitude higher for adhesive incubated at pH 9 when compared to those measured at pH 3. This drastic increase in the viscous dissipation property is attributed to the introduction of reversible complexation into the adhesive network. Based on the Johnson Kendall Roberts (JKR) contact mechanics test, adhesive containing both DMA and AAPBA demonstrated strong interfacial binding properties (work of adhesion (W_{adh}) = 2000 mJ/m^2) to borosilicate glass wetted with an acidic solution (pH 3). When the pH was increased to 9, W_{adh} values (180 mJ/m^2) decreased by more than an order of

---

magnitude. During successive contact cycles, the adhesive demonstrated the capability to transition reversibly between its adhesive and nonadhesive states with changing pH. Adhesive containing only DMA responded slowly to repeated changes in pH and became progressively oxidized without the protection of boronic acid. Although adhesive containing only AAPBA also demonstrated strong wet adhesion ($W_{adh} \sim 500$ mJ/m^2), its adhesive properties were not pH responsive. Both DMA and AAPBA are required to fabricate a smart adhesive with tunable and reversible adhesive properties.

1.2 Introduction

A smart adhesive can switch between its adhesive and non-adhesive states in response to externally applied stimuli. The ability to control interfacial binding properties on command is of critical interests in various fields of materials science and engineering, including manufacturing, development of sustainable packaging, repair of complex structural components, and development of painlessly removable wound dressings.[1-4] However, existing smart adhesives are limited by the need for extreme conditions to promote debonding (e.g., elevated temperature),[2] adhesion to only a specific type of substrate,[5] or weakened adhesive strength under moist conditions.[3] Smart adhesives reported to-date have demonstrated adhesion predominately to dry surfaces. The performance of most man-made adhesives is significantly compromised in the presence of moisture, as water effectively competes for surface bonding and eliminates contributions of van der Waals' interaction.[6, 7]

2

Marine mussels secrete adhesive proteins that enable them to bind to various surfaces (rocks, piers, etc.) in a saline and wet environment.[8, 9] One of the main structural component in these adhesive proteins is the presence of a unique catechol-based amino acid, L-3, 4-dihydroxyphenylalanine (DOPA), which is responsible for interfacial binding and rapid solidification of the proteins.[7] Modification of inert polymers with catechol groups imparted these materials with strong adhesive properties to both organic and inorganic substrates.[10-12] The unique and versatile phenolic chemistries have been employed to design stimuli responsive films,[13] self-healing networks,[14] shape-changing actuators[15-17] and self-assembled capsules.[18] Although smart adhesives inspired by mussel adhesive chemistry have been recently reported, these adhesive demonstrated limited reversibility (i.e., one time activation[19] or one time deactivation[20]).

The adhesive strength of catechol is highly dependent on its oxidation state (**Scheme 1**).[21-23] The interaction between the reduced form of catechol and titanium (Ti) surface was reported to average around 800 pN, which is 40% that of a covalent bond.[24] When the catechol was oxidized to its quinone form in a basic pH (**Scheme 1b**), a drastic reduction in the pull-off force (180 pN) was observed.[24] This indicates that the oxidation state of catechol can be used to tune the adhesive property of this biomimetic adhesive moiety. However, the quinone is highly reactive and can participate in irreversible covalent crosslinking (**Scheme 1c**),[25, 26] which will potentially limit the catechol's ability to function as a reversible adhesive moiety**.**

3

To preserve the reversibility of catechol, the smart adhesive reported here is composed of network-bound phenylboronic acid. Catechol forms pH-dependent, reversible complex with boronic acid.[27] This complex is strong enough to form a self-healing polymer network with modulus approaching those of covalently crosslinked networks.[28] Boronic acid has also been previously used as a temporary protecting group for the synthesis of DOPA-modified polymers, while preserving the reactivity of its catechol side chain.[29] Additionally, the presence of boronic acid has been demonstrated to reduce the adhesive strength of a catechol-based adhesive.[30] Recently, this coordination chemistry was used to design pH responsive capsules for drug delivery.[31]
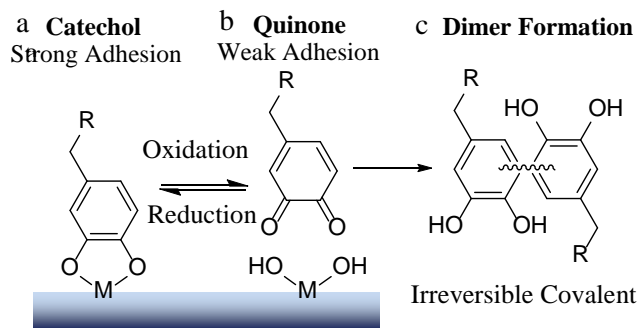
Scheme 1. The reduced form of catechol is responsible for strong interfacial binding (a), while the oxidized quinone exhibits weak adhesion (b). Quinone is also highly reactive and can undergo irreversible covalent crosslinking (c).

We hypothesize that the incorporation of the network-bound boronic acid can provide a protecting mechanism for catechol against irreversible oxidation crosslinking and to preserve the reversibility of the interfacial binding properties of catechol-containing

4

smart adhesive. To this end, adhesive hydrogels were prepared by the copolymerization of dopamine methacrylamide (DMA) and 3-acrylamido phenylboronic acid (AAPBA). DMA contains a catechol side chain that mimics the adhesive properties of DOPA. The formation of the catechol-boronate complex in the adhesive network was characterized by infrared spectroscopy, equilibrium swelling, and oscillatory rheometry experiments. The effect of the complex on the reversibility of adhesive properties was characterized using Johnson Kendall Roberts (JKR) contact mechanics test.

1.3   Materials and Methods

N-Hydroxyethyl acrylamide (HEAA), AAPBA, trichloro(1H,1H,2H,2H-perfluorooctyl)silane (97 %), and toluene (anhydrous, 99.8 %) were purchased from Sigma Aldrich. 2, 2-Dimethoxy-2-phenylacetophenone (DMPA) and methylene bis-acrylamide (MBAA) were purchased from Acros Organics. Dimethyl sulfoxide (DMSO) was purchased from Macron. Ethanol (190 proof) was purchased from Pharmco Aaper. DMA was synthesized following published protocols.[32] The acidic solution was prepared by titrating a 0.1 M NaCl solution to pH 3 using 1 M HCl, while the basic buffer medium was prepared by titrating 10 mM Tris (hydroxymethyl) aminomethane (Tris) base with 1M HCl to pH 9.

1.3.1   Preparation of the adhesive hydrogel

Adhesive hydrogels were prepared by curing a precursor solution containing 1 M of HEAA with up to 10 mol% each of DMA and AAPBA dissolved in 40 v/v% DMSO in

5

deionized (DI) water. The bifunctional crosslinker (MBAA) and the photoinitiator (DMPA) were kept at 3 and 0.1 mol%, respectively, relative to HEAA. The precursor solutions were degassed three times, added to a mold with a spacer (2 mm thick) and photoinitiated in a UV crosslinking chamber (XL-1000, Spectronics Corporation, Westbury, NY) located in a nitrogen-filled glovebox (PLAS LABS, Lansing, MI) for 600 seconds.[15, 16] To form a hemispherical gel, 50 µL of solutions were pipetted on to a fluorinated glass slide and photoinitiated for 600 seconds. Glass slides were submerged in a mixture containing 0.5 mL of trichloro(1H,1H,2H,2H-perfluorooctyl)silane and 49 mL of toluene for 20 min. The glass slides were then washed thrice with fresh toluene and then air dried. Depending on the experiment, the hydrogels were equilibrated in either the acidic (pH 3) or basic (pH 9) solutions for 24-48 hours with gentle nutation and frequent medium changes prior to subsequent experimentation. The adhesive compositions are abbreviated as DxBy where the x and y stand for the mol% of DMA and AAPBA, respectively, relative to the concentration of HEAA.

1.3.2   Equilibrium swelling

Hydrogel discs (thickness = 2 mm and diameter = 15 mm) were equilibrated in 5 mL of either the acidic solution (pH 3) or basic (pH 9) buffer medium for 48 hours, with continuous and gentle nutation. The samples were dried under vacuum for at least 48 hours. Both the swollen (M_s) and dry (M_d) mass of the samples were used to determine the equilibrium swelling ratio using the following equation:[33]

6

$$\text{Equilibrium Swelling} = \frac{M_s}{M_d} \quad (1).$$

1.3.3 Fourier transform infrared (FTIR) spectroscopy

The samples were freeze-dried, crushed into fine powder using a mortar and pestle, and analyzed using a Perkin Elmer Frontier Spectrometer fitted with a GladiATR^{TM} accessory from Pike Technologies.

1.3.4 Oscillatory rheometry

Hydrogel samples (15 mm diameter and 2 mm thick) were equilibrated in pH 3 or 9 with nutation for 48 hours and compressed to a constant gap of 1800 μm using a 20 mm diameter parallel plate geometry. The storage (G') and loss (G'') moduli were determined in the frequency range of 0.1-100 Hz and at a strain of 8% using a TA Discovery Hybrid Rheometer-2 (TA Instruments).

1.3.5 Contact mechanics test

Contact mechanics tests were performed using JKR indentation method to determine the interfacial binding properties of the hydrogels. A custom-built indentation device comprising of a 10-g load cell (Transducer Techniques), high resolution miniature linear stage stepper motor (MFA-PPD, Newport), and an indenter (ALS-06, Transducer

7

Techniques) for affixing a hemispherical gel was used to conduct the contact mechanics testing (**Scheme 2**).[34]
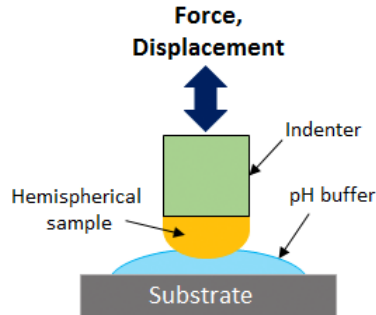
Scheme 2. Schematic representation of the setup used in the contact mechanics adhesion testing.

Two contact mechanics tests were performed. In the first test, samples were equilibrated at pH 3 or 9 for 48 hours prior to testing to determine the effect of pH on their adhesive properties. The hemispherical gel was affixed to the indenter using Super Glue (Loctite Professional Liquid) and was compressed at 1 µm/sec until reaching a maximum preload of 20 mN. The gel sample was retracted at the same rate. A borosilicate glass surface (Pearl microscope slides, cat. no. 7101) was used as test substrate and it was wetted with 25 µL of either pH 3 solution or pH 9 buffer medium.

In the second test, the reversibility of the adhesive to transition between its adhesive and non-adhesive states in response to pH change was examined. The samples were first equilibrated in the pH3 solution for 24 hours with gentle nutation before testing. Reversible adhesion testing was conducted on both a borosilicate glass surface and a quartz surface (Tedpella, Inc., product no. 26011, Redding, CA). A single hydrogel

8

sample was subjected to 3 successive contact cycles on the substrate surface wetted with 25 µL of solution maintained at different pH levels (i.e., pH 3, 9 and then 3 for cycles 1, 2 and 3, respectively). In between cycles, the hemispherical gels were briefly incubated in 100 µL of solution (i.e., pH 9 and 3, after cycles 1 and 2, respectively) for 10 minutes. After removing 75 µL of the solution, the test was carried out in the presence of the remaining 25 µL of the solution.

The force (F) versus displacement (δ) curves were integrated to determine the work of adhesion (W_{adh}), which was normalized by the maximum area of contact (A_{max}) using the following equation:[35]

$$W_{adh} = \frac{\int F \, d\delta}{A_{max}}. \qquad (2)$$

To mathematically calculate A_{max}, the loading portion of the contact curve was fitted with the Hertzian model:[36]

$$\delta_{max} = \frac{a^2}{R}, \qquad (3)$$

where δ_{max} is the maximum displacement at the maximum preload of 20 mN, a is the radius of A_{max}, and R is the radius of curvature of the hemispherical gel. The height (h) and base radius (r) of each individual hemisphere were measured using a digital vernier caliper before testing to determine R:[37]

$$R = \frac{h}{2} + \frac{r^2}{2h}. \qquad (4)$$

9

A$_{max}$ was determined using the following equation:

$$A_{max} = \pi a^2. \qquad (5)$$

Finally, the maximum adhesive force (F$_{max}$) was determined as the highest negative load recorded in the force vs. displacement curve.

1.3.6 Statistical analysis

Statistical analysis was carried out using JMP Pro 12 software (SAS Institute, NC). Student's t-test and one way analysis of variance (ANOVA) with Tukey–Kramer HSD analysis and were performed for comparing means between two and multiple groups, respectively. $p < 0.05$ was considered significant.

1.4 Results and discussions

Hydrogels were prepared with a neutral monomer (HEAA) and network-bound catechol (DMA) and phenylboronic acid (AAPBA) sidechains. We utilize pH to control the oxidation state of the catechol group and its interfacial binding strength. pH 3 was chosen in order to examine the adhesive properties of the reduced from of catechol (i.e., adhesive state).[23, 30] Conversely, pH 9 was chosen to examine the adhesive properties of the oxidized form of the catechol (i.e., non-adhesive state) with weakened interfacial binding strength,[23, 38] and to induce the formation of the catechol-boronate complex. The ideal pH (pH$_{ideal}$) for effective interaction between a diol and a boronic acid has been reported to be the average of their respective acid dissociation constant (pKa) values (pH$_{ideal}$ =

10

(pKa$_{acid}$ + pKa$_{diol}$)/2).[39] Given the reported pKa values for catechol (pKa$_{diol}$ = 9.3)[40] and phenylboronic acid (pKa$_{acid}$ = 8.8),[40, 41] pH 9 ((9.3+8.8)/2 ≈ 9) is an ideal pH for promoting complexation between DMA and AAPBA.

1.4.1 Qualitative analysis

Photographs of hydrogels incubated in pH 3 or 9 for 48 hours confirmed that pH effectively controlled the oxidation states of DMA **(Table 1)**. Both D10B0 and D10B10 remained colorless after incubation in pH 3, indicating that the acidic pH preserved the reduced state of the catechol. However, D10B0 developed a dark brown color (tanning of

Table 1. Images of adhesive samples equilibrated at either pH 3 or 9 for 48 hours.

Composition	pH 3	pH 9
D0B0		
D10B0		
D0B10		
D10B10		

catechol) when it was incubated in pH 9, which is indicative of the oxidation of catecholic groups to quinone.[42, 43] On the other hand, D10B10 developed a slight pinkish tinge at pH 9, indicating that the introduction of boronic acid groups protected the

11

catechol from undergoing oxidation. Samples that were catechol-free (e.g., D0B0 and D0B10) did not display any coloration at both pH levels.

1.4.2 Equilibrium swelling

Hydrogels were equilibrated at either pH 3 or 9 to determine the effect of pH on their swelling ratio **(Figure 1)**. D0B0 did not exhibit any significant change in its swelling ratio with changing pH, confirming that the poly(HEAA) backbone is not pH responsive. Increasing the DMA content to 10 mol% (e.g., D10B0) decreased the swelling ratio of the hydrogel as a result of increased hydrophobicity with the incorporation of the benzene ring in DMA. This change in swelling may also be attributed to the increased molecular interactions between the benzene rings (i.e., $\pi-\pi$ interactions, hydrogen bonding). At pH 9, D10B0 exhibited an increase in swelling ratio when compared to pH 3 (30% increase), potentially due to the increased formation of negatively charged semiquinone with increasing pH **(Scheme 3A)**.[44] Similarly, D0B10 exhibited a higher swelling ratio at pH 9. Phenylboronic acid transforms into a negatively charged trigonal structure when the pH value approaches and becomes higher than its pKa value (pKa = 8.8, **Scheme 3B**).[39] Similar pH dependent swelling have been previously reported for phenylboronic acid containing hydrogels.[45]

12
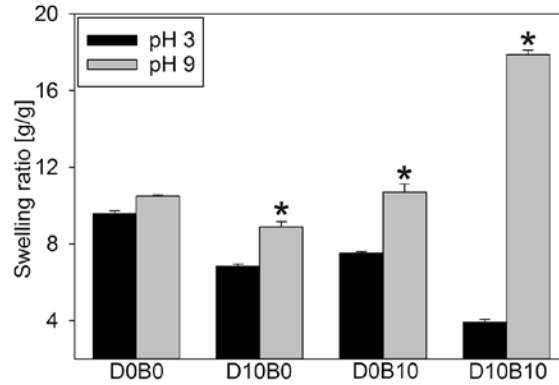
Figure 1. Swelling ratio of adhesives equilibrated at either pH 3 or 9 (n = 3). * p < 0.05 when compared to the adhesive equilibrated at pH 3 for a given composition.

Hydrogels containing both DMA and AAPBA exhibited maximum shrinkage in the acidic solution and maximum swelling in the basic medium. A drastic reduction in swelling at the acidic pH is likely due to the hydrophobicity of the benzyl ring in both DMA and AAPBA as well as their ability to form physical bonds. At pH 9, formation of the catechol-boronate complex results in the formation of negative charge and extensive swelling as a result of electrostatic repulsion (**Scheme 3C**).[39, 45] This pH dependent swelling was observed for hydrogel formulations that contained various amount of DMA and AAPBA (**Figure 2**). D10B10 contained the highest mol% of both DMA and AAPBA and exhibited the largest difference in the swelling ratio between pH 3 and 9 (an increase of 360%).

13

Scheme 3. Chemical structures showing the pH responsive transition between catechol and semiquinone (A), trigonal structure and the negatively charged tetrahedral structure of phenylboronic acid (B), and the unbound catechol and phenylboronic acid moieties and their negatively charged complex (C).
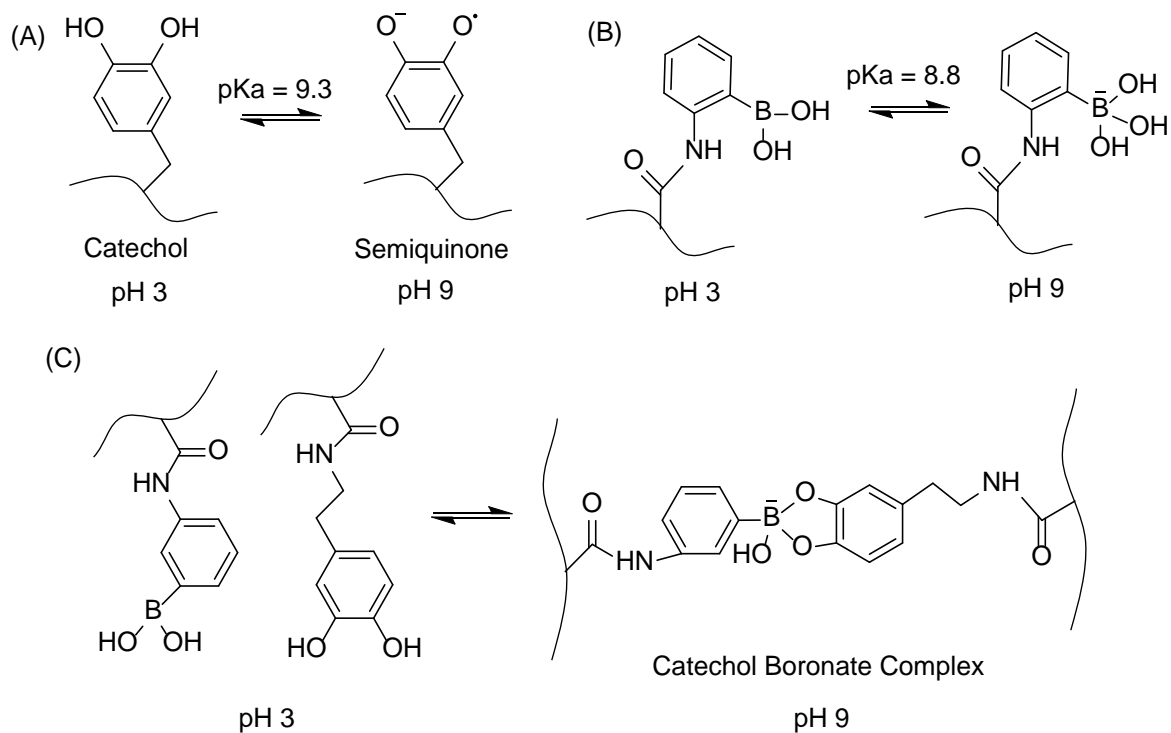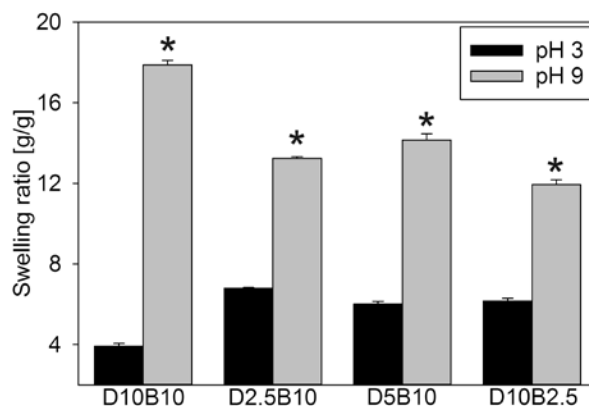
Figure 2. Swelling ratio of adhesives equilibrated at either pH 3 or 9 (n = 3). * $p < 0.05$ when compared to the adhesive equilibrated at pH 3 for a given composition.

1.4.3 FTIR

FTIR spectra confirmed the characteristics peaks for HEAA (–OH 3400-3000 cm^{-1}, secondary amide –NH 1680-1630 cm^{-1}, and C=O 1600-1500 cm^{-1}) and benzene rings (1500-1400 and 800-700 cm^{-1}) in D10B10 (**Figure 3**).[46, 47] When comparing spectra of D10B10 incubated at different pH levels, a new peak was observed at 1489 cm^{-1} at pH 9 (arrow in **Figure 3**), which was not present when D10B10 was incubated at pH 3. This new peak is associated with the benzene ring stretch in aromatic compounds as a result of changing their vibrational states. This peak compares favorably with values (1478-1501 cm^{-1}) previously reported for the catechol-boronate complex.[48]

15
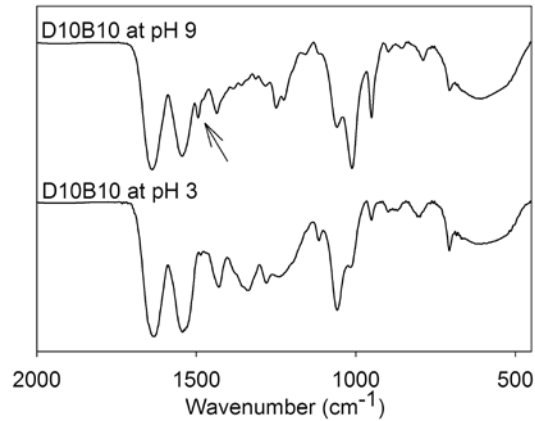
Figure 3. FTIR spectra of D10B10 equilibrated at either pH 3 or 9. The arrow points to the presence of a new peak (1489 cm^{-1}) found at pH 9, corresponding to the formation of catechol-boronate complex.

This peak was not present in samples that did not contain both DMA and AAPBA (i.e., D0B0, D10B0 or D0B10) tested at both pH 3 and 9 (**Figure 4**).
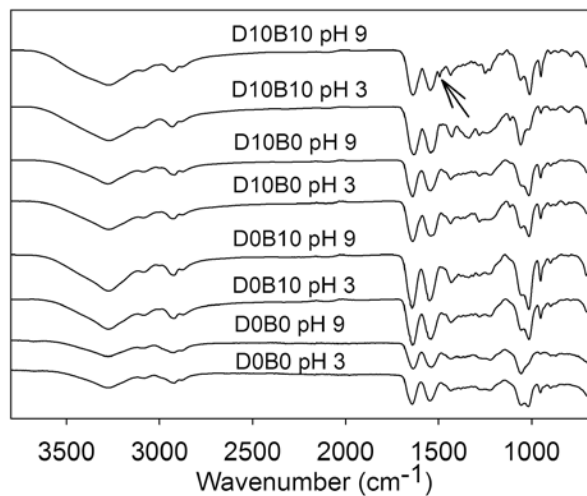
Figure 4. FTIR spectra of adhesives equilibrated at either pH 3 or 9. The arrow points to the presence of a new peak (1489 cm^{-1}) for D10B10 at pH 9, corresponding to the formation of catechol-boronate complex.

16

1.4.4 Oscillatory rheometry

Oscillatory rheometry results indicated that regardless of composition, all the hydrogels were chemically crosslinked, as the G' values were independent of frequencies (< 45 Hz) and the G' values were 1-2 orders of magnitude higher than the G'' values (**Figure 5** and **Figure 6**). There were minimal differences in both the G' and G'' values for the various control groups (D0B0, D10B0, and D0B10) equilibrated at different pH levels (**Figure 6**). On the other hand, D10B10 exhibited an increase in the G' value (a 55% increase at a frequency of 1 Hz) when the pH was increased from pH 3 to 9 (**Figure 5**). An increase in the measured stiffness is a result of increasing crosslinking density, resulting from the formation of new intermolecular crosslinks within the hydrogel network.
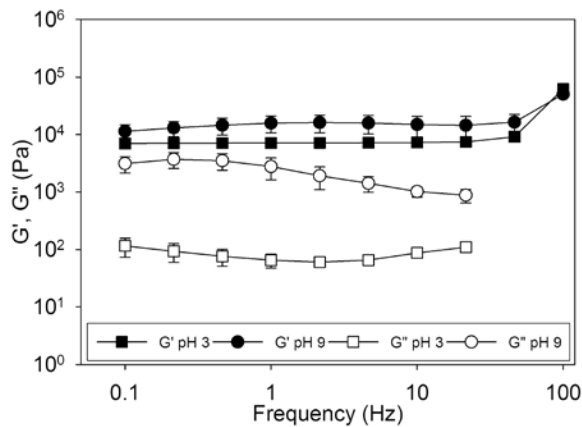
Figure 5. Storage (G', filled symbol) and loss (G'', open symbol) moduli for D10B10 equilibrated at either pH 3 (■, □) or 9 (●, ○) (n = 3).

Most notably, D10B10 incubated at pH 9 exhibited G'' values that were an order of magnitude higher than those incubated at pH 3. This increase in viscous dissipation

17

properties indicates the presence of extensive reversible physical interaction in the hydrogel network attributed to catechol-boronate complexation at pH 9.[49, 50] These enhancements in mechanical properties are remarkable considering these complexes needed to counteract the extensive swelling of the network resulting from electrostatic repulsion of the negatively charged complexes (**Scheme 3C**). This may explain why there was only a marginal increase in the measured G' values in response to changes in pH. Similar pH dependent behaviors were observed for hydrogels containing various ratios of DMA and AAPBA (**Figure 7**).
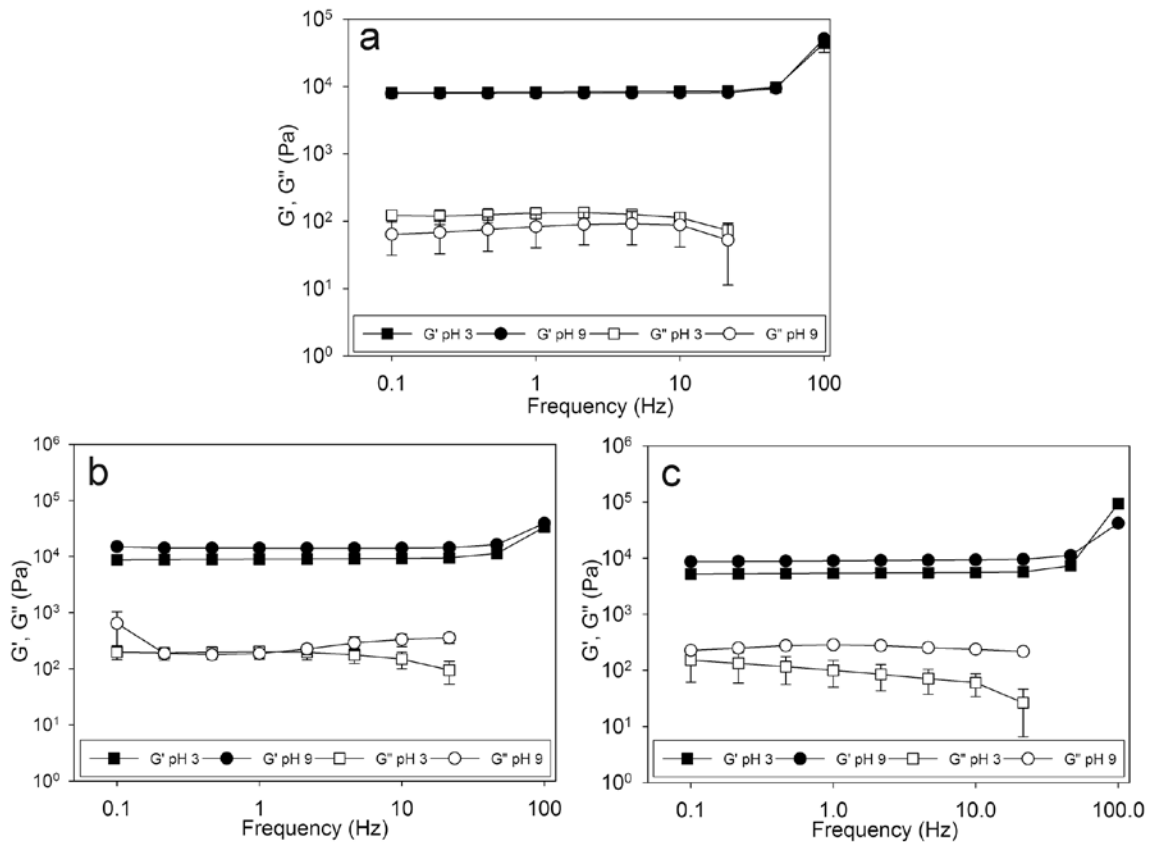
Figure 6. Storage (G', filled symbol) and loss (G", open symbol) moduli for D0B0 (a), D10B0 (b), and D0B10 (c) equilibrated at either pH 3 (■, □) or 9 (●, ○) (n = 3).

18
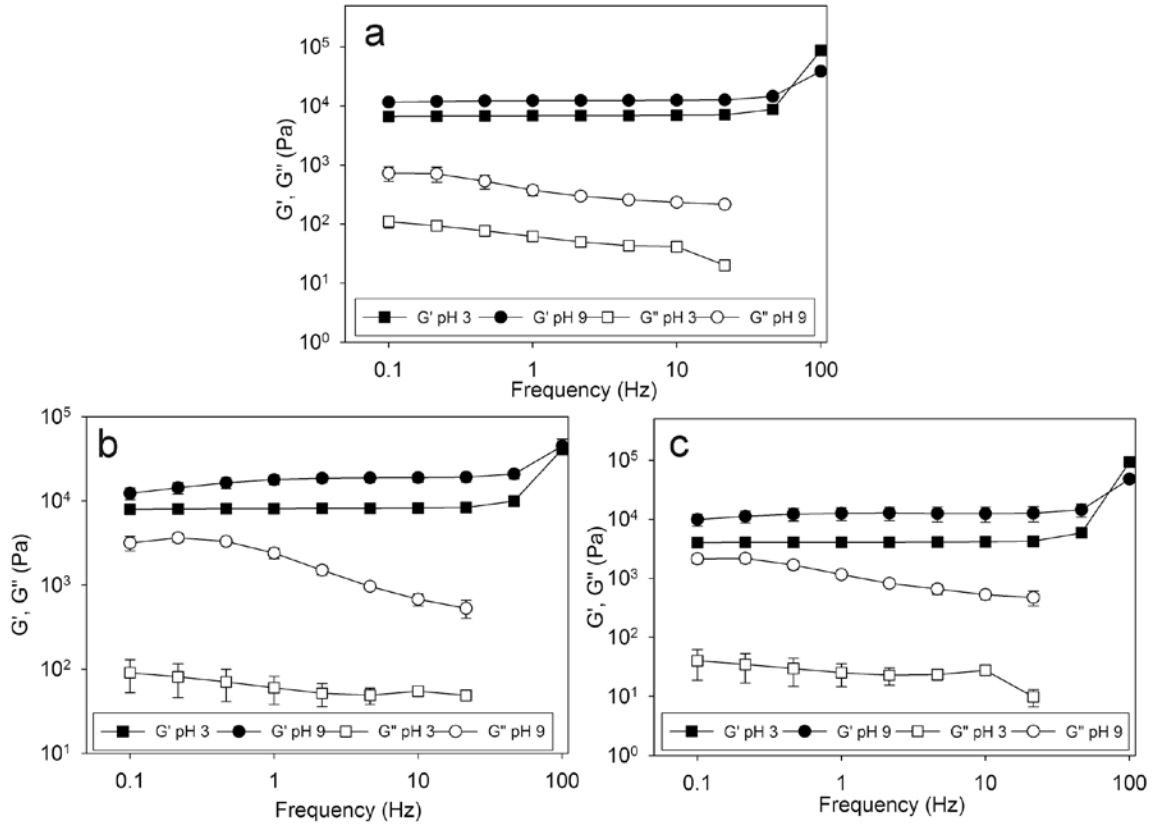
Figure 7. Storage (G', filled symbol) and loss (G'', open symbol) moduli for D10B2.5 (a),
D5B10 (b), and D2.5B10 (c) equilibrated at either pH 3 ($\blacksquare$, $\square$) or 9 ($\bullet$, $\circ$) (n = 3).

1.4.5 Contact mechanics testing of equilibrated adhesive

JKR contact mechanics tests were performed to determine the effect of pH on the
interfacial binding properties of the adhesive. D0B0 exhibited minimal interaction with
the substrate at both pH levels as expected (**Figure 8a, Table 2**). Incorporation of 10
mol% DMA (D10B0) significantly increased the measured adhesive properties at pH 3
(**Figure 8b**). This indicates that the reduced form of catechol is responsible for strong
interfacial binding, potentially through H-bonding or electrostatic interaction with silicon

19

dioxide (SiO_2), which is a major component of borosilicate glass.[51] Density functional

theory analysis revealed that catechol readily displaces water molecules to bind to SiO_2

surface, with a binding energy (33 kcal/mol) value approaching that of catechol-Ti

interaction.[52, 53] D10B0 incubated at pH 9 exhibited a significant reduction in adhesive

properties. Specifically, the measured W_{adh} value for D10B0 measured at pH 9 was not

significantly different from that of D0B0.
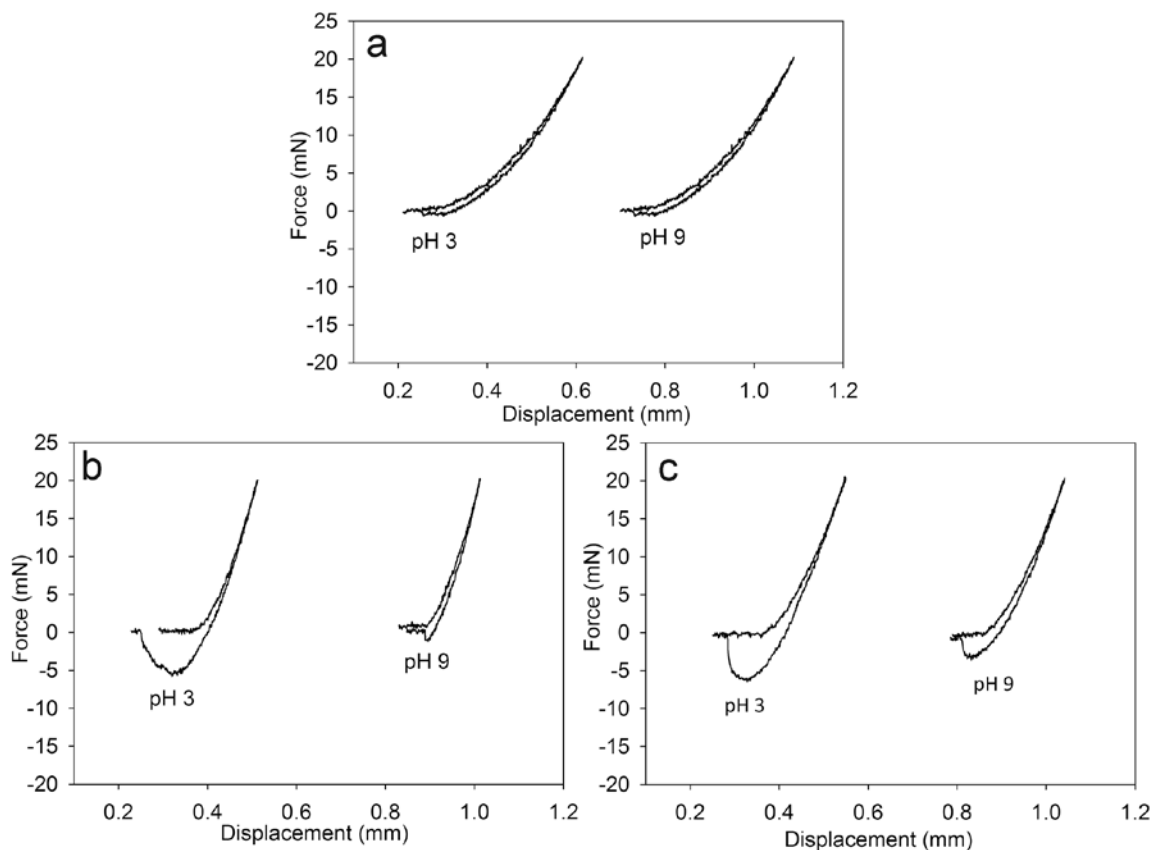
Figure 8. Representative contact curves for D0B0 (a), D10B0 (b), and D0B10 (c)

equilibrated and tested at either pH 3 or 9.

20

Interestingly, D0B10 also demonstrated equivalent or higher adhesive properties when compared to its counterparts (**Figure 8c**). Although the interaction between boronic acid and glass substrates has not been previously reported, AAPBA likely interacted with the surface via H-bonding or electrostatic interaction. However, D0B10 also exhibited significantly higher F_{max} values at pH 9 when compared to D10B0 and D0B0. This indicates that the incorporation of AAPBA alone was not sufficient in creating a smart adhesive due to its ineffective pH responsive characteristics.

Table 2. Average F_{max} and W_{adh} values calculated for adhesives containing varying amounts of DMA and AAPBA equilibrated and tested at either pH 3 or 9 (n = 3).

Composition	F_{max} (mN)		W_{adh} (mJ/m^2)	
	pH 3	pH 9	pH 3	pH 9
D0B0	-1.4 ± 0.25	-0.85 ± 0.24	100 ± 24	76 ± 11
D10B0	-5.9 ± 0.45	-1.6 ± 0.67	170 ± 12	83 ± 28
D0B10	-6.6 ± 0.46	-4.1 ± 0.38	240 ± 28	96 ± 19
D10B10	-11 ± 1.6	-1.1 ± 0.020	460 ± 110	110 ± 6.6

At pH 3, D10B10 demonstrated significantly higher F_{max} (-11 ± 1.6 mN) and W_{adh} (460 ± 110 mJ/m^2) values relative to those obtained from D10B0 and D0B10 (**Figure 9**, **Table 2**). This indicates that both DMA and AAPBA contributed to surface adhesion. At the same time, D10B10 exhibited a 10 and 4.2 time reduction in F_{max} and W_{adh} values,

21

respectively, at pH 9, indicating that the formation of catechol-boronate complex successfully reduced interfacial binding.
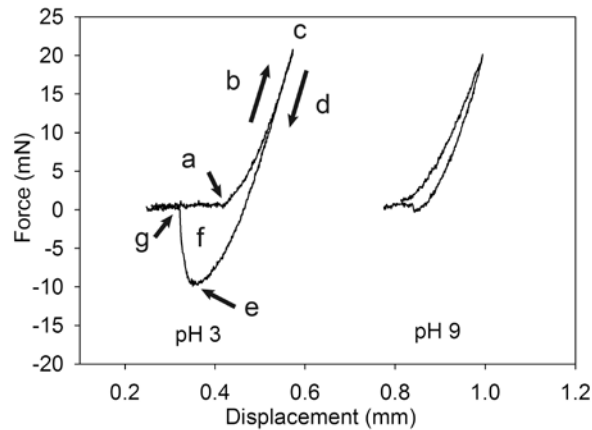
Figure 9. Representative contact curves for D10B10 equilibrated and tested at either pH 3 (left) or 9 (right). The lowercase letters indicate the point of initial contact with the borosilicate glass surface (a), the loading portion of the curve (b), the maximum preload (c), the unloading portion of the curve (d), the maximum adhesive force (F_{max}; e), the area enclosed by the curve corresponding to W_{adh} (f), and the point of detachment from the substrate (g).

1.4.5.1   Reversibility adhesion testing

To confirm the reversible nature of the catechol-boronate complex and its contribution to interfacial binding, samples were repeatedly brought into contact with the substrate while exposing the adhesive to solutions with different pHs. D0B0 exhibited very low adhesive values for all 3 contact cycles (**Figure 10**).

22
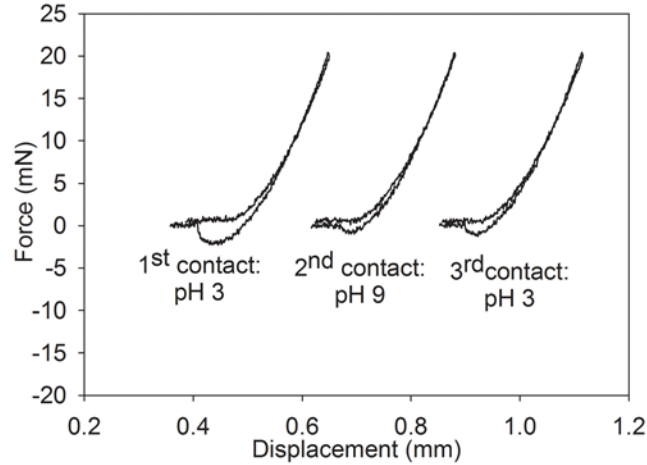
Figure 10. Three successive contact curves for D0B0 tested at pH 3, pH 9, and then pH 3 tested against a borosilicate glass substrate.

D10B0 demonstrated strong adhesion during the first contact cycle performed at pH 3 (**Figure 11a**). However, unlike values obtained from D10B0 that were equilibrated for 48 hrs (**Figure 8b**, **Table 2**), there was no significant change in the measured adhesive values in the second contact cycle measured at pH 9. This may be due to the adhesive's short exposure time to the basic medium and slow oxidation of the catechol to quinone. However, both F_{max} and W_{adh} values were significantly lower in the third contact cycle performed at pH 3. The adhesive network likely traps the basic medium during the second contact cycle and the catechol groups became progressively oxidized with time. D0B10 did not exhibit changes in its adhesive properties with changes in pH (**Figure 11b**).

23
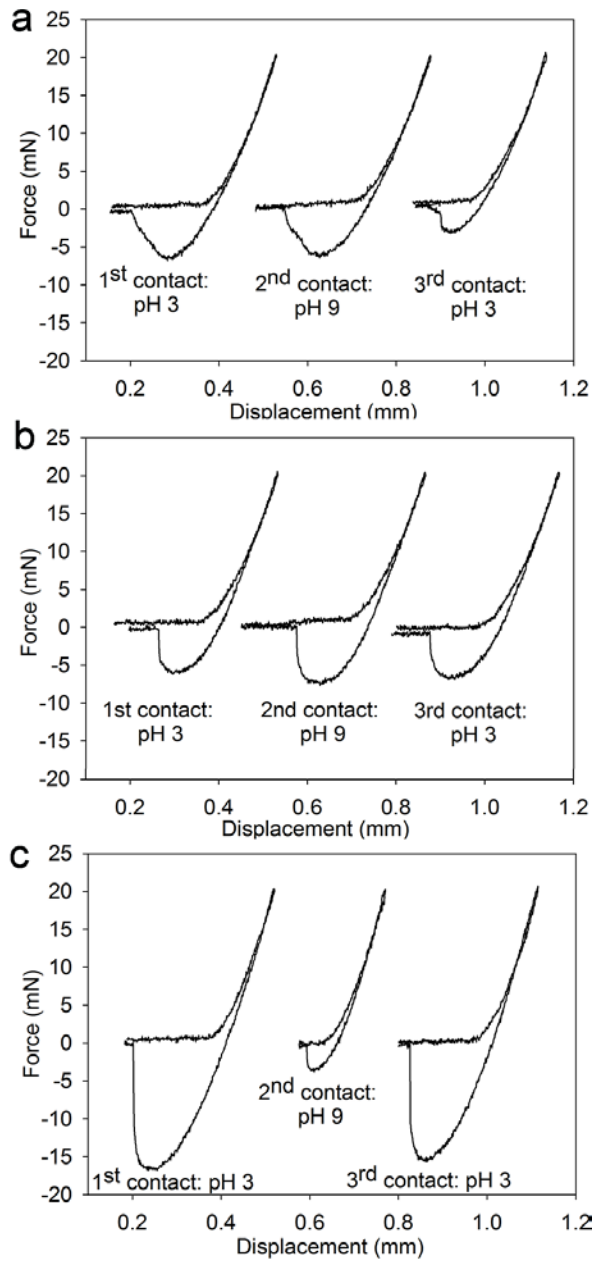
Figure 11. Three successive contact curves for D10B0 (a), D0B10 (b) and D10B10 (c) tested at pH 3, pH 9, and then pH 3 using a borosilicate glass substrate.

D10B10 demonstrated elevated adhesive properties (F_{max} = -16 ± 0.60 mN, W_{adh} = 2000 ± 250 mJ/m^2) during the first contact cycle at pH 3, with adhesion values that were 2-3

24

folds higher when compared to values obtained for D10B0 and D0B10 (**Figures 11 and 12**). During the second contact at pH 9, these values were reduced by more than an order of magnitude (F_{max} = -2.4 ± 1.1 mN, W_{adh} = 180 ± 87 mJ/m^2). These values were two to three times lower when compared to those measured for D10B0 and D0B10 and they were also not significantly different from those of D0B0. In the third contact cycle measured at pH 3, D10B10 recovered 90 and 76% of the F_{max} and W_{adh} values, respectively, measured during the first contact cycle.
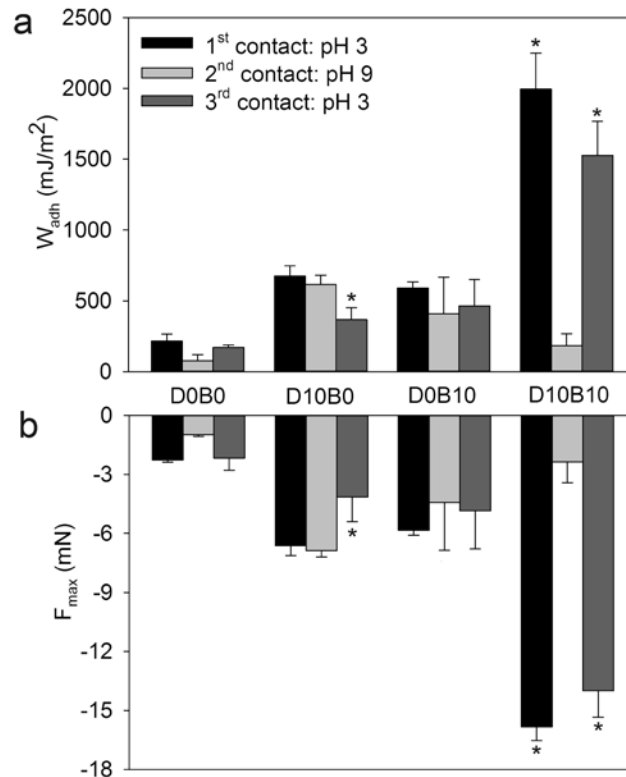
Figure 12. Averaged W_{adh} (a) and F_{max} (b) for adhesives tested in three successive contact cycles using a borosilicate glass as the substrate (n = 3). * $p < 0.05$ relative to the values obtained from the second contact cycle at pH 9 for a given formulation.

25

Similar pH responsive trends was observed using quartz surface (**Figure 13**). D10B10 demonstrated an order of magnitude difference between its adhesive (pH 3) and non-adhesive (pH 9) states. Similarly, D10B0 demonstrated reduced adhesion with successive contact cycles while D0B10 was not pH responsive. Lower adhesive values were obtained for quartz (~14 % reduction for D10B10) when measured at pH 3 indicating that boron (~13%) in the borosilicate glass contributed to adhesion.
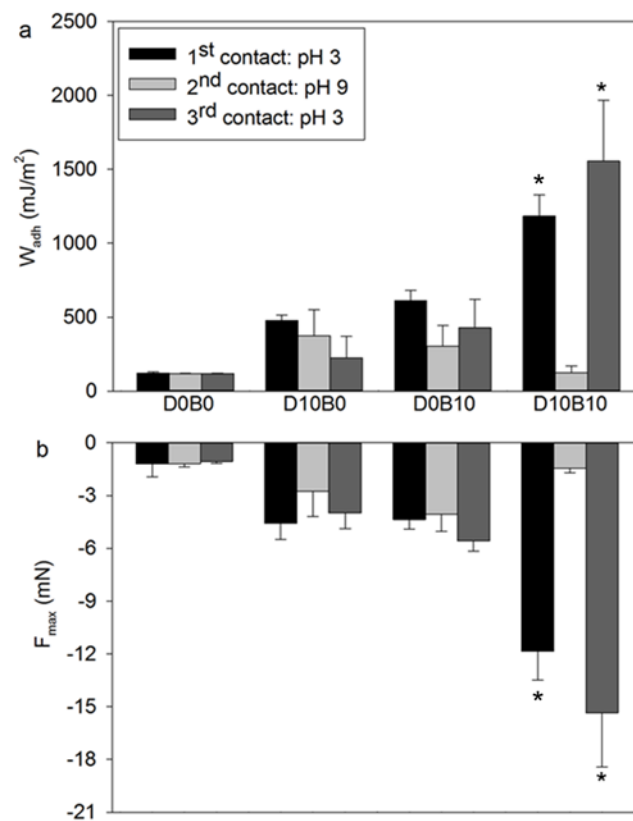
Figure 13. Averaged W_{adh} (a) and F_{max} (b) for adhesives tested in three successive contact cycles using a quartz substrate (n = 3). * $p < 0.05$ relative to the values obtained from the second contact cycle at pH 9 for a given formulation.

Taken together, adhesives containing DMA exhibited strong interfacial binding properties at pH 3, confirming previously published results that the reduced form of catechol is responsible for strong wet adhesion to inorganic substrates.[22, 23, 38] With extensive incubation time at pH 9, the catechol groups were oxidized and exhibited reduced adhesive properties. However, pH-mediated oxidation was relatively slow. The interfacial binding properties of DMA-containing adhesive did not respond to repeated changes in pH but its adhesive properties decreased progressively with repeated contact. Phenylboronic acid also demonstrated strong adhesion to borosilicate surfaces in the presence of water. However, adhesive containing only AAPBA was not pH responsive. These results indicated that adhesives containing either DMA alone or AAPBA alone were not suitable in functioning as a smart adhesive.

When an adhesive contained both DMA and AAPBA, both the catechol and phenylboronic acid moieties contributed to strong interfacial binding at pH 3 (**Scheme 4**). Elevating the pH resulted in the formation of catechol-boronate complex and a significant reduction in the adhesive properties. The reversible nature of this complex allowed both the catechol and phenylboronic acid moieties to become available for interfacial binding once the pH was reduced. AAPBA not only served as an adhesive moiety for interfacial binding, it also functioned as a protecting group to limit catechol oxidation. The combination of catechol and phenylboronic acid provides a basis for designing a novel smart adhesive that is capable of switching between its adhesive and non-adhesive states in the presence of an aqueous environment. To our knowledge, this the first

27

demonstration of a wet adhesive with tunable adhesive properties that exploits the chemistry found in mussel adhesive proteins.
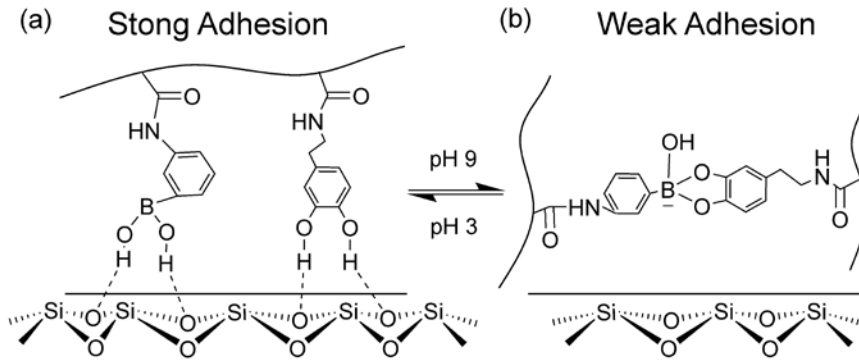
Scheme 4. Schematic representation of the smart adhesive containing catechol and phenylboronic acid functional groups. At an acidic pH, both the catechol and borate functional groups contributed to strong interfacial binding with the wetted borosilicate substrate (a). In a basic pH, formation of catechol-boronate complexation reduced the interfacial binding strength of the adhesive (b). Changing the pH, effectively converts the smart adhesive between its adhesive and non-adhesive states.

1.5 Conclusions

Hydrogel adhesives containing DMA and AAPBA were prepared. FTIR, equilibrium swelling and oscillatory rheometry experiments confirmed the formation of catechol-boronate complex at pH 9. JKR contact mechanics test revealed that adhesives containing both DMA and AAPBA exhibited elevated adhesive properties at pH 3, which were

28

drastically reduced at pH 9. The reversible nature of the catechol-boronate complex enabled the adhesive to reversibly transition between its adhesive and non-adhesive states in response to pH change.

1.6 Acknowledgments

2 Effect of Ionic Functional Groups on the Oxidation State and Interfacial Binding Property of Catechol-Based Adhesive[2]

2.1 Abstract

Adhesive hydrogels were prepared by copolymerizing dopamine methacrylamide (DMA) with either acrylic acid (AAc) or *N*-(3-aminopropyl)methacrylamide hydrochloride (APMH). The effect of incorporating the anionic and cationic side chains on the oxidation state of catechol was characterized using the FOX assay to track the production of hydrogen peroxide (H_2O_2) byproduct generated during the autoxidation of catechol while the interfacial binding property of the adhesive was determined by performing Johnson-Kendall-Roberts (JKR) contact mechanics tests tested over a wide range of pH values (pH 3.0-9.0). The ionic species contributed to interfacial binding to surfaces with the opposite charge, with measured work of adhesion values that were comparable to or in some cases higher than those of catechol. Addition of AAc minimized the oxidation of catechol even at a pH of 8.5 and correspondingly preserved the elevated adhesive property of catechol to both quartz and amine-functionalized surfaces. However, AAc lost its buffering capacity at pH 9.0 and catechol was oxidized at this pH. On the other

---

hand, catechol formed cohesive covalent bond with network-bound amine side chain of APMH at a basic pH, which interfered with the interfacial binding capability of APMH and the catechol.

2.2 Introduction

Designing adhesives capable forming strong bonds to wet surfaces is critical for many biomedical and underwater marine applications.[54-56] The presence of a surface liquid layer on a substrate acts as a barrier for interfacial binding and interferes with adhesion.[8, 57-59] Marine mussels secrete a mixture of different adhesive mussel foot proteins (mfp) to anchor themselves to a wide variety of substrates in a wet environment.[57, 60] These proteins contain a unique amino acid, L-3,4-dihydroxyphenylalanine (DOPA), which contains a catechol side chain that is responsible for moisture resistant interfacial binding. In particular, mfp-3 and 5 contain up to 30 mol % DOPA, indicating that catechol plays a major role in wet adhesion. Adhesives containing catechol functionality have hence been used to develop adhesives and coatings for various biomedical as well as industrial applications.[10, 61-63]

The majority of existing literature focused on incorporating catechol adhesive moiety alone in designing synthetic mimics of mussel foot proteins.[57, 64, 65] However, many of the adhesive foot proteins, especially those found at the interface are highly charged (i.e., mfp-5 contains approximately 28 % cationic and 7 % anionic functional groups).[66] Recently, different research groups demonstrated that the incorporation of cationic

31

functional groups to catechol containing adhesive enhanced its adhesive property to various inorganic surfaces (e.g., aluminum, mica, and steel) in simulated seawater or saline.[67-69] The presence of cations likely enhanced wetting to these surfaces that has a surface negative charge.[67] Additionally, the positively charged cation displaces positively charged salt ions on the surface, subsequently allowing the catechol to form stable interfacial bonds.[68] However, incorporation of anionic functional group alone did not enhance the interfacial binding property of catechol containing adhesive.[69]

While recent publications have begun to elucidate the contributions of ionic species to interfacial binding, the effect of these functional groups on the oxidation state of catechol has yet to be systemically studied. The adhesive strength of catechol is highly dependent on its oxidation state as well as the type of surface it adheres to.[21-23, 70] The reduced catechol is responsible for strong interfacial binding to inorganic surfaces.[71] On the other hand, catechol needs to be oxidized to its quinone form in order to participate in intermolecular covalent crosslinking with nucleophilic groups (e.g., $-NH_2$, $-SH$) found on biological substrates.[70] To counteract the basic and oxidizing environment of seawater, mussel utilize antioxidant interfacial proteins (i.e., mfp-6 and mfp-3s) to preserves the reduced state of catechol and facilitate interfacial binding.[72, 73] Similarly, the hydrophobic nature of mfp-3s as well as its ability to form self-coacervates limits catechol's contact with seawater.[74] However, adopting these strategies in the design of synthetic adhesives is challenging and potentially expensive because these strategies not only involve multiple proteins but are also dependent on a highly controlled sequence of surface deposition of these proteins. Qualitative evidence has suggested that incorporating an

32

acidic moiety can preserve the catechol in its reduced state.[75, 76] However, there has been no systematic study that correlates the effect of ionic side chain on the oxidation state and interfacial binding property of catechol.

In this study, we determined the effect of incorporating anionic and cationic functional groups on the oxidation state of catechol. Adhesives hydrogels were prepared by copolymerizing either acrylic acid (AAc) or *N*-(3-aminopropyl)methacrylamide hydrochloride (APMH) with dopamine methacrylamide (DMA), which contain an anionic –COOH, a cationic –NH$_2$, and an adhesive catechol moiety, respectively. The oxidation state of catechol was characterized using ferrous ion oxidation xylenol orange (FOX) assay to track the hydrogen peroxide (H$_2$O$_2$) byproduct generated during the autoxidation of catechol. The interfacial binding property of the adhesives was determined by performing Johnson-Kendall-Roberts (JKR) contact mechanics tests on both inorganic (e.g., quartz) and organic (e.g., amine-functionalized glass) model substrates over a wide range of pH (3.0-9.0).

2.3 Materials and methods

2.3.1 Materials

APMH was purchased from Polysciences, Inc. (Warrington, PA). AAc, *N*-hydroxyethyl acrylamide (HEAA), trichloro(1H,1H,2H,2H-perfluorooctyl)silane (97 %), (3-aminopropyl) trimethoxysilane (APTS), and toluene (anhydrous, 99.8 %) were purchased from Sigma-Aldrich (St. Louis, MO). Methylene bis-acrylamide (MBAA) and 2,2-

33

dimethoxy-2-phenylacetophenone (DMPA) were purchased from Acros Organics (New Jersey, USA). Dimethyl sulfoxide (DMSO) was purchased from Macron (Center Valley, PA), and ethanol (190 proof) was purchased from Pharmco Aaper (Brookfield, CT). DMA was synthesized following previously published protocols.[32] Glass slides were purchased from Fisher Scientific (cat. no. 12-550- A3; Hampton, NH). Quartz slides were purchased from Ted Pella (Redding, CA).

2.3.2   Preparation of the Coated Substrates

Amine-functionalized substrates were prepared by silane chemistry following published procedures with minor modification.[77-79] Glass slides were sonicated in acetone and subsequently dipped into 3 v/v % APTS solution in acetone for 10 min with no agitation, 5 min with sonication and 15 min with no agitation. Slides were soaked in acetone for 10 min, dried at room temperature, and baked overnight at 60°C. To prepare hydrophobic, fluorinated glass slides for making adhesive hydrogel in the hemispherical shape, glass slides were submerged in a solution containing 0.5 mL of trichloro(1H,1H,2H,2H-perfluorooctyl)silane and 49 mL of toluene for 20 min before washing them thrice with fresh toluene, and then air dried.[80]

2.3.3   Preparation of the Testing Media

The acidic pH 3.0 solution was prepared by adding appropriate quantities of 1 M HCl to a solution containing 0.1 M NaCl.[80] The pH 5.0 buffer was prepared by mixing 0.1 M acetic acid and 0.1 M sodium acetate in the ratio 0.56:1. pH 7.5, 8.5 and 9.0 buffers were

34

prepared by adjusting the pH of 10 mM Tris (hydroxymethyl)aminomethane (Tris) buffer containing 0.1 M NaCl with 1 M HCl.

2.3.4   Preparation of the Adhesive Hydrogel

Adhesive hydrogels were prepared by photo-curing precursor solutions containing 1 M HEAA with 10 mol % of DMA and 0 – 10 mol % of either AAc or APMH dissolved in 40% (v/v) DMSO and deionized (DI) water. The crosslinker (MBAA) and photoinitiator (DMPA) were kept constant at 3 and 0.1 mol % respectively, in relation to HEAA. Precursor solutions were degassed three times with N_2 gas, and added to a mold composed of 2 pieces of glass separated by a silicone rubber spacer (2 mm thick). To make hemispherical samples for contact mechanics tests, a maximum of 80 µL of the precursor solution was pipetted onto a hydrophobic, fluorinated glass slide. All samples were photo-cured in a ultra violet (UV) crosslinking chamber (XL-1000, Spectronics Corporation; Westbury, NY) placed inside a N_2 filled glove box (Plas laboratories; Lansing, MI) for a total of 600 s.[15, 80, 81] Immediately after curing, samples were washed in a pH 3.0 solution for overnight to remove any unreacted monomers. Samples for swelling, rheometry, and FOX assay experiments were formed into disk shape using a punch with a diameter of 10, 15, and 6.35 mm, respectively. Samples were further equilibrated at the desired pH for 24 h with constant nutation. The composition of the hydrogels was abbreviated as DxAAy where x and y stand for the mol % of DMA and AAc, respectively, or DxAPz where x and z stand for mol % of DMA and APMH, respectively. All mol % are relative to the molar concentration of HEAA. D10AA0 and

35

D10AP0 are the same composition and will be denoted as D10 for simplicity. Similarly, the control hydrogel with no DMA and no ionic monomers was abbreviated as D0.

2.3.5   Equilibrium Swelling

Hydrogel discs (thickness = 2 mm and diameter = 10 mm) equilibrated at different pH levels were dried in vacuum for at least 48 h. The mass of the swollen (M_s) and dried (M_d) samples were used to calculate the equilibrium swelling ratio by using the following equation:[80]

$$\text{Equilibrium Swelling} \quad = \quad \frac{M_s}{M_d} \quad (6)$$

In the case of FOX assay samples, dry weights were taken into consideration to account for the effect of swelling at different pH values.

2.3.6   Oscillatory Rheometry

Hydrogel discs (thickness = 2 mm and diameter = 15 mm) were compressed to a constant gap of 1800 µm using a parallel plate geometry with a diameter of 20 mm. The storage modulus (G') was measured at frequencies ranging from 0.1 – 100 Hz, and at a strain of 8 % using a TA Discovery Hybrid Rheometer-2 (TA Instruments; New Castle, DE).

36

2.3.7 FOX Assay for Quantifying Hydrogen Peroxide Concentration

The concentration of H_2O_2 generated by the adhesive hydrogel was measured using the Quantitative Peroxide Assay Kit (Thermo Scientific[TM]; Waltham, MA).[82, 83] Hydrogel samples (thickness = 2 mm diameter = 6.35 mm) were briefly rinsed with DI water and submerged in 1000 µL of buffer solution with a desired pH at room temperature for up to 24 h. At a given time point, 20 µL of the hydrogel extract was mixed with 200 µL of the FOX assay reagent, incubated at room temperature for 15 min, and examined using a microplate reader (Synergy[TM] HT, BioTek; Winooski, VT) at 595 nm. 20 µL of fresh buffer solution was added back to the hydrogel extract to keep the volume of the extracting solution constant. H_2O_2 standard curve was prepared by preparing a stock solution (2000 µM of H_2O_2) from 30 % H_2O_2 solution and serially diluting it to a concentration of 7.8 – 2000 µM. H_2O_2 concentrations were normalized by the concentration of DMA as calculated based on the combined volumes of the hydrogel and the extraction fluid.

2.3.8 Contact Mechanics Test

Contact mechanics tests were conducted using a custom-built setup consisting of 10-g load cell (Transducer Techniques; Temecula, CA) and a miniature linear stage stepper motor (MFA-PPD, Newport; Irvine, CA).[80] Hemispherical samples equilibrated at different pH levels were affixed to an indenter (ALS-06, Transducer Techniques; Temecula, CA) using super glue (Gorilla glue or Adhesive systems MG100). Samples were compressed against the test substrate at 1 µm/sec until reaching a maximum preload

37

of 20 mN before the samples were retracted at the same rate. Quartz or APTS-coated glass slides were used as the substrates. The surfaces were wetted with at least 25 µL of buffer solution with the same pH as those used to equilibrate the hemispheres. The force (F) versus displacement (δ) curves were integrated to determine the work of adhesion (W_{adh}), which was normalized with the calculated maximum area of contact (A_{max}) according to the following equation:[80]

$$W_{adh} = \frac{\int F \, d\delta}{A_{max}} \quad (7)$$

A_{max} was mathematically calculated by fitting the loading portion of the force vs displacement curve with the Hertzian model:[84]

$$\delta_{max} = \frac{a^2}{R}, \quad (8)$$

where δ_{max} is the maximum displacement at the maximum preload of 20 mN, a is the radius of A_{max}, and R is curvature of the hemispherical sample. The height (h) and base radius (r) of the each hemisphere were measured using digital Vernier calipers before the start of each test, to determine R:[85]

$$R = \frac{h}{2} + \frac{r^2}{2h} \quad (9)$$

A_{max} was calculated by using the following equation:

$$A_{max} = \pi a^2 \quad (10)$$

38

The adhesion strength (S_{adh}) was calculated by normalizing the maximum pull-off force (F_{max}) by the maximum area of contact (A_{max}) as follows:[86]

$$S_{adh} = \frac{F_{max}}{A_{max}} \quad (11)$$

2.3.9   Statistical Analysis

Statistical analysis was determined using One way analysis of variance (ANOVA) with Tukey−Kramer HSD analysis using JMP Pro 13 software (SAS Institute, NC). $p < 0.05$ was considered significant.

2.4   Results and discussion

We incorporated anionic (AAc) and cationic (APMH) functional groups into DMA containing hydrogels and tested the effect of these ionic side chains on the oxidation state and interfacial binding property of catechol (**Scheme 5**). Our experiments were conducted over a set of five pH values ranging from pH 3.0 to 9.0. pH levels 3.0 and 9.0 were chosen to examine the catechol at its reduced and oxidized states, respectively, and the adhesive properties of catechol under these conditions have been well characterized.[23, 80, 87] A pH of 5.0 and 7.5 were used to simulate the expected physiological pH values of tissues ranging from the acidic skin tissues to oxygenated, internal organs.[88-90] We also chose to test at pH of 8.5 because seawater pH typically ranges between 7.5 and 8.4, while natural freshwater and coastal seawater are more acidic (pH 6.5 to 8.0).[91]

39

Scheme 5. Chemical structures of dopamine methacrylamide (DMA), acrylic acid (AAc) and N-(3-aminopropyl)methacrylamide hydrochloride (APMH).

DMA   AAc   APMH
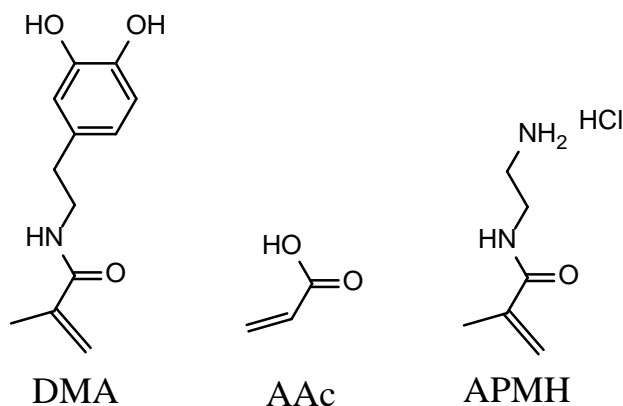
2.4.1 Hydrogel Formation and Characterization

Prior to photo-polymerization, pH testing strips (Fisher, cat. no. 13-640-508; Hampton, NH) were used to determine the pH of the precursor solutions. While all of the formulations exhibited pH range of around 5.0 and 6.0, solutions containing 10 mol % AAc (e.g., D0AA10 and D10AA10) were highly acidic with a pH range between 2.0 and 4.0. This indicated that the carboxylate side chain of AAc drastically lowered the pH value of these solutions. Oscillatory rheology was used to verify that the hydrogels were covalently crosslinked. For all the formulation tested and regardless of incubation pH, the storage modulus (G') values were independent of frequencies (< 45 Hz) (**Figure 14**) and G' values were an order of magnitude higher than those of the loss modulus values (data not shown). These results indicated that all the samples were covalently crosslinked.[50] G' for all the hydrogel formulations were comparable and averaged around 4–10 kPa.

40
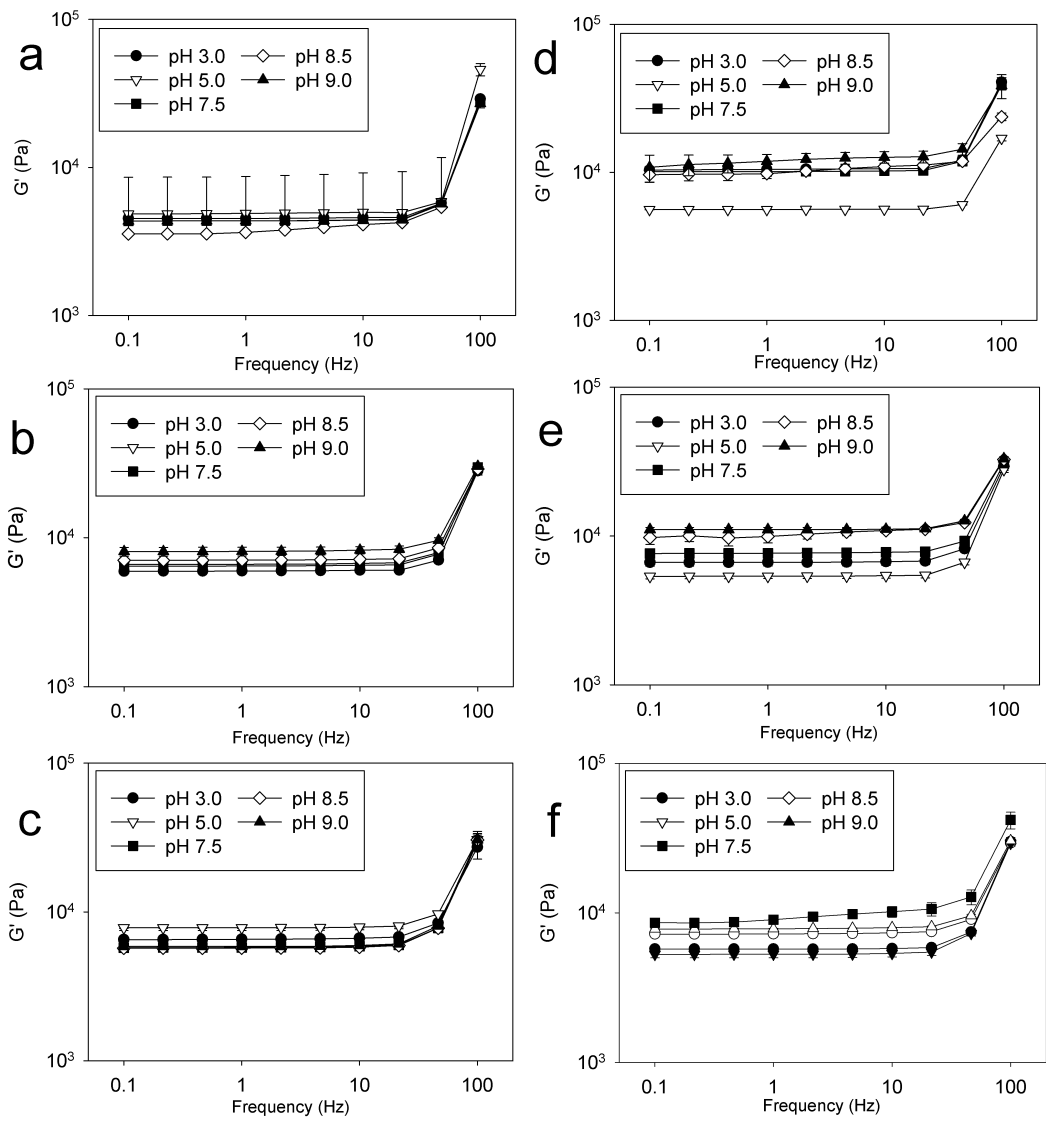
Figure 14. Storage modulus (G') for D0 (a), D0AA10 (b), D0AP10 (c), D10 (d), D10AA10 (e) and D10AP10 (f) equilibrated at pH 3.0-9.0 for 24 h (n = 3).

Incorporating DMA into HEAA gels (i.e., D10) drastically reduced the measured swelling ratio (**Figures 15 and 16**), which is potentially due to π-π interactions and H-bonding between catechol moieties.[92] For D10AA10, increasing pH increased its swelling ratio as AAc (pKa $\approx$ 4.25)[93] became progressively more deprotonated (**Figure 15**).

41

Electrostatic repulsion of the negatively charged AAc resulted in increased swelling.[93] On the other hand, D10AP10 contains APMH (pKa $\approx$ 10)[94] with a –NH$_2$ side chain that reduces charge density and becomes deprotonated with increasing pH, which resulted in deswelling. The swelling ratio for D10AP10 measured at pH 8.5 and higher were drastically lower when compared to those for D10. This indicated that there was an increase in the crosslinking density of the D10AP10 network potentially due to covalent crosslinking between catechol and –NH$_2$ side chain of APMH through either Michael-type addition or the formation of Schiff's base.[95, 96]
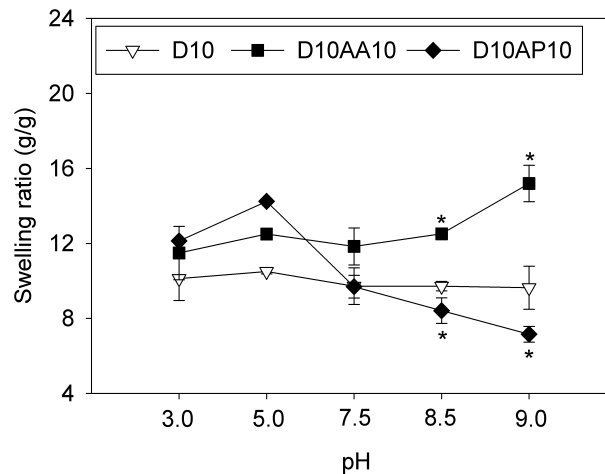
Figure 15. Swelling ratios of adhesive hydrogels equilibrated at pH 3.0-9.0 for 24 h (n = 3). * $p < 0.05$ when compared to D10 at the same pH. D10, D10AA10 and D10AP10 represent adhesive hydrogels containing DMA (catechol), AAc (-COOH) and APMH (-NH$_2$) respectively.

42
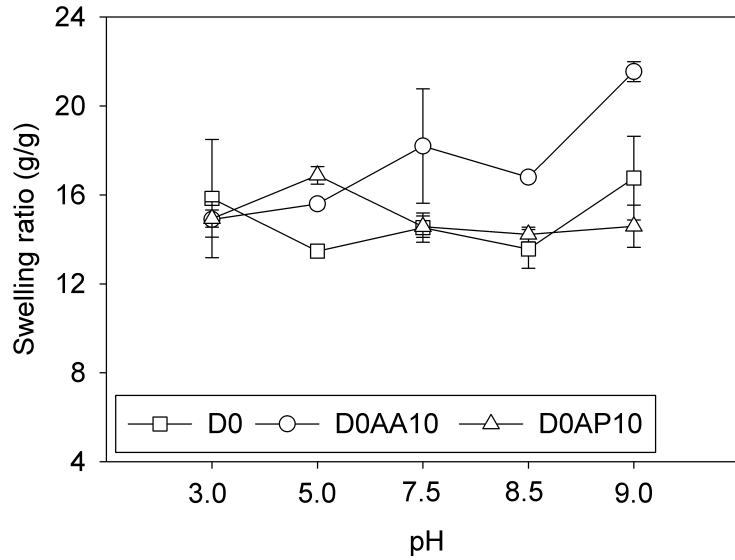
Figure 16. Swelling ratios of control hydrogels equilibrated at pH 3.0-9.0 for 24 h (n = 3).

2.4.2 Characterizing the Oxidation State of Catechol using FOX assay

Adhesive hydrogels reported here are covalently crosslinked and insoluble, which made it difficult to employ the oft-used spectroscopy methods to directly determine the oxidation state of catechol in these samples.[87] During the autoxidation of catechol, reactive oxygen species (ROS) such as superoxide ($O_2^{\bullet-}$) and hydrogen peroxide (H_2O_2) are generated as byproducts (**Scheme 6**).[83] Dismutation of $O_2^{\bullet-}$ also generates H_2O_2, which is significantly more stable when compared to $O_2^{\bullet-}$.[97] As such, H_2O_2 can be quantified using the conventional FOX assay as it is being generated and released from the hydrogel samples.

43

Scheme 6. Schematic representation of the generation of hydrogen peroxide (H_2O_2) as a result of catechol autoxidation.
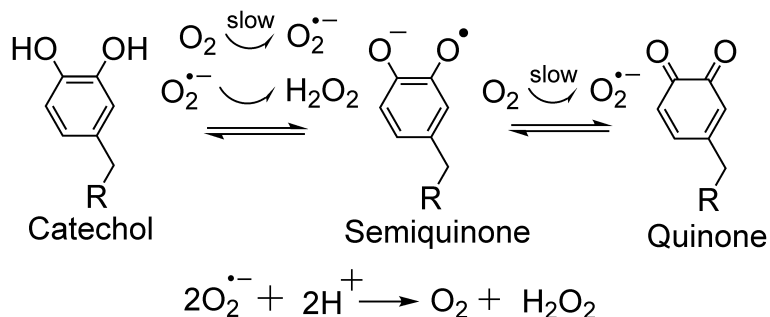
Tracking the concentration of H_2O_2 over time provided a convenient approach for determining the oxidation state of catechol in our samples at different pH values. D10 incubated at pH 3.0 and 5.0 did not generate H_2O_2 even after 24 h (**Figures 17 and 18**) and these samples remained clear and colorless (**Table 3**). As expected, catechol remained in its reduced state in an acidic pH.[71] However, when the pH was raised to 7.5, D10 generated detectable amount of H_2O_2 within 2 h and the H_2O_2 concentration continued to increase for 24 h (0.0481 ± 0.00373 µM H_2O_2 /µM catechol by 24 h), indicating that catechol were increasingly oxidized over time. Given the half-life of H_2O_2 at room temperature ($\approx$ pH 7.0) can range from $12 - 30$ h,[98] D10 continued to generate H_2O_2 over time. D10 generated more H_2O_2 when these samples were incubated at a more basic pH (1.5 and 1.9 fold increase at pH 8.5 and 9.0, respectively, when compared to pH 7.5). These samples also turned brown when incubated at a pH of 7.5 and higher, which is an indication of catechol oxidation (**Table S1**). Catechol becomes increasingly more oxidized when the pH of the solution approach the pK_a of catechol ($\approx$ 9.3).[40]

44
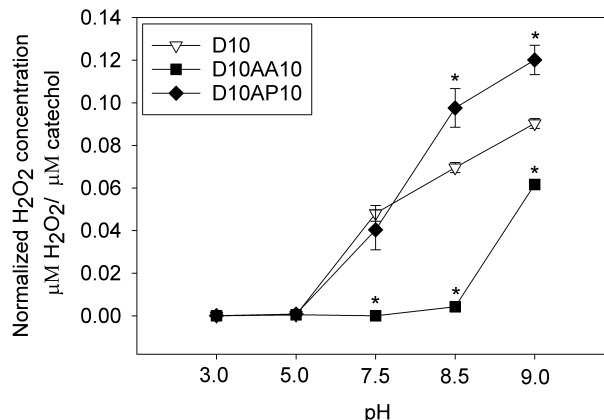
Figure 17. Normalized concentration of H_2O_2 released from hydrogels equilibrated at pH 3.0-9.0 after 24 h of incubation (n = 3). * $p < 0.05$ when compared to D10 at the same pH. . D10, D10AA10 and D10AP10 represent adhesive hydrogels containing DMA (catechol), AAc (-COOH) and APMH (-NH$_2$) respectively.

When AAc was incorporated, D10AA10 did not generate H_2O_2 even when it was incubated at pH 7.5 and only a small amount of H_2O_2 was detected at pH 8.5 (**Figure 17**). Correspondingly, D10AA10 remained colorless when incubated at a pH that was 7.5 or less and D10AA10 only developed minor discoloration around its edge after it was incubated at pH 8.5 for 24 h (**Table 3**). When the pH was raised to 9.0, a significantly higher amount of H_2O_2 was generated (0.0617 ± 0.00202 μM H_2O_2/μM catechol after 24 h) and D10AA10 appeared brown in color (**Table 3**), indicating catechol oxidation. However, the amount of H_2O_2 generated from D10AA10 was 1.5 fold lower compared to that of D10 tested at the same pH. These results suggest that the carboxyl side chain of AAc buffered the local pH within the adhesive network and contributed to maintaining the reduced form of catechol. Precursor solutions containing AAc (e.g., D0AA10 and

45

D10AA10) were also significantly more acidic (pH 2.0-4.0) when compared to those (e.g., D0, D10, D10AP10, etc.) that do not contain AAc (pH 5.0-6.0). However, AAc lost its buffering capacity when the surrounding media was highly basic.
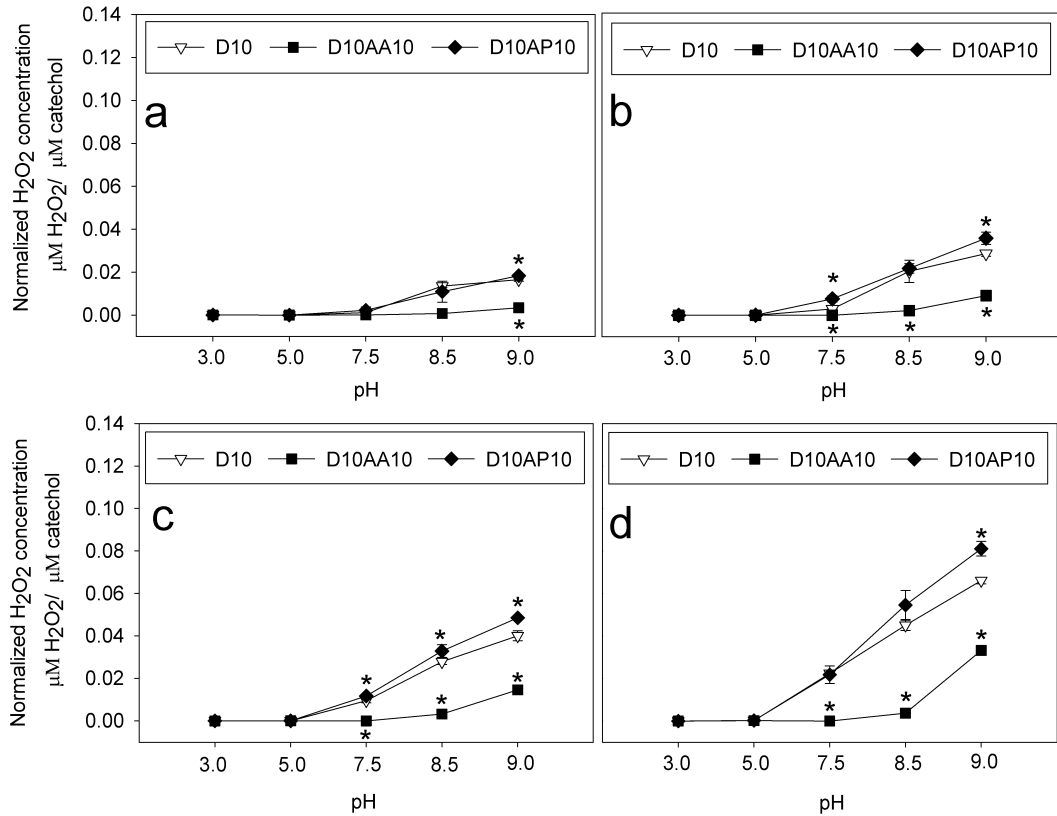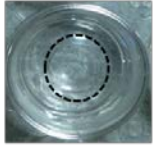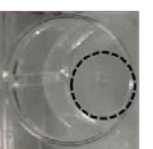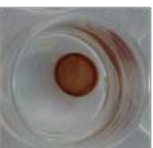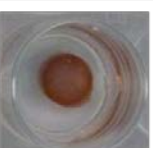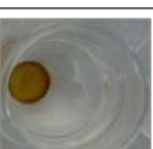
Figure 18. Normalized concentration of H_2O_2 released from hydrogels equilibrated at pH 3.0-9.0 after 2 (a), 4 (b), 6 (c) and 12 (d) hours of incubation (n = 3). * $p < 0.05$ when compared to D10.

Samples containing APMH (e.g., D10AP10) generated similar amount of H_2O_2 as D10 at pH levels between 3.0 and 7.5 (**Figure 17**). At a more basic pH, D10AP10 generated higher amount of H_2O_2 when compared to D10 (2.5 and 3 fold increase at pH 8.5 and 9.0,

46

respectively). Previously, we reported that dopamine with a free $-NH_2$ group generated significantly more H_2O_2 when compared to DMA, potentially due to the polymerization of dopamine to form polydopamine.[83] Autoxidation of dopamine involves intracyclization and formation of intramolecular Michael-type adduct to form dopamine indole.[62] On the other hand, the primary amine group in DMA was functionalized with a methacrylamide and was unavailable for covalent crosslinking. This increase in the measured H_2O_2 from D10AP10 may be attributed to covalent crosslinking between the $-NH_2$ of APMH and oxidized quinone.

Table 3. Images of adhesive hydrogels equilibrated at pH 3.0-9.0 for 24 h. The dashed circles highlights the location of colorless hydrogels.

Composition	pH 3.0	pH 5.0	pH 7.5	pH 8.5	pH 9.0
D0					
D0AA10					
D0AP10					
D10					
D10AA10					
D10AP10					

The measured H_2O_2 concentration was lower than the concentration of catechol in the hydrogel network. While H_2O_2 was constantly being generated, H_2O_2 decomposition also occurred concurrently. Additionally, the hydrogel network also served as a cage that

48

hinders the diffusion of H_2O_2 into the extracting solution.[82, 83] Nevertheless, H_2O_2

quantification served as useful approach to measure the extent of catechol oxidation *in situ*. Samples that did not contain DMA (e.g., D0, D0AA10 and D0AP10) did not

generate H_2O_2 over 24 h for all the pH values (data not shown) and these samples

remained colorless (**Table 3**), confirming that the source of H_2O_2 is associated with

autoxidation of catechol.

2.4.3   Contact Mechanics Tests

JKR contact mechanics test was performed to assess the effect of incorporating AAc and

APMH on the interfacial binding property of catechol to two types of surfaces (e.g.,

quartz and APTS-coated glass). Quartz was used as a model inorganic surface as silica-

based materials are commonly used as medical and dental implants,[99, 100] while APTS-

coated glass was used to simulate amine functional group found on tissue surfaces.[101]

Most importantly, interaction between catechol and these surfaces have been well

documented.[70, 71]

2.4.3.1   *Adhesion to Quartz Surface*

The control HEAA hydrogels (D0) exhibited weak adhesion to quartz surface with W_{adh}

values that averaged around 11-130 mJ/m^2 depending on the pH (**Table 4**). Addition of

DMA to HEAA hydrogels (D10) significantly increased W_{adh} values and D10

demonstrated elevated adhesive property at acidic pH (444.7 ± 123.7 mJ/m^2 at pH 3.0;

Figure 19a). This is due to the strong interfacial binding (i.e., H-bond) between catechol

49

and SiO$_2$ surface (**Scheme 7a**).[51, 80] W$_{adh}$ values for D10 were greatly reduced at a pH of 7.5 or higher (90 % reduction when compared to pH 3.0) as a result of catechol oxidation. Addition of an anionic monomer, AAc, to HEAA hydrogels (D0AA10) showed negligible W$_{adh}$ value over the entire range of pH values except some weak interactions at pH 3.0. With increasing pH, both- the –COOH group of AAc and the quartz surface become highly negatively charged[102, 103] and electrostatic repulsion between D0AA10 and quartz surface greatly minimized the measured adhesion values (**Scheme 7b**).

Table 4. Work of adhesion (W$_{adh}$) for D0 tested against a wetted quartz and APTS-functionalized glass substrate at pH 3.0-9.0 (n = 3).

Surface	W$_{adh}$ (mJ/m^2)				
	pH 3.0	pH 5.0	pH 7.5	pH 8.5	pH 9.0
Quartz	128.9 ± 39.46	115.9 ± 37.50	91.55 ± 29.64	25.16 ± 9.464	11.06 ± 8.217
APTS	142.7 ±21.83	132.7 ± 41.94	170.0 ± 7.705	54.03 ± 13.87	82.41 ± 53.61

50

Scheme 7. Schematic representation of adhesive hydrogels D10 (a), D10AA10 (b), D0AP10 (c) and D10AP10 (d) interacting with a wetted quartz substrate at pH ranging from 3.0 to 9.0 (from left to right).
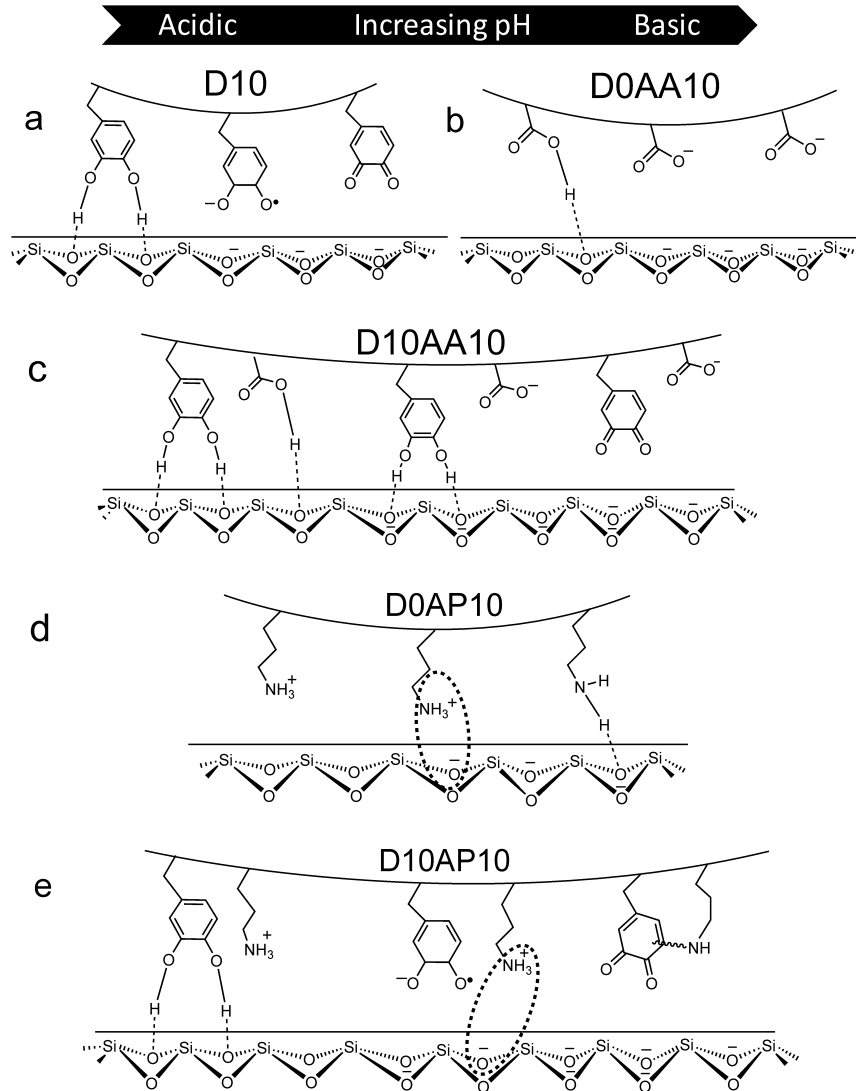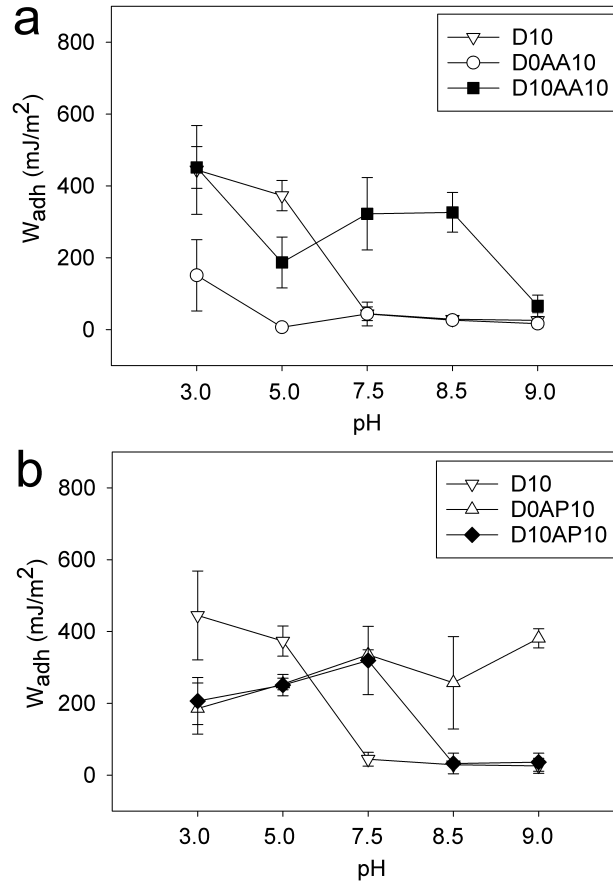
Figure 19. Work of adhesion (W_{adh}) for adhesive hydrogels containing AAc (-COOH) (a) and APMH (-NH$_2$) (b) tested against a wetted quartz substrate at pH 3.0-9.0 (n = 3). Refer to Tables 5-7 for results of statistical analysis.

When AAc was incorporated into DMA-containing hydrogel (D10AA10), there was a drastic increase in the measured W_{adh} values at pH 7.5 and 8.5 when compared to those of D10 (~ 7 and 11 fold increase, respectively) (**Figure 19a**). Given that D0AA10 was poorly adhesive to quartz at this pH range, the elevated adhesive values measured for D10AA10 can be attributed to catechol's ability to from strong interfacial bonds (**Scheme 7c**). The W_{adh} at pH 7.5 and 8.5 was not significantly different from the value measured

52

at pH 5.0 (**Table 7**). The presence of AAc likely maintained catechol in its reduced and adhesive state in a neutral to mildly basic pH, which was confirmed by the FOX assay results (**Figure 17**) and the photographs of the hydrogel (**Table 3**). The adhesive property of D10AA10 was drastically diminished at pH 9.0 as a result of catechol oxidation, as the basic buffer overcame the buffering capacity of AAc. The FOX assay data also supported this as the measured concentration of H_2O_2 was the highest at pH 9.0. Our data confirmed previously published results that indicated anions do not actively participate in interfacial binding to inorganic surfaces.[69] However, our new findings suggest that the anionic functional groups contributed by buffering the local pH to preserve the adhesive property of catechol.

Table 5. Statistical analysis for W_{adh} of adhesive hydrogels containing anionic AAc tested against a wetted quartz substrate. Compositions not connected by the same letter at a given pH are significantly different.

Composition	pH 3.0	pH 5.0	pH 7.5	pH 8.5	pH 9.0
D10	A	A	A	A	A
D0AA10	B	B	A	A	A
D10AA10	A	C	B	B	A

53

Table 6. Statistical analysis for W_{adh} of adhesive hydrogels containing cationic APMH tested against a wetted quartz substrate. Compositions not connected by the same letter at a given pH are significantly different.

Composition	pH 3.0	pH 5.0	pH 7.5	pH 8.5	pH 9.0
D10	A	A	A	A	A
D0AP10	B	B	B	B	B
D10AP10	B	B	B	A	A

Table 7. Statistical analysis for W_{adh} of adhesive hydrogels containing anionic AAc or cationic APMH tested against a wetted quartz substrate. pHs not connected by the same letter for a given composition are significantly different.

pH	D10	pH	D0AA10	pH	D10AA10	pH	D0AP10	pH	D10AP10
3.0	A	3.0	A	3.0	A	3.0	A	3.0	A
5.0	A	5.0	B	5.0	B C	5.0	A B	5.0	A
7.5	B	7.5	A B	7.5	A B	7.5	A B	7.5	A
8.5	B	8.5	A B	8.5	A B	8.5	A B	8.5	B
9.0	B	9.0	B	9.0	C	9.0	B	9.0	B

54

Adding a cationic monomer, APMH, to the HEAA hydrogels (D0AP10) exhibited W_{adh} values (200-380 mJ/m^2) that were comparable to those of D10 (452.6 ± 58.18 mJ/m^2 at pH 3.0; **Figure 19b**). This result is in agreement with previous findings that indicated cationic functional groups contributed significantly to interfacial binding to inorganic surfaces.[67-69] APMH likely interacted with the quartz surface using a combination of electrostatic interaction and H-bonding (**Scheme 7d**). The W_{adh} values for D10AP10 mirrored those of D0AP10 for pH between 3.0 and 7.5. There was no additive effect with the addition of both catechol and –NH$_2$ into the adhesive network. Most noticeably, W_{adh} values for D10AP10 was more than 10 fold higher when compared to that observed for D10 at pH 7.5. Based on the FOX assay, both D10 and D10AP10 produced equivalent amount of H$_2$O$_2$ over 24 h (**Figure 17**), indicating that catechol in both adhesives were equally oxidized. The elevated adhesive property demonstrated by D10AP10 was likely contributed by the presence of –NH$_2$ side chain of APMH. With further increase in pH (i.e., pH 8.5 and 9.0), W_{adh} values for D10AP10 decreased drastically and became equivalent to those of oxidized D10. However, W_{adh} values for D0AP10 remained constant and average around 300-380 mJ/m^2. These results indicated that the oxidized catechol in D10AP10 likely formed covalent crosslinks with –NH$_2$ of APMH, leading to reduced availability of APMH for interfacial binding (**Scheme 7e**). This observation is in agreement with the FOX assay data, which also showed that D10AP10 generated significantly higher amount of H$_2$O$_2$ at pH 8.5 and 9.0 as compared to D10, possibly due to the formation of adducts with the nucleophile.[83] S_{adh} data (**Figures 20a and 20b, Tables 8-10**) was largely in agreement with the W_{adh} results.

55
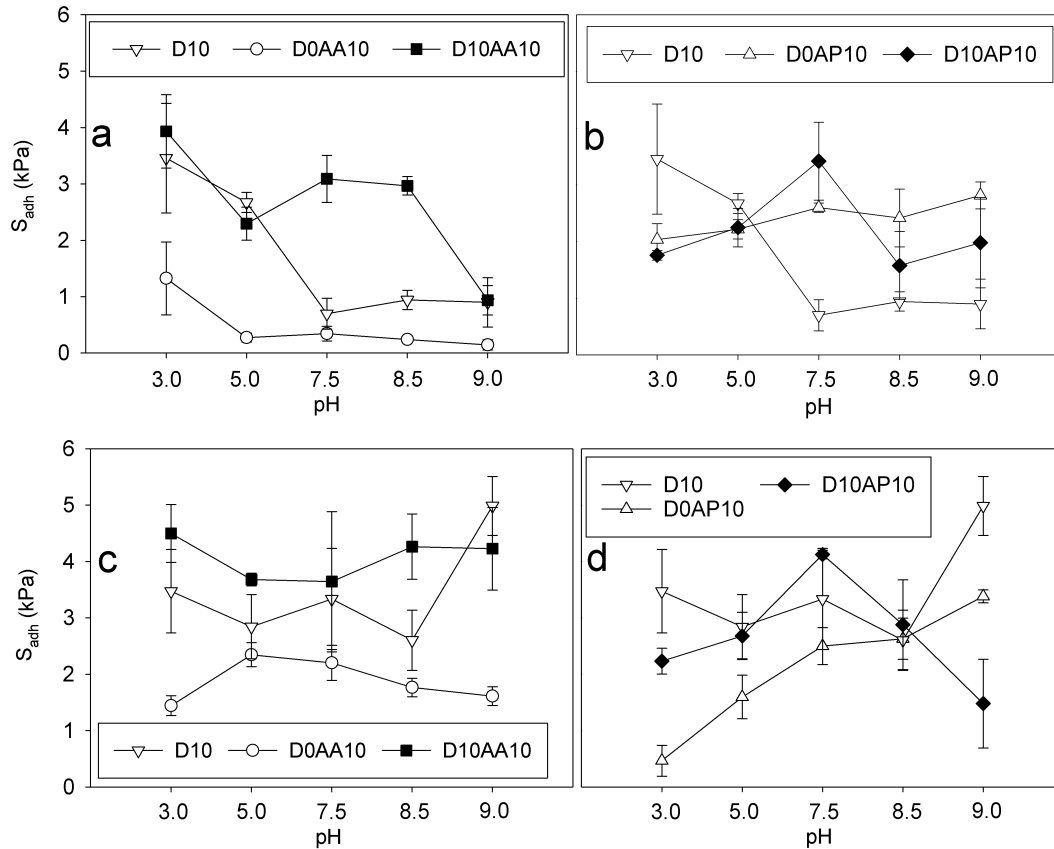
Figure 20. Adhesion strength (S_{adh}) for adhesive hydrogels containing anionic AAc or cationic APMH tested against a wetted quartz (a and b) or APTS-functionalized substrate (c and d) at pH 3.0-9.0 (n=3). Refer to Tables 8-10 and 14-16 for statistical analysis.

56

Table 8. Statistical analysis for S_{adh} of adhesive hydrogels containing anionic AAc tested against a wetted quartz substrate. Compositions not connected by the same letter at a given pH are significantly different.

Composition	pH 3.0	pH 5.0	pH 7.5	pH 8.5	pH 9.0
D10	A	A	A	A	A
D0AA10	B	B	A	A	A
D10AA10	A	C	B	B	A

Table 9. Statistical analysis for S_{adh} of adhesive hydrogels containing cationic APMH tested against a wetted quartz substrate. Compositions not connected by the same letter at a given pH are significantly different.

Composition	pH 3.0	pH 5.0	pH 7.5	pH 8.5	pH 9.0
D10	A	A	A	A	A
D0AP10	A B	A	B	B	B
D10AP10	B	A	B	A B	A B

57

Table 10. Statistical analysis for S_{adh} of adhesive hydrogels containing anionic AAc or cationic APMH tested against a wetted quartz substrate. pHs not connected by the same letter for a given composition are significantly different.

pH	D10	pH	D0AA10	pH	D10AA10	pH	D0AP10	pH	D10AP10
3.0	A	3.0	A	3.0	A	3.0	A	3.0	A
5.0	A	5.0	B	5.0	B	5.0	A	5.0	A B
7.5	B	7.5	B	7.5	A B	7.5	A	7.5	B
8.5	B	8.5	B	8.5	A B	8.5	A	8.5	A
9.0	B	9.0	B	9.0	C	9.0	A	9.0	A B

2.4.3.2 Adhesion to –NH₂-functionalized Glass

W_{adh} values for D10 decreased with increasing pH ($W_{adh} = 471.7 \pm 138.5$ and 107.6 ± 62.11 mJ/m^2 for pH 3.0 and 8.5, respectively.) (**Figure 21a**). The strong interaction at acidic pH was due to the strong cation-π interactions between catechol and the positively charged APTS substrate (**Scheme 8a**).[60, 65] This interaction may have weakened as the pH was increased due to reduced surface charge density and the deprotonation of –NH$_2$. D10 may have transitioned to form weaker H-bond or electrostatic interactions. Interestingly, elevated W_{adh} value was obtained for D10 at pH 9.0 ($W_{adh} = 340.0 \pm 41.15$ mJ/m^2), which

58

suggested the formation of interfacial covalent bond formation between oxidized quinone and primary amine on the surface.[71]
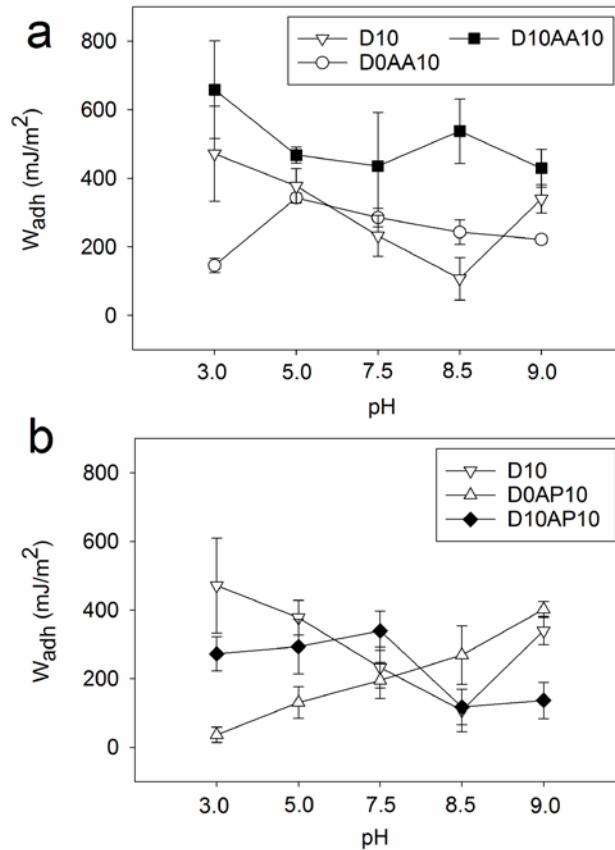
Figure 21. Work of adhesion (W_{adh}) of adhesive hydrogels containing AAc (-COOH) (a) and APMH (-NH$_2$) (b) tested against a wetted APTS-functionalized glass substrate at pH 3.0-9.0 (n = 3). Refer to Tables 11-13 for results of statistical analysis.

Scheme 8. Schematic representation of adhesive hydrogels D10 (a), D0AA10 (b), D10AA10 (c), D0AP10 (d) and D10AP10 (e) interacting with a wetted amine-functionalized substrate (APTS-coated glass) at pH ranging from 3.0 to 9.0 (from left to right).
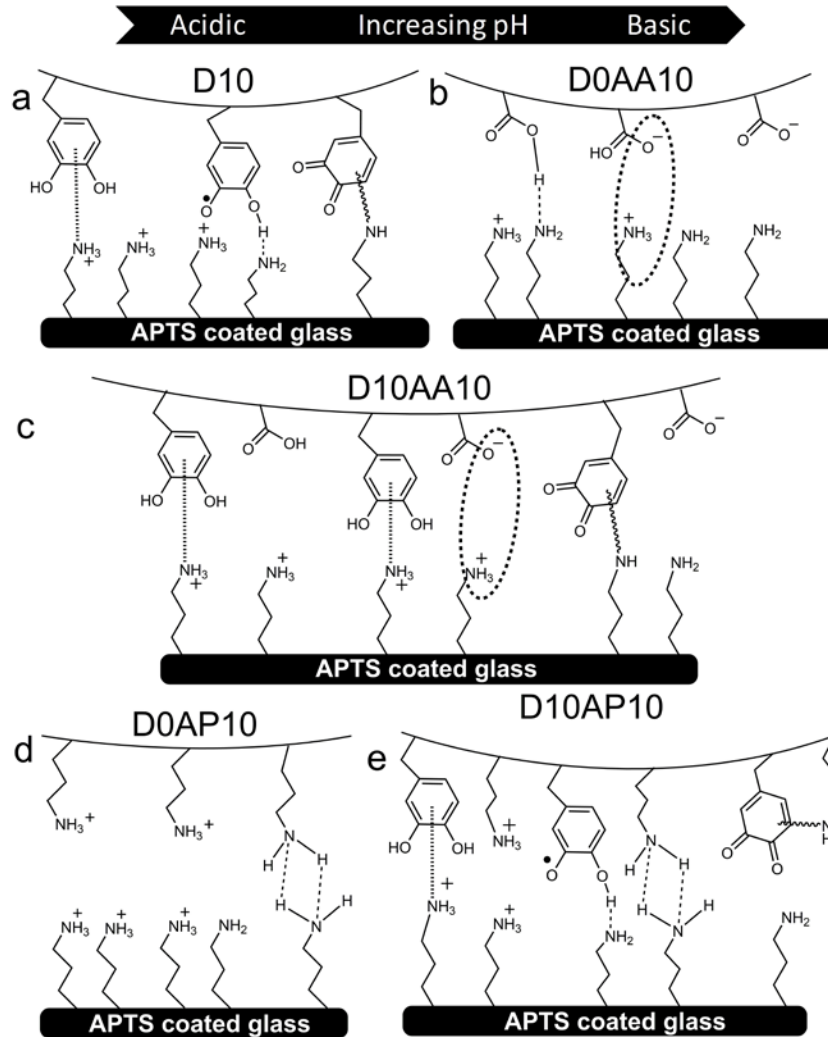
W_{adh} for hydrogel containing only the anionic AAc (i.e., D0AA10) initially increased with increasing pH reaching a maximum at pH 5.0 (W_{adh} = 343.1 ± 13.93 mJ/m^2; **Figure 21a**, **Scheme 8b**). At pH 3.0, the carboxyl group of AAc was mostly protonated and interacted weakly with APTS through H-bonding. When the solution pH exceeded the dissociation constant of AAc (pKa ≈ 4.25),[93] the carboxyl group became more negatively charged and interacted with APTS through electrostatic interaction. However, further increase in pH resulted in reduced W_{adh} values as the surface positive charge density decreased and APTS becomes progressively more deprotonated. Nevertheless, AAc demonstrated considerable amount of adhesion to APTS-functionalized surface and outperformed catechol at pH 7.5 and 8.5.

Table 11. Statistical analysis for W_{adh} of adhesive hydrogels containing anionic AAc tested against a wetted APTS-functionalized glass substrate. Compositions not connected by the same letter at a given pH are significantly different.

Composition	pH 3.0	pH 5.0	pH 7.5	pH 8.5	pH 9.0
D10	A	A	A	A	A
D0AA10	B	A	A	A	B
D10AA10	A	B	A	B	A

61

Table 12. Statistical analysis for W_{adh} of adhesive hydrogels containing cationic APMH tested against a wetted APTS-functionalized glass substrate. Compositions not connected by the same letter at a given pH are significantly different.

Composition	pH 3.0	pH 5.0	pH 7.5	pH 8.5	pH 9.0
D10	A	A	A B	A	A
D0AP10	B	B	B	A	A
D10AP10	A	A	A	A	B

Table 13. Statistical analysis for W_{adh} of adhesive hydrogels containing anionic AAc or cationic APMH tested against a wetted APTS-functionalized glass substrate. pHs not connected by the same letter for a given composition are significantly different.

pH	D10	pH	D0AA10	pH	D10AA10	pH	D0AP10	pH	D10AP10
3.0	A	3.0	A D	3.0	A	3.0	A	3.0	A B C
5.0	A B	5.0	B	5.0	A	5.0	A B	5.0	A B
7.5	B C	7.5	B C	7.5	A	7.5	B C	7.5	A
8.5	C	8.5	C D	8.5	A	8.5	C D	8.5	C
9.0	A B	9.0	D	9.0	A	9.0	D	9.0	B C

62

Table 14. Statistical analysis for S_{adh} of adhesive hydrogels containing anionic AAc tested against a wetted APTS-functionalized glass substrate. Compositions not connected by the same letter at a given pH are significantly different.

Composition	pH 3.0	pH 5.0	pH 7.5	pH 8.5	pH 9.0
D10	A	A B	A	A	A
D0AA10	B	B	A	A	B
D10AA10	A	A	A	B	A

Table 15. Statistical analysis for S_{adh} of adhesive hydrogels containing cationic APMH tested against a wetted APTS-functionalized glass substrate. Compositions not connected by the same letter at a given pH are significantly different.

Composition	pH 3.0	pH 5.0	pH 7.5	pH 8.5	pH 9.0
D10	A	A	A B	A	A
D0AP10	B	B	B	A	B
D10AP10	C	A B	A	A	C

63

Table 16. Statistical analysis for S_{adh} of adhesive hydrogels containing anionic AAc or cationic APMH tested against a wetted APTS-functionalized glass substrate. pHs not connected by the same letter for a given composition are significantly different.

pH	D10	pH	D0AA10	pH	D10AA10	pH	D0AP10	pH	D10AP10
3.0	A B	3.0	A	3.0	A	3.0	A	3.0	A
5.0	A	5.0	B	5.0	A	5.0	B	5.0	A B
7.5	A B	7.5	B	7.5	A	7.5	C	7.5	B
8.5	A	8.5	A B	8.5	A	8.5	C D	8.5	A B
9.0	B	9.0	A B	9.0	A	9.0	D	9.0	A

When both DMA and AAc were introduced into HEAA (D10AA10), both functional groups (i.e., catechol and carboxylate group) appeared to interact synergistically with the APTS surface, as the measured W_{adh} values were significantly higher than the formulations containing either of the two functional groups alone (i.e., D10 or D0AA10; **Figure 21a**). The W_{adh} values measured in this series were also the highest among the adhesive-surface combinations that were investigated in this study (i.e., $W_{adh} = 658.5 \pm 141.9$ mJ/m^2 at pH 3.0). The combination of cation-π and electrostatic interactions likely contributed to the elevated adhesive property (**Scheme 8c**). While the W_{adh} values for both D10 and D0AA10 decreased with increasing pH, W_{adh} values for D10AA10 did not change significantly with changing pH (**Table 13**). Based on FOX assay results, addition

64

of AAc preserved the reduced state of catechol at pHs 5.0-8.5, which suggest that catechol in its reduced form is required for strong interaction with $-NH_2$-functionalized surface. Additionally, long range interaction (i.e., electrostatic attraction between $-COO^-$ and $-NH_3^+$) likely promoted catechol surface adsorption, potentially similar to how cations promoted adhesion of catechol adsorption to inorganic substrates.[104] When the pH was raised to 9.0, D10AA10 exhibited W_{adh} of 429.1 ± 55.45 mJ/m^2 even though AAc lost its buffering capacity at this pH. Similar to D10, the elevated adhesion values is likely resulted from the formation of interfacial covalent bond.[71]

Both D0AP10 and APTS-functionalized surface contained $-NH_2$ functional groups, which were positively charged at an acidic pH. Electrostatic repulsion between the hydrogel and surface resulted in reduced interaction at pH 3.0 ($W_{adh} = 36.23 \pm 22.38$ mJ/m^2; **Figure 21b**, **Scheme 8d**). W_{adh} value increased with increasing pH as the charge density for both the adhesive and substrate decreased, resulting in increased interfacial binding. Specifically, at pH 9.0, the interfacial binding was the strongest ($W_{adh} = 402.0 \pm 23.64$ mJ/m^2) potentially due to interfacial H-bond formation.

At pH 3.0 and 5.0, D10AP10 exhibited comparable W_{adh} values as D10 (**Figure 21b**). This indicated that catechol needed to form strong interfacial cation-π interactions while overcoming electrostatic repulsion between network bound $-NH_3^+$ of APMH and positively charged surface ($-NH_3^+$ of APTS; **Scheme 8e**). As the pH was increased to 7.5, W_{adh} value for D10AP10 averaged around 339.7 ± 57.07 mJ/m^2, which was ~ 1.5 fold higher compared to those of D10 and D0AP10. With increasing pH, a reduction in

65

charge density allowed both catechol and network-bound –NH$_2$ group to from interfacial bonds. However, further increase in the pH resulted in a statistically significant decrease in interfacial binding (W$_{adh}$ at pH 8.5 = 117.3 ± 51.59 mJ/m^2 and pH 9.0 = 136.4 ± 52.95 mJ/m^2) (**Table 13**). This is possibly due to the cohesive crosslinking between network-bound–NH$_2$ of APMH and quinone,[95, 96] resulting in reduced availability of APMH and catechol at pH 8.5 and 9.0, respectively, for interacting with the amine functionalized surface. S$_{adh}$ data (**Figures 20c and 20d, Tables 14-16**) was largely in agreement with W$_{adh}$ data.

Taken together, both anionic and cationic functional groups contributed considerably to interfacial binding through electrostatic attraction to surfaces with the opposite charges. Measured W$_{adh}$ values for these ionic species were comparable to and in some cases exceeded those measured for catechol. Most noticeably, the carboxylate side chain of AAc buffered local pH to preserve the reduced state of catechol, which was critical for binding to both quartz and –NH$_2$-functionalized surfaces. Unlike strategies devised by marine mussels that require multiple foot proteins with unique features (i.e., antioxidant property, surface drying property, etc.) to preserve the reduced and adhesive state of catechol,[72, 74] adding anionic functional group provided a simple yet effective approach in designing synthetic mussel-mimetic adhesives for applications suitable for mildly basic conditions. On the other hand, the –NH$_2$ side chain of APMH promoted cohesive crosslinking with oxidized quinone in a basic pH, which limited interfacial interactions. Although we did not test adhesives that combined both ionic species; natural interfacial foot proteins (i.e., mfp-5 and mfp-3) containing both anionic and cationic functional

66

groups[73, 105] and synthetic mimics that contain both species have demonstrated enhanced adhesion under simulated seawater conditions.[69] The anionic and cationic side chains in these adhesives likely contributed synergistically to interfacial binding by separately preserving the reduced state of catechol and promoting adhesion to inorganic surfaces (i.e., electrostatic interaction, repelling surface anions), respectively. The adhesion testing described here consisted of a soft hydrogel contacting a rigid substrate and additional testing is required to determine of the same trends can be obtained for contacting a soft, compliant substrate (i.e., soft tissue).[106] Finally, our report provided a useful guide for designing synthetic adhesives and coatings depending on the intended application (i.e., different surface type and pH).

2.5 Conclusions

In this study, we systemically evaluated the effect of incorporating anionic (AAc) and cationic (APMH) functional groups on catechol adhesion to both model inorganic and organic surfaces across a wide range of pH levels. Specifically, we correlated the effect of these ionic species on the oxidation state and interfacial binding property of catechol. Both ionic functional groups contributed considerably to interfacial binding through electrostatic attraction to surfaces with the opposite charges. In some situations, measured adhesion values for these ionic species were comparable to and can exceed those of catechol. Addition of AAc preserved the reduced and adhesive form of catechol in a mildly basic condition. On the other hand, the $-NH_2$ of APMH resulted in covalent

67

crosslinking between oxidized quinone in a basic pH, which interfered with interfacial binding.

2.6 Acknowledgements

3 Incorporation of Anionic Monomer to Tune the Reversible Catechol-Boronate Complex for pH Responsive, Reversible Adhesion[3]

3.1 Abstract

Up to 30 mol% of acrylic acid (AAc) was incorporated into a pH responsive smart adhesive consisting of dopamine methacrylamide (DMA) and 3-acrylamido phenylboronic acid (APBA). FTIR spectroscopy and rheometry confirmed that the incorporation of AAc shifted the pH of catechol-boronate complexation to a more basic pH. Correspondingly, adhesive formulations with elevated AAc contents demonstrated strong adhesion to quartz substrate at a neutral t[3]o mildly basic pH (pH 7.5-8.5) based on Johnson-Kendall-Roberts (JKR) contact mechanics test. When pH was further increased to pH 9.0, there was a drastic reduction in the measured work of adhesion (18 and 7 fold reduction compared to values measured at pH 7.5 and 8.5, respectively) due to the formation of catechol-boronate complex. The complex remained reversible and the interfacial binding property of the adhesive was successfully tuned with changing pH in successive contact cycles. However, an acidic pH (pH 3.0) was required to break the

---

69

catechol-boronate complex to recover the elevated adhesive property. Adding AAc enables the smart adhesive to function in physiological or marine pH ranges.

3.2 Introduction

Smart adhesives can transform reversibly between its adhesive and non-adhesive states with an externally applied stimulus. This property is particularly important for the development of painless and removal dressings, sustainable packaging materials, recyclable bonded structures, and robust walking mechanisms for microrobotics.[1-3, 107] Currently available smart adhesives are limited by the need for elevated temperatures for debonding,[3] adhesion to a specific substrate,[5] or poor adhesion in a wet environment.[2] In particular, the presence of a liquid layer on the substrate acts as an obstacle to adhesion, making most synthetic adhesives ineffective in a wet environment.[8, 57, 59]

Mussels secrete adhesive proteins that contain a catecholic amino acid, 3,4–dihydroxyphenylalanine (DOPA), which enables them to bind to wet substrates.[57, 60] In its reduced form, catechol has the ability to interact inorganic surfaces (e.g., metals) through formation of coordination bonds, while in its oxidized form, it is capable of forming interfacial covalent bonds with organic surfaces (e.g., tissues).[71, 108] Incorporating catechol into inert polymers has imparted these materials with strong, wet adhesive properties for various applications.[10, 109, 110] Several labs have recently reported different catechol-based adhesives that are responsive to light,[20] enzyme,[19] or temperature.[111]

70

The adhesive property of catechol is highly dependent on its oxidation state.[22, 23, 55, 70] At an acidic pH, catechol is in its reduced state, and forms strong interfacial bonds with inorganic substrates.[71] However, when the pH approaches the dissociation constant of catechol ($pK_a \approx 9.3$), catechol is progressively oxidized and its strength of interfacial interaction is significantly reduced.[71] Recently, we exploited this pH-dependent adhesive property of catechol to design a smart adhesive.[80] This adhesive consisted of both network-bound catechol and boronic acid, which demonstrated elevated adhesion at pH 3.0. At pH 9.0, the formation of catechol-boronate complex reduced the measured work of adhesion by over an order of magnitude. Boronic acid not only contributed to adhesion, but also protected catechol from irreversible oxidation and crosslinking. Even though the ideal pH for catechol-boronate complexation is 9.0,[80, 112] the complex forms readily at a neutral and mildly basic pH,[39] which will limit the potential for using this smart adhesive for applications at physiological or marine pH ranges (i.e., pH 7.5-8.5).[89, 91]

To tune the pH of catechol-boronate complexation, we introduced an acidic anionic monomer, acrylic acid (AAc), into the adhesive network. Incorporating an acidic moiety has been demonstrated to preserve the catechol in its reduced state.[75, 76] Similarly, we previously demonstrated that the incorporation of AAc preserved the reduced and adhesive state of catechol even at a pH of 8.5, potentially due to the localized buffering capacity of the carboxylic acid side chain.[113] We hypothesized that incorporating AAc will shift the catechol-boronate complexation pH to a more basic pH, and thus control the pH at which the adhesive transitions between adhesive and non-adhesive states.

71

To this end, we synthesized adhesives containing dopamine methacrylamide (DMA), 3-acrylamido phenylboronic acid (APBA) and AAc consisting of an adhesive catechol moiety, protective boronic acid functional group, and an anionic –COOH side chain, respectively. Johnson–Kendall–Roberts (JKR) contact mechanics tests were carried out to determine the effect of AAc concentration on adhesion over a wide range of pH (3.0-9.0). Additionally, Fourier-transform infrared (FTIR) spectroscopy and rheometry experiments were used to characterize the effect of AAc on the formation of the catechol-boronate complex.

3.3 Materials and methods

3.3.1 Materials

APBA, AAc, N-hydroxyethyl acrylamide (HEAA), trichloro($1H$,$1H$,$2H$,$2H$-perfluorooctyl)silane (97%), and toluene (anhydrous, 99.8%) were purchased from Sigma-Aldrich (St. Louis, MO). Methylene bis-acrylamide (MBAA) and 2,2-dimethoxy-2-phenylacetophenone (DMPA) were purchased from Acros Organics (New Jersey, USA). Dimethyl sulfoxide (DMSO) was purchased from Macron (Center Valley, PA), and ethanol (200 proof) was purchased from Pharmco Aaper (Brookfield, CT). DMA was synthesized by following previously published protocols.[32] Quartz slides were purchased from Ted Pella (Redding, CA). The acidic pH 3.0 solution was prepared by adding appropriate quantities of 1 M HCl to a solution containing 0.1 M NaCl, while pH 7.5, 8.5, and 9.0 buffers were prepared by adjusting the pH of 10 mM Tris

72

(hydroxymethyl)aminomethane (Tris) buffer containing 0.1 M NaCl with 1 M HCl.[113] Fluorinated glass slides were prepared by submerging glass slides (Fisher Scientific; cat. no. 12-550-A3; Hampton, NH) in a solution containing 0.5 mL of trichloro(1*H*,1*H*,2*H*,2*H*-perfluorooctyl)silane and 49 mL of toluene for 20 min, washed three times with fresh toluene, and air-dried.[80]

3.3.2   Preparation of the Adhesive

Adhesive hydrogels were prepared by curing precursor solutions containing 1 M HEAA with 10 mol % of DMA, 10 mol % of APBA and 0–30 mol % of AAc dissolved in 40 % (v/v) DMSO and deionized (DI) water. The cross-linker (MBAA) and photoinitiator (DMPA) were kept constant at 3 and 0.1 mol %, respectively. All of the monomer, cross-linker, and photoinitiator concentrations in the precursor solutions were reported in relation to the concentration of the HEAA (**Scheme 9**). Precursor solutions were degassed three times with N$_2$ gas and added to a mold composed of two pieces of glass separated by a silicone rubber spacer (2.0 mm thick). All samples were photocured in an ultraviolet (UV) cross-linking chamber (XL-1000, Spectronics Corporation; Westbury, NY) placed inside a N$_2$-filled glovebox (Plas Laboratories; Lansing, MI) for a total of 600 s.[15, 81, 113] After the curing process, all samples were washed in a pH 3.0 solution overnight to remove any unreacted monomers. Samples for swelling and rheometry experiments were formed into a disk shape using a punch with a diameter of 7.9 mm. They were further rinsed twice in deionized (DI) water and equilibrated at the desired pH for 24 h with constant nutation. For contact mechanics tests, hemispherical samples were

73

prepared by irradiating 50 µL of the precursor solution on a hydrophobic, fluorinated

glass slide with UV and purified in the similar manner as described above.[113] Adhesive

compositions were abbreviated as DxByAz where x, y and z denote the mol % of DMA,

APBA and AAc respectively, in relation to HEAA.

Scheme 9. Chemical structures of N-hydroxyethyl acrylamide (HEAA), dopamine

methacrylamide (DMA), 3-acrylamido phenylboronic acid (APBA), acrylic acid (AAc),

methylene bis-acrylamide (MBAA) and 2,2-dimethoxy-2-phenylacetophenone (DMPA).
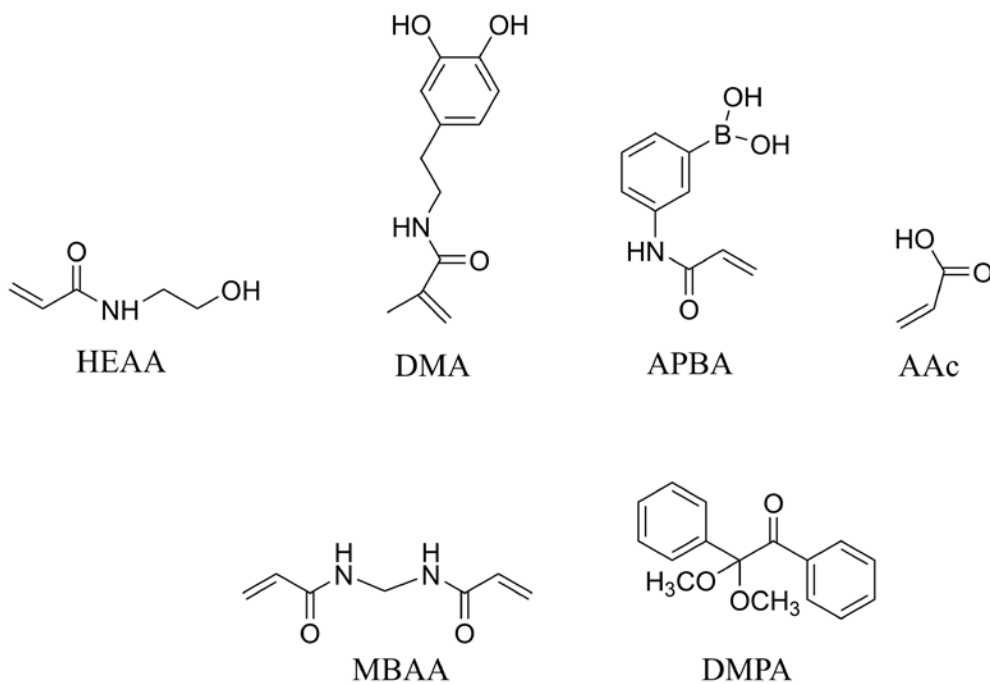
3.3.3   Equilibrium Swelling

Hydrogel discs (thickness = 2.0 mm and diameter = 7.9 mm) were equilibrated at

different pH levels for 24 h, and then dried in vacuum for at least 48 h. The masses of the

74

swollen (M_s) and dried (M_d) samples were obtained to determine the equilibrium swelling ratio by using the equation:[113]

$$\text{Equilibrium Swelling} \quad = \quad \frac{M_s}{M_d} \quad (12)$$

3.3.4 FTIR

The samples were freeze-dried, crushed into powder using a mortar and pestle, and analyzed using a PerkinElmer Frontier Spectrometer fitted with a GladiATR^{TM} accessory from Pike Technologies.

3.3.5 Oscillatory Rheometry

Hydrogel discs (thickness = 2.0 mm and diameter = 7.9 mm), were compressed to a fixed gap of 1800 μm using an 8 mm diameter parallel plate geometry. The storage (G′) and loss (G′′) moduli were determined in the frequency range of 0.1-100 Hz and at a constant strain of 8 % using a TA Discovery Hybrid Rheometer-2 (TA Instruments; New Castle, DE).

3.3.6 Contact Mechanics Test

JKR contact mechanics tests were performed using a custom-built setup comprising of a 10-g load cell (Transducer Techniques; Temecula, CA) and a miniature linear stage stepper motor (MFA-PPD, Newport; Irvine, CA). Hemispherical adhesives were affixed to an indenter stem (ALS-06, Transducer Techniques; Temecula, CA) using Super Glue

75

(Adhesive Systems MG 100) and compressed at a rate of 1 µm/sec against a buffer-wetted quartz surface until a fixed maximum preload of 20 mN was reached (**Figure 22**).[80, 113] The hemispheres were then retracted at the same speed. One contact cycle comprised of bringing the hemispheres into contact with the substrate at a constant speed until the fixed preload was reached and then retracting it at the same speed.
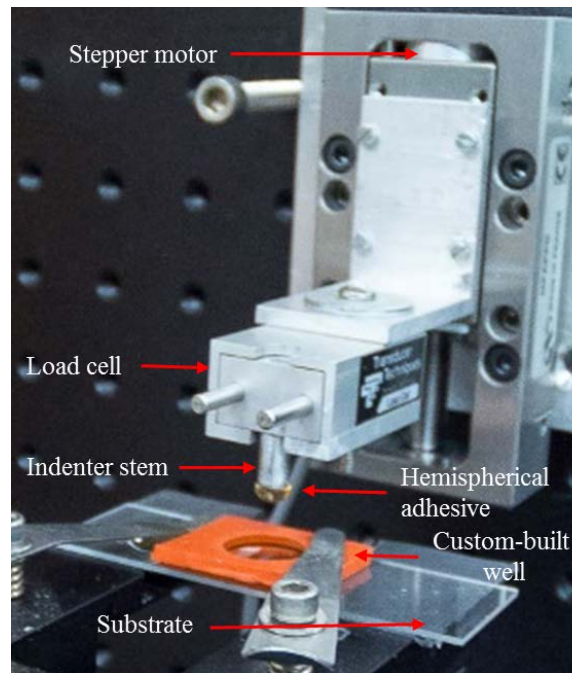
Figure 22. Photograph of the contact mechanics setup used for the adhesion experiments.

Two types of adhesion tests were performed. For the first test, samples were equilibrated at pH 3.0, 7.5, 8.5 or 9.0 for 24 h and tested against a quartz slide wetted with 25 µL of buffer with the same pH to determine the effect of AAc concentration on interfacial binding properties at these different pH levels. For the second test, adhesives were examined for their ability to switch between adhesive and non-adhesive states in response to pH. A single sample was subjected to 3 successive contact cycles. Samples were first

76

incubated at pH 7.5 for 3 h. The first and the second contacts were carried out in the presence of pH 7.5 and 9.0, respectively, while the third contact was carried out in the presence of either pH 7.5, or pH 3.0. Between two cycles, the samples were incubated for 30 min in a custom-built well that contained ≈ 350 µL of either pH 9.0 (between first and second cycle), or pH 7.5 or 3.0 (between second and third cycles) buffer solution. In order to ensure that the target pH was reached before testing (i.e., pH 9.0 for incubation prior to the second cycle), the custom-built well was rinsed twice with ≈ 350 µL of buffer with the desired pH before the start of the subsequent cycle. Additionally, the medium used to incubate the hemispherical adhesive was changed every 10 min during the 30 min incubation period.

The force (F) versus displacement (δ) curves were integrated to determine the work of adhesion (W_{adh}), which was normalized by the maximum area of contact (A_{max}) by using the following equation:[80]

$$W_{adh} = \frac{\int F \, d\delta}{A_{max}} \qquad (13)$$

A_{max} was calculated by fitting the loading portion of the F versus δ curve with the Hertzian model:[84]

$$\delta_{max} = \frac{a^2}{R}, \qquad (14)$$

77

where δ_{max} is the maximum displacement at the maximum preload of 20 mN, a is the radius of A_{max}, and R is the curvature of the hemispherical sample. The height (h) and base radius (r) of each hemisphere were measured using digital Vernier calipers before the start of each test to determine R:[85]

$$R = \frac{h}{2} + \frac{r^2}{2h} \qquad (15)$$

A_{max} was calculated by using the equation:

$$A_{max} = \pi a^2 \qquad (16)$$

The adhesion strength (S_{adh}) was calculated by normalizing the maximum pull-off force (F_{max}) by the maximum area of contact (A_{max}) using the equation:[86]

$$S_{adh} = \frac{F_{max}}{A_{max}} \qquad (17)$$

3.3.7 Statistical Analysis

Statistical analysis was performed using JMP Pro 13 application (SAS Institute, NC). One-way analysis of variance (ANOVA) with Tukey-Kramer HSD analysis was performed for comparing means. $p < 0.05$ was considered significant.

78

3.4 Results and discussion

Up to 30 mol % of AAc was formulated into an adhesive hydrogel containing DMA and APBA and its effect on the formation of catechol-boronate complex and interfacial binding property were evaluated over a wide range of pH (3.0-9.0). pH 3.0 was chosen because the adhesive properties of catechol with inorganic substrates at this pH have been widely documented.[23, 113] Additionally, we have previously confirmed that adhesives containing both DMA and APBA do not form complex at this pH.[80] pH 7.5 and 8.5 were chosen to represent physiological and marine pH ranges.[89, 91] pH 9.0 was selected to promote the formation of the catechol-boronate complex and to inactivate the adhesive.[80]

3.4.1 Equilibrium Swelling

Equilibrium swelling tests were performed to confirm the addition of AAc in the adhesives. The equilibrium swelling ratio of AAc-containing adhesives increased with increasing pH (**Figure 23**). Additionally, formulations containing higher AAc concentrations also demonstrated higher increase in swelling with increasing pH. For example, the equilibrium swelling ratio of D10B10A30 exhibited the highest difference between values measured at pH 9.0 and 3.0 (over 2 fold increase). The carboxylic acid side chain of AAc becomes progressively deprotonated with increasing pH ($pK_a \approx$ 4.25).[93] The negatively charged AAc resulted in charge repulsion of the polymer chains and increased the swelling ratio of the adhesive network.[102]

79
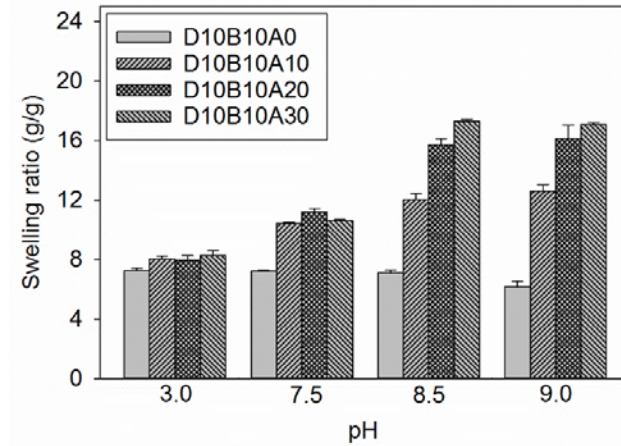
Figure 23. Equilibrium swelling ratio for adhesive equilibrated at pH 3.0, 7.5, 8.5 or 9.0
for 24 h (n = 3). Refer to Table 17 for statistical analysis.

Table 17. Statistical analysis for equilibrium swelling ratio of adhesive equilibrated at pH
3.0, 7.5, 8.5 or 9.0 for 24 h. Compositions not connected by the same letter at a given pH
are significantly different.

	pH 3.0	pH 7.5	pH 8.5	pH 9.0
D10B10A0	A	A	A	A
D10B10A10	A B	B	B	B
D10B10A20	A B	C	C	C
D10B10A30	B	B	D	C

80

3.4.2 FTIR

All adhesive formulations exhibited signature peaks for HEAA ($-OH$ 3400-3000 cm^{-1}, secondary amide $-NH$ 1680-1630 cm^{-1}, and $C=O$ 1600-1500 cm^{-1}), and benzene rings (1500-1400 and 800-700 cm^{-1}) in their FTIR spectra (**Figures 24 and 25**).[81, 114] Formulations containing AAc also exhibit characteristics peak of carboxylic acid ($-C=O$ $\approx$ 1700 cm^{-1}),[114] which increased in peak intensity with increasing AAc content in the adhesive (**Figure 24a**). With increasing pH, formulations containing both DMA and APBA exhibited a new peak at 1490 cm^{-1} (arrows in **Figure 24**). This peak corresponds to the benzene ring stretch as a result of catechol-boronate complexation.[48, 80] For formulations with no AAc or low AAc content (e.g., D10B10A0 and D10B10A10, respectively), this new peak appeared at a pH as low as 7.5 (**Figure 24b**). For formulations with higher AAc concentrations (e.g., D10B10A20 and D10B10A30), the complexation peak was not observed until a pH of 8.5 (**Figure 24c**). FTIR results confirmed that the presence of the acidic AAc monomer interfered with the formation of catechol-boronate complexation, potentially due to the ability of the network-bound anion to maintain a more acidic pH environment within the adhesive network. Adhesive formulations with elevated AAc contents required a higher pH in the incubation medium to form the complex. FTIR spectra for formulations that did not contain both DMA and APBA (e.g., D0B10A20, D10B0A20) did not exhibit a peak at 1490 cm^{-1} (**Figure 25**), further confirming that this peak is attributed to the catechol-boronate complex.

81
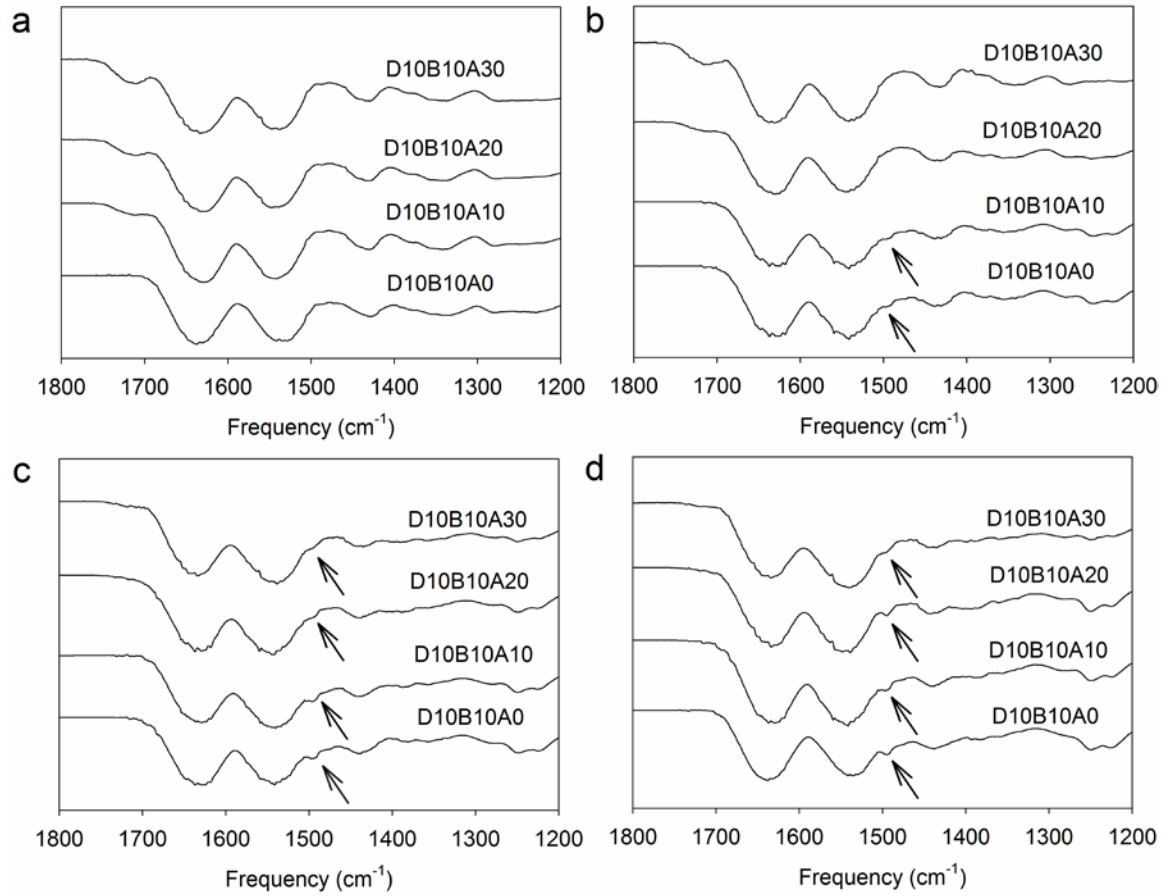
Figure 24. FTIR spectra of adhesive equilibrated at pH 3.0 (a), pH 7.5 (b), pH 8.5 (c) or pH 9.0 (d). The arrows indicate peaks corresponding to formation of the catechol-boronate complex at 1490 cm^{-1}.
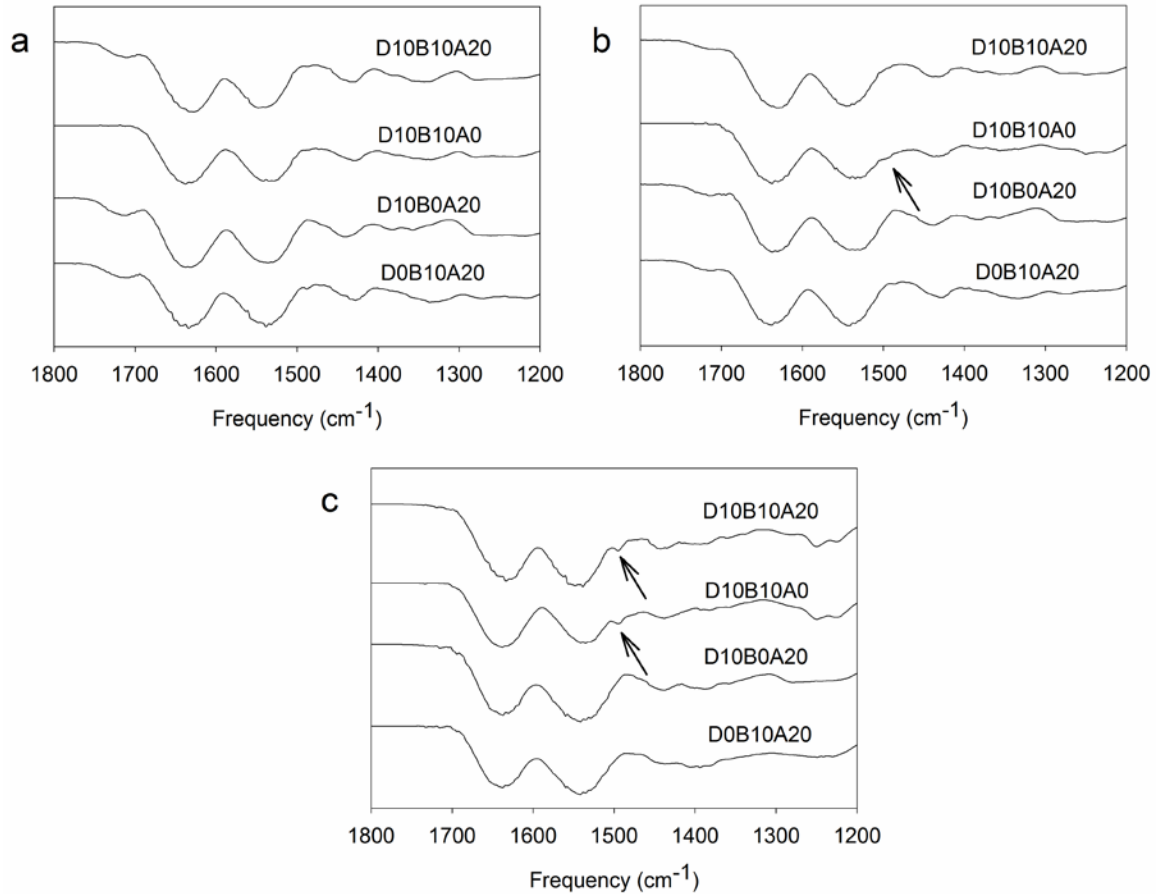
Figure 25. FTIR spectra of adhesives equilibrated at pH 3.0 (a), pH 7.5 (b) or pH 9.0 (c). The arrows indicate peaks corresponding to formation of the catechol-boronate complex at 1490 cm^{-1}.

3.4.3   Oscillatory Rheometry

Frequency sweep experiments were performed to determine the storage and loss moduli (G' and G", respectively) of the adhesive (**Figure 26**) and the values obtained at a frequency of 1 Hz were further summarized in **Figure 27**. For all the adhesive formulations, G' values were comparable (averaged around 10^4 Pa) and did not change

greatly with changing pH. Contrastingly, G" values increased by 1 to 2 orders of magnitude with increasing pH. An elevated G" value corresponded to the dissipation of reversible physical bonds between catechol and boronic acid within the polymer network.[50, 115] We have previously observed a similar pH-induced change in the measured G" values as a result of catechol-boronate complexation.[80] For D10B10A0, the onset of change in the G" values occurred between pH 3.0 and 7.5 (**Figure 27a**). With increasing AAc content, a higher solution pH was required to induce a similar increase in the G" values. For D10B10A30, G" values remained constant around 10^2 Pa and did not increase to 10^3 Pa until pH 9.0. Rheometry data corroborated FTIR data in showing that the presence of AAc interfered with the catechol-boronate complexation. Specifically, the pH responsive nature of the complex correlated with the concentration of the anionic monomer. Formulations that did not contain both DMA and APBA (e.g., D0B10A20 and D10B0A20) did not exhibit a large increase in the measured G" values with increasing pH (**Figure 28**).

84
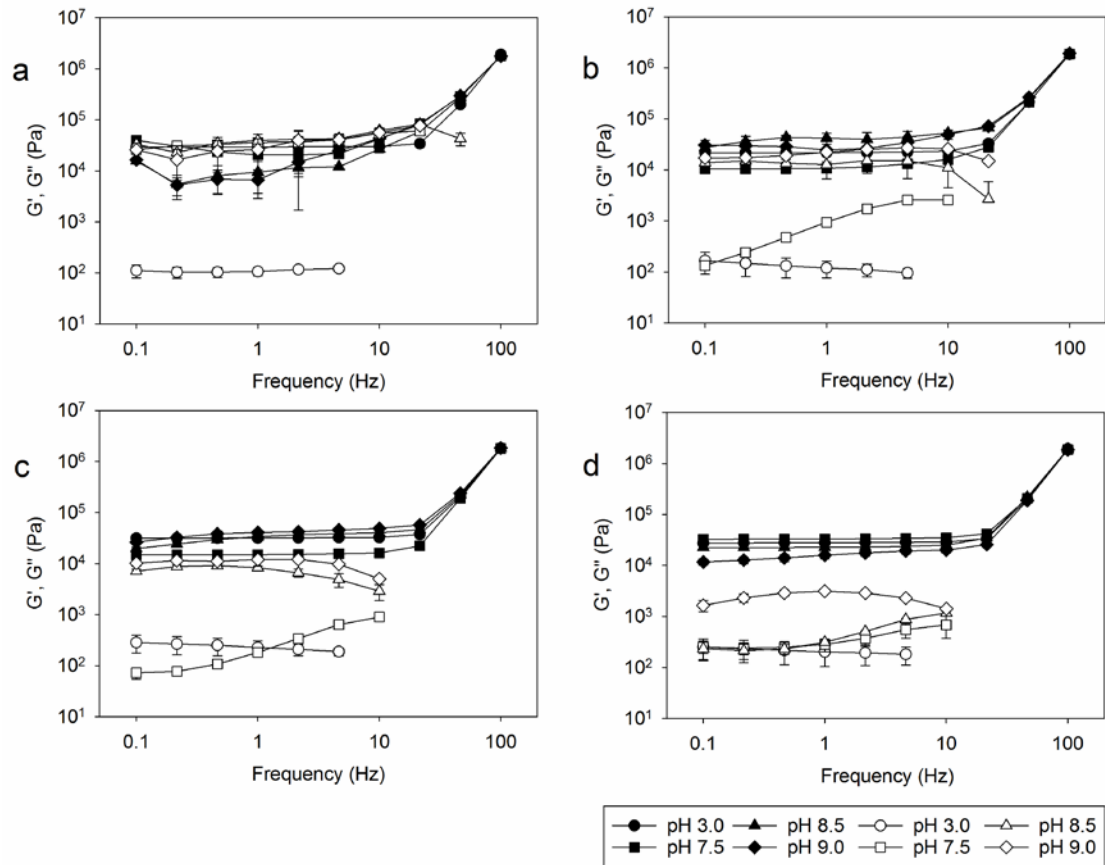
Figure 26. Storage (G′, filled symbols) and loss (G″, empty symbols) moduli for D10B10A0 (a), D10B10A10 (b), D10B10A20 (c) and D10B10A30 (d) equilibrated at pHs 3.0, 7.5, 8.5 or 9.0 and tested in the frequency range of 0.1-100 Hz and 8 % strain (n = 3).
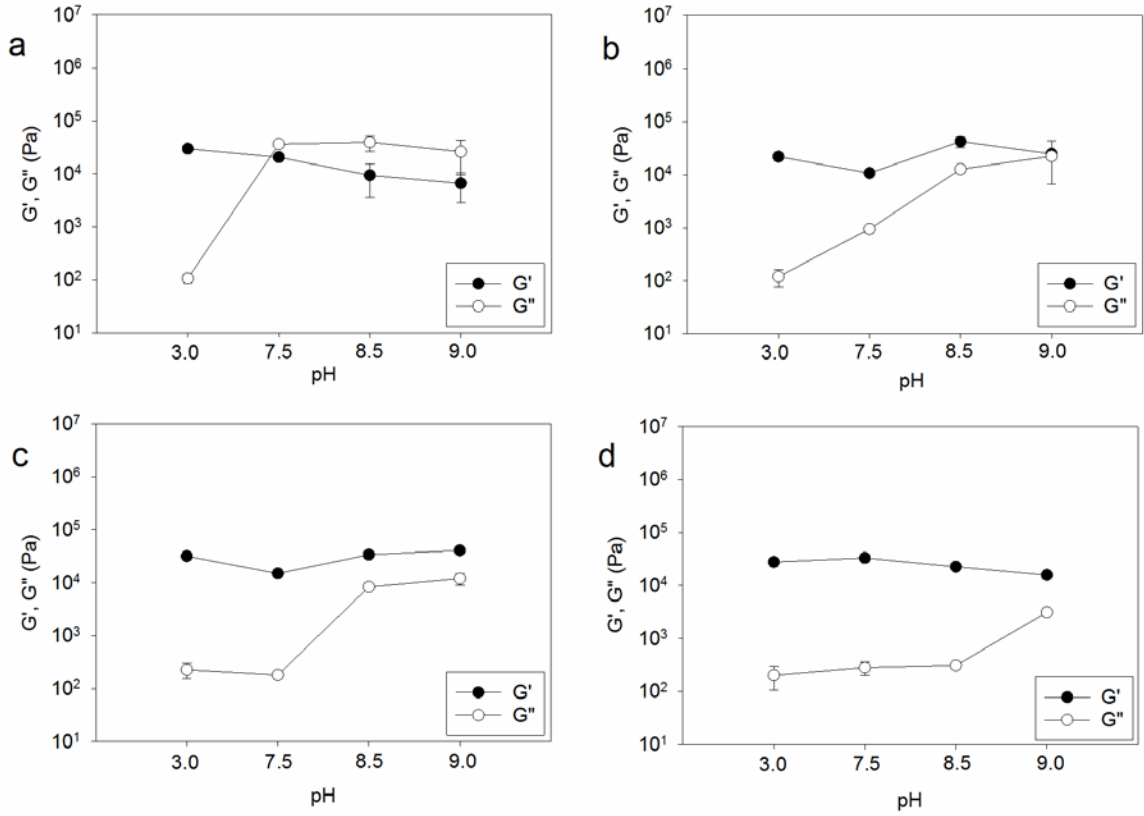
Figure 27. Storage (G', filled symbols) and loss (G", empty symbols) moduli for

D10B10A0 (a), D10B10A10 (b), D10B10A20 (c) and D10B10A30 (d) equilibrated at

pHs 3.0, 7.5, 8.5 or 9.0 tested at a frequency of 1 Hz and 8 % strain (n = 3).
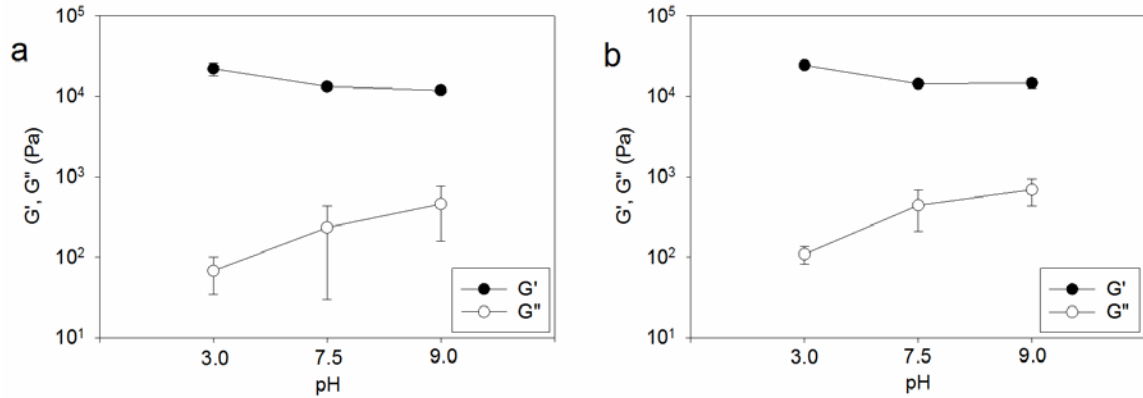
Figure 28. Storage (G', filled symbols) and loss (G", empty symbols) moduli for D0B10A20 (a), and D10B0A20 (b) equilibrated at pHs 3.0, 7.5 or 9.0 tested at a frequency of 1 Hz and 8 % strain (n = 3).

3.4.4 Contact Mechanics Test: Single Contact

JKR contact mechanics test was performed to determine the effect of AAc concentration on interfacial binding property over a wide range of pH (3.0-9.0) using quartz (SiO_2) surface as the test substrate (**Figure 29**). Adhesive formulation without AAc (e.g., D10B10A0) exhibited the strongest adhesive interaction with quartz at pH 3.0 (W_{adh} = 1830 ± 170 mJ/m², S_{adh} = 10.8 ± 0.209 kPa), when both the reduced form of catechol and the boronic acid contributed to strong interfacial interaction (i.e., hydrogen bonding) with the quartz surface.[71, 80] Correspondingly, all formulations exhibited low G" values ($\approx 10^2$ Pa, **Figure 27**). When D10B10A0 was incubated at a pH of 7.5 or higher, there was a significant decrease in the measured adhesive values (W_{adh} = 487 ± 21.9 mJ/m², S_{adh} = 4.66 ± 0.704 kPa for pH 7.5). The measured adhesive values for D10B10A0 further decreased with increasing pH (W_{adh} = 264 ± 10.1 mJ/m², S_{adh} = 0.515 ± 0.613 kPa for pH

87

9.0). Both FTIR and rheometry results (**Figures 24** and **27**, respectively) indicated that catechol-boronate complexation formed at a pH as low as 7.5 for D10B10A0, suggesting that the formation of the complex limited the availability of the adhesive molecules for interfacial binding. A large reduction in the measured adhesive values at a neutral to mildly basic pH made D10B10A0 impractical for many applications at this pH range. Additionally, at low AAc concentration, the adhesive values for D10B10A10 at pH 3.0 were lower than the other tested formulations. This is perhaps due to the H-bond interactions between AAc chains in the bulk,[116] which interfered with the ability of catechol to form interfacial bonds.

Incorporating 20 mol % or higher AAc resulted in a significant increase in the measured adhesive values at both pH 7.5 and 8.5 (**Figure 29** and **Table 19**). For example, measured W_{adh} values for D10B10A20 and D10B10A30 equilibrated at pH 7.5 were 3 fold higher when compared to those measured for D10B10A0. This indicated that network-bound AAc was able to counteract the solution pH and maintain a local acidic pH within the adhesive network.[113] At pH 7.5, no catechol-boronate complex peaks were observed for both D10B10A20 and D10B10A30 (**Figure 24b**), and these formulations also exhibited low G" values ($\approx 10^2$ Pa; **Figures 27c and 27d**). These observations further suggest that both DMA and APBA were available for strong interfacial binding at pH 7.5. With further increase in pH, measured adhesive values decreased. At pH 8.5, both D10B10A20 and D10B10A30 showed complexation peak in their FTIR spectra (**Figure 24c**), which correspondingly resulted in reduced adhesion, and D10B10A20 also exhibited high G" values ($\approx 10^4$ Pa), while G" values of D10B10A30 continued to remain low ($\approx 10^2$ Pa).

88

However, values measured at pH 8.5 were still around 3 fold higher when compared to those measured for D10B10A0. Regardless of adhesive formulation, lowest adhesive values were measured at pH 9.0, and all formulations exhibited high G" values ($10^3 - 10^4$ Pa, **Figure 27**). Although the incorporation of AAc preserved the interfacial binding property of the adhesive at a neutral to mild basic pH, the anion lost its buffering capability at an elevated pH, which was corroborated with elevated G" values. Nevertheless, the W_{adh} values for D10B10A20 at pH 7.5 and pH 8.5 were 18 and 7 fold higher, respectively, when compared to values measured at pH 9.0. This difference in the measured adhesive values makes the adhesive a good candidate to function as a smart adhesive.
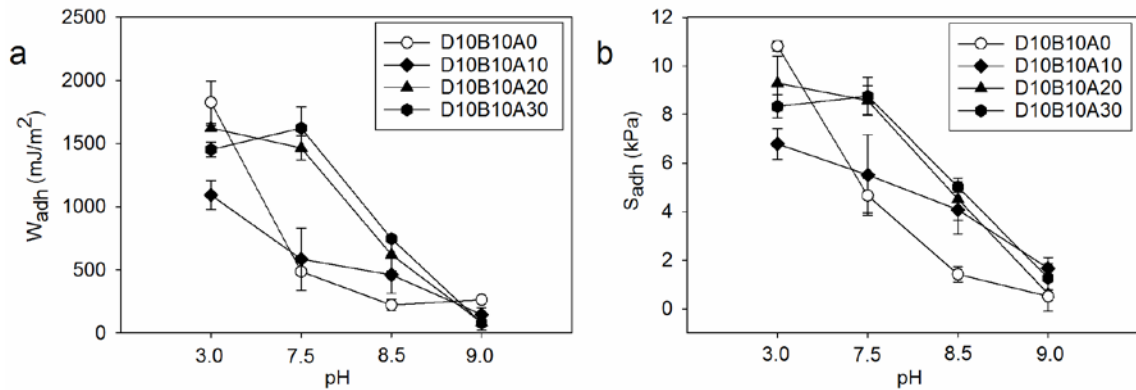
Figure 29. Work of adhesion (W_{adh}) (a) and adhesion strength (S_{adh}) (b) for single contact experiments tested between wetted quartz substrate and adhesive equilibrated at pH 3.0, 7.5, 8.5 or 9.0 (n = 3). Refer to Table 18 for statistical analysis.

89

Table 18. Statistical analysis for work of adhesion (W_{adh}) and adhesion strength (S_{adh}) of adhesives tested against a wetted quartz substrate. Compositions not connected by the same letter at a given pH are significantly different.

Composition	W_{adh}				S_{adh}			
	pH 3.0	pH 7.5	pH 8.5	pH 9.0	pH 3.0	pH 7.5	pH 8.5	pH 9.0
D10B10A0	A	A	A	A	A	A	A	A
D10B10A10	C	A	A B	A B	C	A B	B	A
D10B10A20	A B	B	B	B	A B	B	B	A
D10B10A30	B	B	B	B	B C	B	B	A

3.4.5   Contact Mechanics Test: Reversible Adhesion Testing

To evaluate the feasibility for AAc to control the pH responsive characteristics of the catechol-boronate complex, adhesive samples were subjected to three successive contact cycles at pH 7.5, 9.0 and then at 7.5 again (**Figure 30**). D10B10A20 showed strong adhesion during the first contact at pH 7.5 ($W_{adh} = 677 \pm 173$ mJ/m^2, $S_{adh} = 4.76 \pm 0.557$ kPa) and significantly reduced adhesion during the second contact at pH 9.0 ($W_{adh} = 230.$ ± 33.2 mJ/m^2, $S_{adh} = 2.59 \pm 0.185$ kPa) as expected. However, the adhesion values

90

remained low for the final contact at pH 7.5 ($W_{adh} = 311 \pm 174$ mJ/m^2, $S_{adh} = 2.80 \pm 1.13$ kPa). The adhesive samples were incubated for only 30 min at pH 7.5 in between the last two contact cycles and may not have had sufficient ionic exchange to break the strong, reversible complex. D10B10A0 was not responsive to changes in pH as the catechol-boronate complexation readily formed at a pH 7.5 and higher and it does not contain anionic monomer to modulate complexation pH.
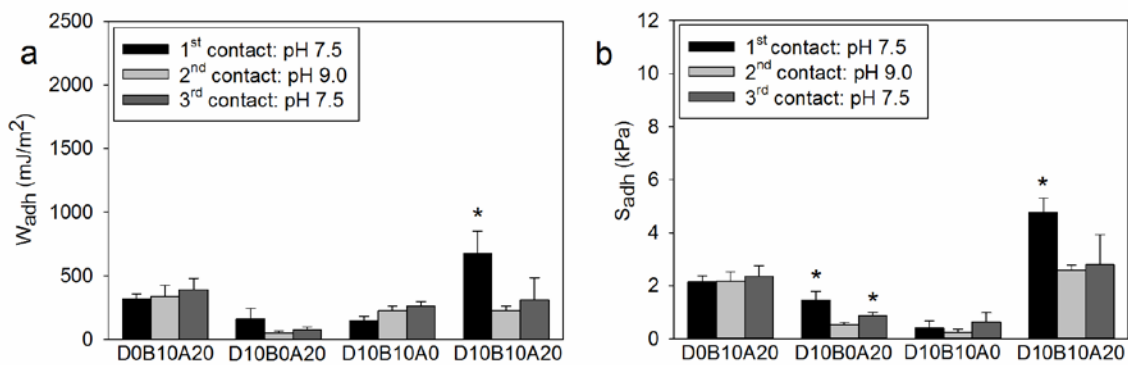
Figure 30. Averaged W_{adh} (a) and S_{adh} (b) for adhesives tested in three successive contact cycles using quartz as the substrate (n = 3). * $p < 0.05$ relative to the values obtained from the second contact cycle at pH 9.0 for a given formulation.

To confirm the reversible nature of the catechol-boronate complex, the pH for the third contact cycle was lowered to 3.0 (**Figures 31** and **32**). D10B10A20 exhibited elevated and reduced adhesion at pH 7.5 ($W_{adh} = 663 \pm 65.1$ mJ/m^2, $S_{adh} = 5.63 \pm 0.488$ kPa) and 9.0 ($W_{adh} = 85.9 \pm 47.6$ mJ/m^2, $S_{adh} = 1.34 \pm 1.03$ kPa), respectively, as observed in the previous series of reversible adhesion testing (**Figure 30**). However, when the pH was decreased to 3.0 during the third contact cycle, the adhesive recovered its adhesive properties ($W_{adh} = 1540 \pm 171$ mJ/m^2, $S_{adh} = 6.99 \pm 0.983$ kPa). The measured W_{adh} and

91

S_{adh} values were 17 and 5 fold higher, respectively, when compared to values measured for the second contact at pH 9.0. Similarly, D10B10A0 exhibited low adhesive properties during the first two contact cycles conducted at pH 7.5 and 9.0, but recovered elevated adhesive properties during the third contact cycle conducted at pH 3.0 ($W_{adh} = 1800 \pm 439$ mJ/m^2, $S_{adh} = 9.20 \pm 1.19$ kPa). These observations indicate that the catechol-boronate complex within the adhesive remained reversibly bonded, and an acidic pH was required to break the complex and recover the strong interfacial binding.

During both series of reversible adhesion testing (**Figures 30** and **31**), the presence of boronic acid in D0B10A20 contributed to adhesion potentially via hydrogen bonding or electrostatic interaction.[80] However, D0B10A20 did not demonstrate pH responsive adhesive property, indicating that the presence of boronic acid alone was not sufficient to design a smart adhesive. D10B0A20 demonstrated reversible adhesion resulting from pH dependent oxidation and reduction of the catechol moiety. Although catechol readily oxidizes at a pH of 7.5, the presence of the network-bound anion preserved the reduced state of catechol for strong adhesion.[113] AAc lost its buffering capacity when the pH was increased to pH 9.0. However, pH 7.5 was insufficient to reduce catechol for strong adhesion and pH 3.0 was required to recover its adhesive property. This observation further confirmed that poor ion diffusion is the main factor that limited pH responsive property of the hydrogel based adhesive. Although D10B0A20 was pH responsive, the measured adhesion values were relatively low when compared to D10B10A20. This confirms our previous findings that both catechol and boronic acid contributed to strong adhesion.[80]

92
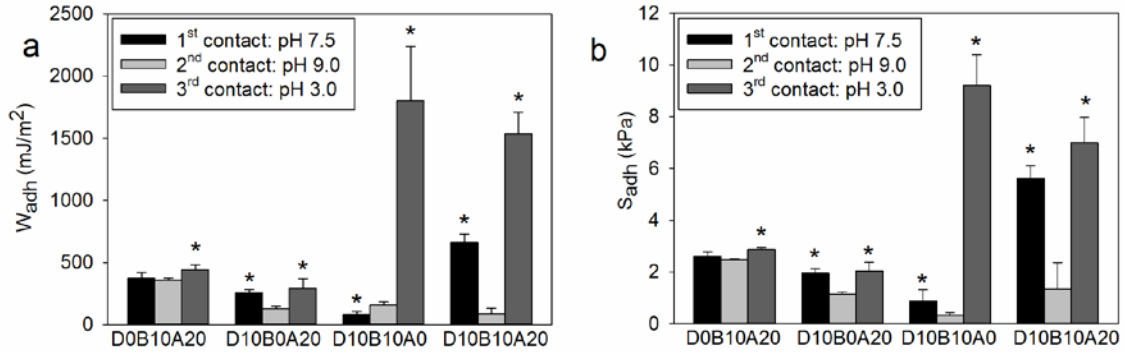
Figure 31. Averaged W_{adh} (a) and S_{adh} (b) for adhesives tested in three successive contact cycles using quartz as the substrate (n = 3). * $p < 0.05$ relative to the values obtained from the second contact cycle at pH 9.0 for a given formulation.
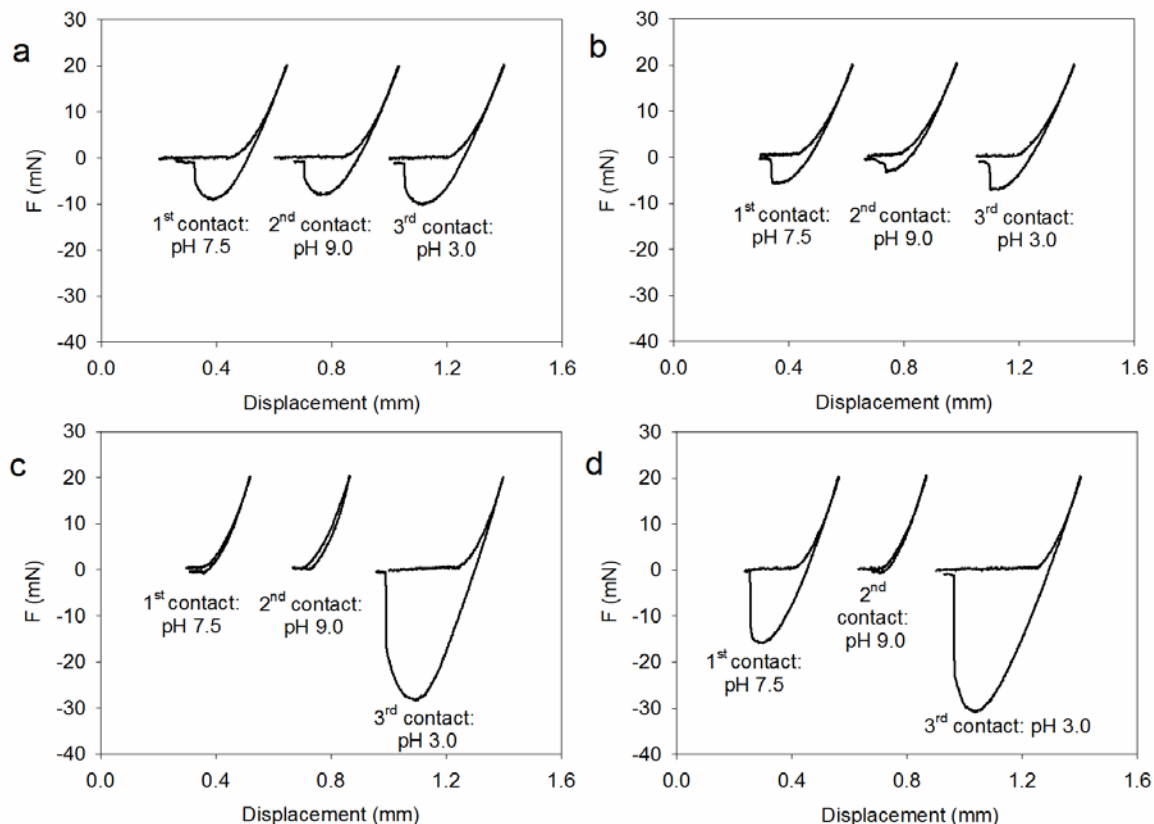
Figure 32. Three successive contact curves for D0B10A20 (a), D10B0A20 (b), D10B10A0 (c) and D10B10A20 (d) tested at pH 7.5, pH 9.0, and then pH 3.0 using a quartz substrate.

The ideal pH for complexation between catechol ($pK_a = 9.3$)[40] and phenylboronic acid ($pK_a = 8.8$)[40, 41] has been reported to be the average of their respective pKa values (($9.3+8.8$)/2 ≈ 9).[39] As such, the complex forms as the pH approached 9 and resulted in poor adhesion at a neutral and mildly basic pH. The addition of AAc acidified the local pH within the adhesive network and shifted the pH for catechol-boronate complexation to a more basic pH. This disruption of the complex permitted both catechol and phenylboronic acid to participate in strong interfacial binding at pH 7.5 to 8.5 (**Scheme**

94

10). Incorporation of elevated amount of AAc did not prevent complexation at pH 9.0, which is necessary for the inactivation of the adhesive. Although the JKR technique used to calculate W_{adh} takes into account only the maximum area of contact and minimizes the sample volume to reduce losses due to the bulk dissipation within the adhesive hydrogel, the hysteresis in the JKR curves which indicates a likely contribution of bulk dissipative behavior due to pH responsive changes in the adhesive network, would require further probing.[117-119] The incorporation of AAc provides an effective strategy for designing adhesives for applications that demand strong adhesion at physiological or marine pH levels, while preserving the adhesive's ability to transition between its adhesive and non-adhesive states in response to pH.

Scheme 10. Schematic representation of a smart adhesive consisting of acrylic acid in addition to catechol and phenylboronic acid interacting with a wetted quartz substrate.
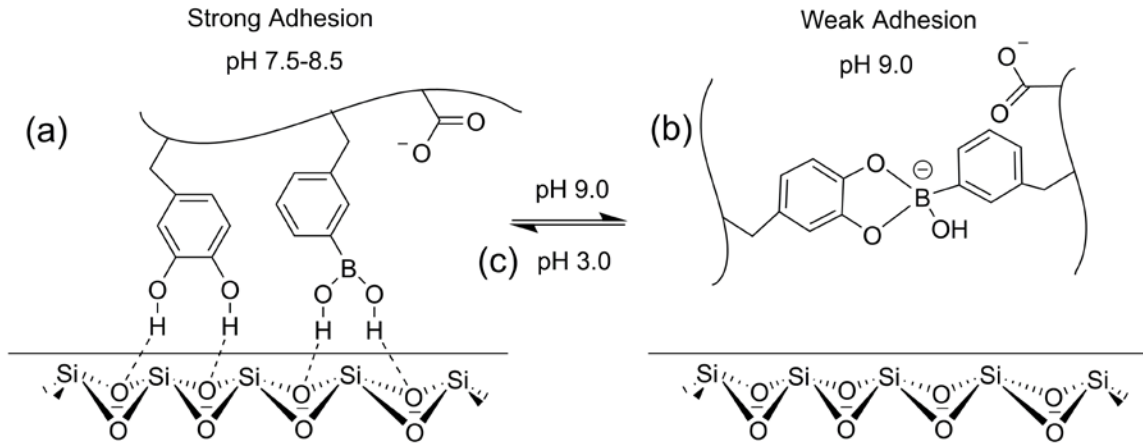
4

3.5 Conclusions

DMA and APBA–containing adhesive hydrogels were formulated with up to 30 mol % of AAc to tune the pH responsive characteristics of catechol-boronate complexation. FTIR and rheometry confirmed that formulations with elevated AAc contents required a higher pH to form the catechol-boronate complex, which corresponded to elevated adhesive

---

[4] The presence of the anionic AAc reduced local pH, which prevented catechol-boronate complexation while enabled these adhesive molecules to form strong interfacial bonds with the quartz substrate even at a neutral mildly basic pH (a). When the pH was raised to a more basic value (i.e. pH 9.0), AAc lost its buffering capacity, which resulted in the formation of the catechol-boronate complex while inactivating the adhesive (b). Decreasing the solution pH to pH 3.0, effectively breaks the catechol-boronate complex and recovers strong interfacial binding behavior of the adhesive molecules (c).

property measured at a neutral to mildly basic pH (pH 7.5-8.5). This is potentially due to the ability for the anionic AAc side chain to acidify the local pH within the adhesive network. At pH 9.0, measured adhesive values reduced dramatically due to the formation of the catechol-boronate complex. The catechol-boronate complex remained reversible and the interfacial binding property of the adhesive was successfully tuned with changing pH in successive contact cycles. However, an acidic pH (pH 3.0) was required to break the catechol-boronate complex to recover the elevated adhesive property.

3.6 Acknowledgements

4 Evaluating the Enhanced Adhesion, Rapid Switching and Reversibility of Adhesive Hydrogel-Coated Polydimethylsiloxane Micropillars

4.1 Abstract

Adhesive hydrogels with 10 mol % each of dopamine methacrylamide (DMA) and 3-acrylamido phenylboronic acid (APBA) were coated on chemically modified micropillared polydimethylsiloxane (PDMS) templates of different aspect ratios (ARs) to obtain hybrid adhesive structures. Field Emission-Scanning Electron Microscopy (FE-SEM), X-ray Photoelectron Spectroscopy (XPS), Contact Angle (CA) measurements and Fourier- Transform Infrared Spectroscopy (FTIR) confirmed the presence of the coating on the PDMS templates. Environmental Scanning Electron Microscopy (ESEM) images showed that the adhesive coating was deswollen at an acidic pH and swollen at a basic pH. Johnson-Kendall-Roberts (JKR) contact mechanics tests indicated strong adhesion for hybrid adhesives with template ARs 0.4 and 1 incubated at pH 3, which decreased significantly at pH 9 (5-fold decrease in the work of adhesion for hybrid structures with template AR 1). The increase in adhesion at low pH was attributed to contact splitting effects obtained by micropatterning combined with the wet interfacial binding offered by catechol and boronic acid. On the other hand, formation of the reversible catechol-

boronate complex and the associated swelling decreased the interfacial binding and surface area, respectively, which together contributed to the dramatic decrease in adhesion. Although the flat adhesives showed strong adhesion, it was not pH responsive. Hybrid structures with template AR 1 exhibited strong adhesion at pH 3, which decreased dramatically when the pH was raised to 9. Reversible transitions between strong and weak adhesion were observed during the successive contact cycles. Moreover, they also displayed rapidly switching adhesion (average strength of adhesion at pH 3 was around 4-fold higher than pH 9) over multiple cycles. The increased rate of transitions was due to the large surface area which promoted quick diffusion of the ions in the pH medium. Thus, integration of adhesive hydrogel coating and micropatterning was essential for designing hybrid adhesives with enhanced adhesion and rapid switching between strong and weak adhesion.

4.2 Introduction

Smart adhesives can reversibly transition between strong and weak adhesion states in response to externally applied stimuli. This control of adhesion is of particular interest in various applications including painless removal of wound dressings, effortless disassembly of bonded structural components, sustainable recycling of materials without damaging substrates, controlled locomotion of robots underwater, etc.[1, 3, 107, 120] Current smart adhesives have limited applications due to adhesion mainly in a dry environment,[2] lack of switchable adhesion (ability to turn the adhesion on and off),[32] or slow switching between strong and weak adhesion.[121] Thus, it is desirable to develop a smart adhesive

99

that can demonstrate strong wet adhesion, and reversibly and rapidly transform between adhesive and non-adhesive states.

Marine mussels secrete several foot proteins that contain a unique catecholic amino acid, 3,4-dihydoxyphenylalanine, which is responsible for adhesion to wetted surfaces (e.g. rocks, piers, etc.).[57, 60] The adhesion offered by catechol depends on its oxidation state.[21-23] Catechol in its reduced form interacted strongly with titanium (Ti), and reported pull-off forces of around 800 pN, which is 40 % that of a covalent bond.[71] When the pH was elevated to a basic value, catechol was oxidized to its quinone form, which significantly diminished its adhesive properties.[78] This suggested that the oxidation state of catechol could be exploited to tune its adhesive properties. However, quinone is highly reactive and can undergo irreversible crosslinking and polymerization, making it unfavorable to employ catechol alone for reversible adhesion. Even though some labs have reported smart adhesives that mimic mussel adhesive chemistry, they are limited in terms of their reversibility (i.e., one-time triggered adhesion activation[19] or deactivation[20]).

Recently, we synthesized a smart adhesive containing catechol and boronic acid, which demonstrated strong interfacial binding at pH 3. When the pH was elevated to 9, the formation of the catechol-boronate complex led to a decrease of over an order of magnitude in the work of adhesion. The presence of the boronic acid not only served as a temporary protecting group for catechol and facilitated reversible adhesion, but also contributed to adhesion at acidic pH.[80] However, long incubation time, deactivation, and reversible switching between adhesive states, still need to be addressed.

Several research groups have established theories regarding gecko adhesion mechanisms by studying the specific geometry of the gecko's feet which suggest that the adhesion is dominated by weak secondary forces such as van der Waals interactions.[122, 123] Gecko-inspired adhesives having different geometries and orientations of the gecko-mimicking fibers have demonstrated reversible adhesion to various surfaces. However, their adhesion was drastically reduced upon immersion in water due to diminished van der Waals' interactions.[2, 124, 125] Existing reports have demonstrated synergistic wet adhesion offered by combining gecko-inspired PDMS pillars with mussel-inspired polymeric coatings. Even though multiple cycles of attachment and detachment were reported, the adhesives lack reversible transformation between strong and weak adhesive states.[32, 126, 127] A recent study illustrated that coating a catechol-containing polymer onto PDMS posts enhanced the switching between adhesive states of the structures due to the increased area offered by micropatterning.[120]

We hypothesize that by coating our previously synthesized smart adhesives onto micropillared PMDS templates, we can demonstrate strong wet adhesion, along with reversible and rapid switching between high and low adhesion values. We fabricated hybrid structures composed of a gecko-inspired PMDS micropillar array with aspect ratios (ARs) ranging from around 0.4-1, carried out their chemical modification and coated them with an adhesive hydrogel containing dopamine methacrylamide (DMA) and 3-acrylamido phenylboronic acid (APBA). The bare PDMS templates were characterized using 3D profiling. The adhesive hydrogel coating on the bare templates was characterized using Field Emission-Scanning Electron Microscopy (FE-SEM),

101

Environmental Scanning Electron Microscopy (ESEM), contact angle (CA) measurements, Fourier- Transform Infrared Spectroscopy (FTIR) and X-ray Photoelectron Spectroscopy (XPS). The effect of AR of the pillars and applied maximum preloads on the adhesive properties of these adhesive hydrogel-coated PDMS templates was studied using Johnson-Kendall-Roberts (JKR) contact mechanics tests.

4.3 Materials and Methods

4.3.1 Materials

APBA, *N*-hydroxyethyl acrylamide (HEAA) and 3-(trimethoxysilyl)propyl methacrylate (TMSPMA), and trichloro(1H,1H,2H,2H-perfluorooctyl)silane were purchased from Sigma-Aldrich (St. Louis, MO). Methylene bis-acrylamide (MBAA) and 2,2-dimethoxy-2-phenylacetophenone (DMPA) were purchased from Acros Organics (New Jersey, USA). Dimethyl sulfoxide (DMSO) was purchased from Macron (Center Valley, PA), and ethanol (200 proof) was purchased from Pharmco Aaper (Brookfield, CT). DMA was synthesized by following previously published protocols.[32] Hydrogen peroxide (30% stock solution) (H_2O_2) was purchased from Fisher Scientific (Fair Lawn, NJ). Polydimethylsiloxane (PDMS) monomer and crosslinking agent (Sylgard 184 Silicone Elastomer kit) was purchased from Dow Corning (Midland, MI). The acidic pH 3.0 solution was prepared by adding appropriate quantities of 1 M HCl to deionized (DI) water. The pH 9.0 medium was prepared by adjusting the pH of 10 mM Tris (hydroxymethyl) aminomethane (Tris) buffer with 1 M HCl.

102

4.3.2   Si master mold and preparation of the PDMS micropillared template

Si wafers having holes with height (h), diameter (d) and pitch (p) ranging from 4-20 µm, 10 µm and 20 µm respectively, were fabricated. For the fabrication of the Si master, a Si wafer with 100 nm of silicon dioxide (SiO_2) was used as the base substrate. The wafer was solvent cleaned in acetone, isopropanol, and deionized (DI) water before baking at 200°C for 5 min on a hot plate. For the patterning process, a photoresist, Shipley 1813 (Shipley; Marlborough, MA) was spun on at 4000 rpm for 40 sec and baked at 100°C, before exposing to UV light in a EV 620 mask alignment system (EV Group; Albany, NY) to give a dose of 160 mW/cm^2. The photomask used had 10 µm diameter pores spaced in a square array with a 20 µm pitch. The developed wafer was hard baked at 120°C for 10 min, and then the SiO_2 was etched in 10:1 buffered oxide etchant (BOE) to produce openings to the Si surface. To etch the Si wafer, a pseudo Bosch etch process was used in a Trion ICP/RIE Etch PHTII-4301 (Trion Technology, Inc.; Clearwater, FL). 100 sccm of sulfur hexafluoride (SF_6) was used to etch the Si at a reactor pressure of 35 mTorr, inductively coupled plasma power of 600W, and RIE (Reactive Ion Etch) power of 60 W for 13 sec. 75 sccm of octafluorocyclobutane (C_4F_8) was used to passivate the Si sidewall at a reactor pressure of 120 mTorr, with inductively coupled plasma power of 600 W for 40 sec. These two steps were cycled 10, 24 and 48 times to achieve around 4, 10 and 20 µm deep pores, respectively. The photoresist and SiO_2 were removed in acetone and BOE, respectively, to complete the Si master fabrication. The Si wafer was cleaned with pressurized N_2 gas. It was then placed inside a desiccator chamber in which two drops (≈ 100 µL) of the silanizing agent, trichloro(1H,1H,2H,2H-perfluorooctyl)silane

103

were placed on a glass slide. The desiccator chamber was pumped down for 10 min using laboratory vacuum to accelerate the evaporation of silane and maintained in a sealed condition for 10 additional minutes. The wafer was retrieved and placed on a hot plate at 150°C for 10 min to evaporate the excess silane. PDMS prepolymer and curing agent (Sylgard 184 Elastomer kit; Dow Corning Corporation, Canada) were mixed in the weight ratio 10:1 and degassed to remove all the bubbles. The mixture was then poured over a Si wafer and cured at 60°C for 4 hours in an oven. The cured PDMS was allowed to cool overnight and then peeled off, followed by washing with ethanol and DI water. Hereon, the PDMS micropillared templates will be referred to as 'bare templates' for simplicity. For specific notations, bare templates were addressed as 'Bare ARx', where x represents the AR (AR was calculated as $h/2r_1$, where h and r_1 stand for the height and radius of the respective PDMS templates).

4.3.3   Chemical modification of the bare template

Chemical modification was carried out according to a previously published protocol.[128] Briefly, the surface of the micropillared PDMS samples was treated with oxygen plasma at 100 W power, 200 mTorr pressure for 1 min (Jupiter II, March Instruments; Westlake, OH). They were then immersed in a solution containing H_2O-H_2O_2-HCl in a volume ratio of 5:1:1 for 5 min followed by a DI water rinse. Further, they were introduced into a 1.5 v/v % TMSPMA solution of ethanol-DI water (volume ratio of 1:1) for 1 hour (**Scheme 11a-11c**). The samples were washed with DI water and dried with compressed air and N_2.

Scheme 11. Schematic representation of a bare template (a) O₂ plasma and hydrogen peroxide (H_2O_2) + HCl treatment (b), chemical modification using TMSPMA (c), DMPA priming, precursor (HEAA only shown) coating and UV irradiation of the bare template (d).
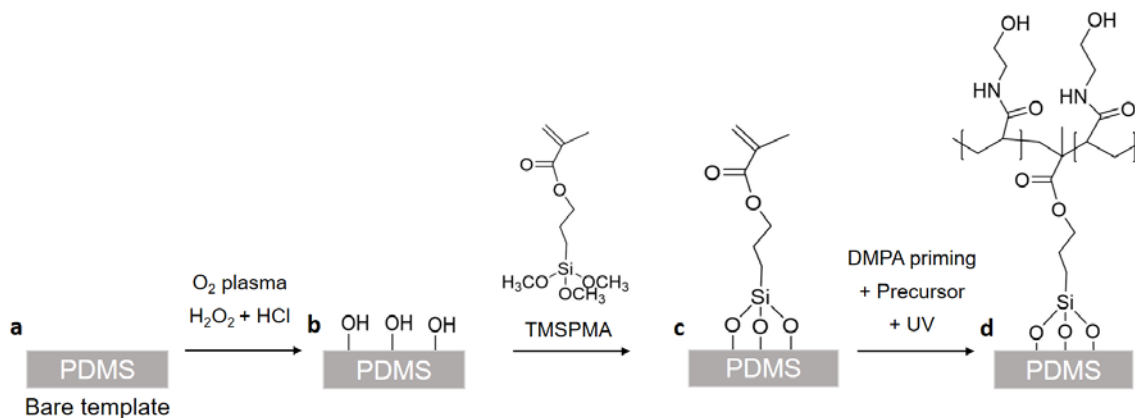
4.3.4 Preparation of adhesive hydrogel and coating the bare template

Adhesive hydrogels were prepared by curing a precursor solution containing 1 M of HEAA with 10 mol % each of DMA and APBA dissolved in 40% (v/v) dimethyl sulfoxide DMSO in DI water. The bifunctional cross-linker methylene bis-acrylamide MBAA and the photoinitiator DMPA were kept at 3 and 0.1 mol %, respectively, relative to HEAA. To prepare a flat adhesive film, precursor solutions were degassed three times with N_2 gas and added to a mold composed of two glass pieces separated by a silicone rubber spacer (0.75 mm thick), and photoinitiation was carried out in a UV cross-linking chamber (XL-1000, Spectronics Corporation; Westbury, NY) located in a nitrogen-filled glovebox (PLAS LABORATORIES; Lansing, MI) for a total of 200 sec.[15, 81, 129]

105

To prepare the adhesive hydrogel-coated bare templates, the chemically modified bare templates were primed with $\approx$ 6 µL of the 0.1 mol % DMPA solution in ethanol to promote free radical initiated polymerization,[130] followed by pipetting $\approx$ 10 µL of the precursor solutions onto them. A cover glass was placed on top and photoinitiation was carried out for 100 sec (**Scheme 11d** and **Scheme 12**). Both - the film and the hybrid structures were immersed in DI water overnight with gentle nutation. The PDMS substrate was gently peeled off from the cover glass, rinsed briefly in DI water, and the samples were used for further analysis. The flat adhesive film was referred to as 'AD-Flat' and the adhesive hydrogel-coated bare templates were referred to as 'hybrid structures' in general and 'AD-ARx' for specific notations where 'x' represents the AR of bare template.

Scheme 12. Schematic representation of the separate components involved in coating the bare template (a) and the assembled configuration (b).

106
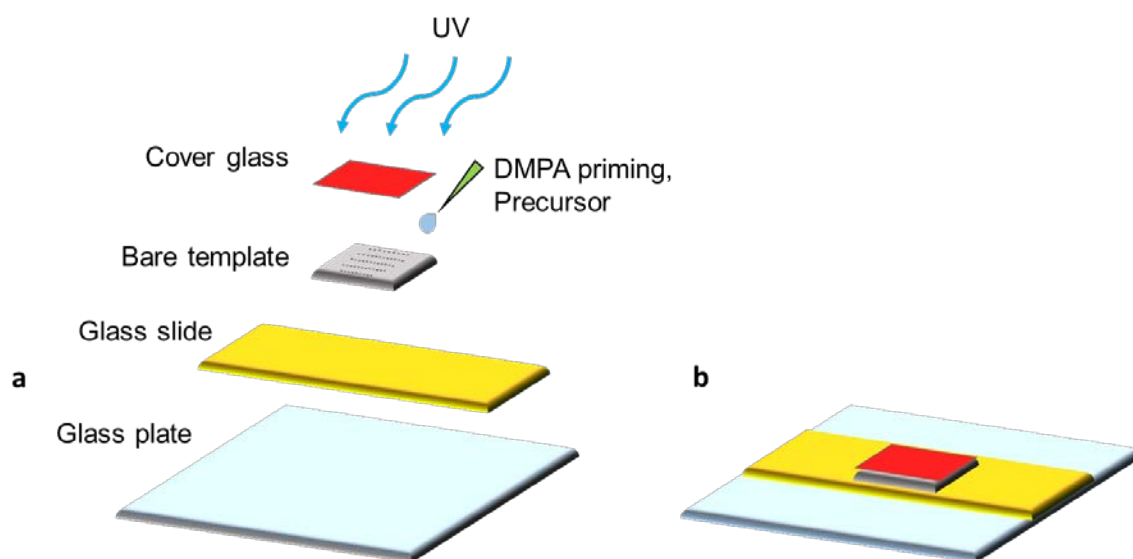
4.3.5 3D Profiling

The bare templates were sputter-coated with a 20 nm Pt/Pd coating (Cressington 208HR; Watford, England, UK) and analyzed using a Profilm3D white light interferometer (Filmetrics Inc., San Diego, CA).

4.3.6 FE-SEM

Samples were incubated in pH 3 for 5 min, air-dried for at least 72 hours under the fume hood. They were then coated with 5 nm Pt/Pd coating (Cressington 208HR; Watford, England, UK), and imaged at 10 kV using the FE-SEM (S-4700, Hitachi; Tarrytown, NY).

4.3.7 ESEM

Samples were incubated in pH 3 or pH 9 for 5 min and imaged using the ESEM (XL 40, Philips; Andover, MA) at an accelerating voltage of 30 kV and working distances of 7.7 mm or 12.5 mm, respectively, for the pH 3 or pH 9 samples. The water vapor inside the chamber was maintained at 868 Pa and saturated vapor pressure was achieved by setting the temperature of the Peltier stage around 5°C.

4.3.8 CA Measurements

Samples were incubated in 5 mL pH 3 buffer for 5 min. The excess buffer was then removed and the sample was maintained in a parafilm-sealed petri dish along with a 200 µL drop of pH 3 buffer for 30 minutes before analysis. A drop of approximately 0.66 µL

107

of DI water was manually placed on the sample surface using $1/8^{th}$ rotation of a threaded plunger syringe (81242, Hamilton; Reno, NV) fitted with a small gauge metal needle. The droplet image was taken 10 sec after the deposition. The values for the CA were measured using ImageJ software for an average of 3 values of CA on different areas of a single sample.

4.3.8.1   Details of the Imaging Setup for CA Measurements

The contact angle measurement system comprises of an illumination source, a stage for droplet deposition on the sample and a microscope coupled to CCD camera. A carousel projector (Kodak Medalist, Eastman Kodak Company; Rochester, NY) was used as the source of illumination. A labjack (L200, Thorlabs; Newton, NJ) was mounted on a translation stage (AXY2509W, Velmex; Bloomfield, NY) enabling X-Y-Z movement of the sample stage. A long distance microscope (K2/S, Infinity; Boulder, CO) was coupled to a CCD camera (TM-1325CL, Pulnix; Sunnyvale, CA) for focusing and image acquisition. Images were captured on an IBM thinkpand T60 laptop using the EPIX XCAP software and the EPIX EL1DB framegrabber.

108

4.3.9 FTIR

The samples were dried in vacuum overnight and analyzed using a PerkinElmer Spectrum One Spectrometer (Waltham, MA) fitted with a GladiATR accessory from Pike Technologies (Madison, WI).

4.3.10 XPS

The samples were dried in vacuum overnight and their surface was analyzed using the X-ray photoelectron spectrometer (PHI 5800, Physical Electronics; Chanhassen, MN). A Mg anode operated at 15 kV, 27 mA and 400 W was used to generate X-rays (hυ = 1253.6 eV) and a hemispherical analyzer angled at 45 degrees from the sample was used to detect electrons from an analysis area with a nominal diameter of 800 µm. Survey spectra were collected for 5 min, in a range of 0 to 1150 electron volts (eV), a step size of 0.8 eV/step, a 20 ms/step dwell time and a 187.85 eV pass energy. High resolution spectra were collected for the time required to generate adequate signal to noise, in a 20 eV range per element (with the combined Cl2p and B1s region spanning a range of 30 eV), a step size of 0.1 eV/step, a 100 ms/step dwell time and a 23.50 eV pass energy. Charge correction was accomplished with a neutralizer that generated 6 eV electrons at a current necessary for the major peak in the C1s region to present at 284.8 eV.

109

4.3.11 Contact Mechanics Test

Contact mechanics tests were performed using the JKR indentation method to determine the interfacial binding properties of the adhesive hydrogel coated samples. A custom-built indentation device with a 10-g load cell (Transducer Techniques; Temecula, CA), high resolution miniature linear stepper motor (MFA-PPD, Newport; Irvine, CA) with a SiO_2 hemispherical indenter with a diameter of 6 mm and thickness of 3 mm (QU-HS-6, ISP Optics; Irvington, NY) affixed using super glue (Gorilla glue) to the load stem (ALS-06, Transducer Techniques; Temecula, CA) was used to conduct the tests. The samples washed in DI water were placed under the fume hood for drying for 10 min. During a contact cycle, the SiO_2 hemisphere was compressed against the samples at 0.5 µm/sec until a maximum preload of 20 mN was reached (except in effect of preload tests), maintained in contact with the substrate for 30 sec, and then retracted at the same rate. The SiO_2 hemisphere was cleaned with a DI water-wetted kimwipe before the start of each contact cycle. Three contact mechanics tests were performed.

For the first series of tests, the bare templates, AD-Flat and the hybrid structures with different ARs were first incubated in either pH 3 or 9 for 5 min. A single contact cycle was then carried out in the presence of ≈ 2 µL of either pH 3 or 9. Further, the hybrid structures were tested out in the presence of ≈ 2 µL of pH 3 or 9 while varying the maximum preload from 10-80 mN.

For the second test, the samples were probed for their ability to transition between adhesive and non-adhesive states in response to pH. They were subjected to three successive contact

110

cycles. The first and the third contacts were carried out in the presence of ≈ 2 µL of pH 3, while the second contact was carried out in the presence of ≈ 2 µL pH 9. Between the cycles, the samples were briefly rinsed in DI water and incubated for 5 min in a petri dish that contained 10 mL of either pH 9 (between first and second cycle) or pH 3 (between second and third cycles).

For the third test, a single sample was tested for its ability to repeatedly switch between adhesive and non-adhesive states in response to changing pH. The sample washed in DI water was incubated at pH 3 for 5 min prior to the first contact cycle. It was then tested in the presence of pH 3 (≈ 2 µL). The sample was then briefly rinsed in DI water before incubating in a pH 9 solution for 1 min. Following the incubation, it was tested in the presence of pH 9 (≈ 2 µL). It was thus tested at pH 3 and pH 9 in the same alternating manner with 1 min incubations in between for three more contact cycles.

The force (F) versus displacement (δ) curves were integrated to determine the work of adhesion (W_{adh}), which was normalized by the apparent maximum area of contact (A_{max}) by using the following equation:[80]

$$W_{adh} = \frac{\int F \, d\delta}{A_{max}}, \qquad (18)$$

where A_{max} was calculated by fitting the loading portion of the F versus δ curve with the Hertzian model:[84]

111

$$\delta_{max} = \frac{a^2}{R}, \qquad (19)$$

where δ_{max} is the maximum displacement at the applied maximum preloads (10-80 mN), a is the radius of A_{max}, and R is the curvature of the hemispherical SiO_2 indenter. The thickness (t = 3 mm) and base radius (r = 3 mm) of the SiO_2 hemisphere was used to determine R:[85]

$$R = \frac{t}{2} + \frac{r^2}{2t} \qquad (20)$$

A_{max} was calculated by using the equation:

$$A_{max} = \pi a^2. \qquad (21)$$

The adhesion strength (S_{adh}) was calculated by normalizing the maximum pull-off force (F_{max}) by the apparent maximum area of contact (A_{max}) using the equation:[86]

$$S_{adh} = \frac{F_{max}}{A_{max}} \qquad (22)$$

The Young's modulus (E) was obtained by determining the slope of the advancing portion of the F versus δ curve at a fixed point near the maximum preload.

112

4.3.12 Statistical Analysis

Statistical analysis was performed using JMP Pro 13 application (SAS Institute, NC). One-way analysis of variance (ANOVA) with Tukey-Kramer HSD analysis was performed for comparing means. $p < 0.05$ was considered significant.

4.4 Results and Discussion

To facilitate covalent interaction between the bare template and the adhesive hydrogel network, the surface of the bare templates was activated with hydroxyl (-OH) groups using the O_2 plasma treatment and then modified using H_2O-H_2O_2-HCl. Further, TMSPMA was employed as an intermediate bridge to interact with the hydroxyl groups and also facilitate covalent binding of the adhesive hydrogel to the -OH modified templates. The adhesive hydrogel was introduced into the spaces between the micropillars by capillary action, followed by UV photopolymerization.

4.4.1 3D profiler

3D profiling of the bare templates was carried out to ensure their integrity after peel-off (**Figure 33**).
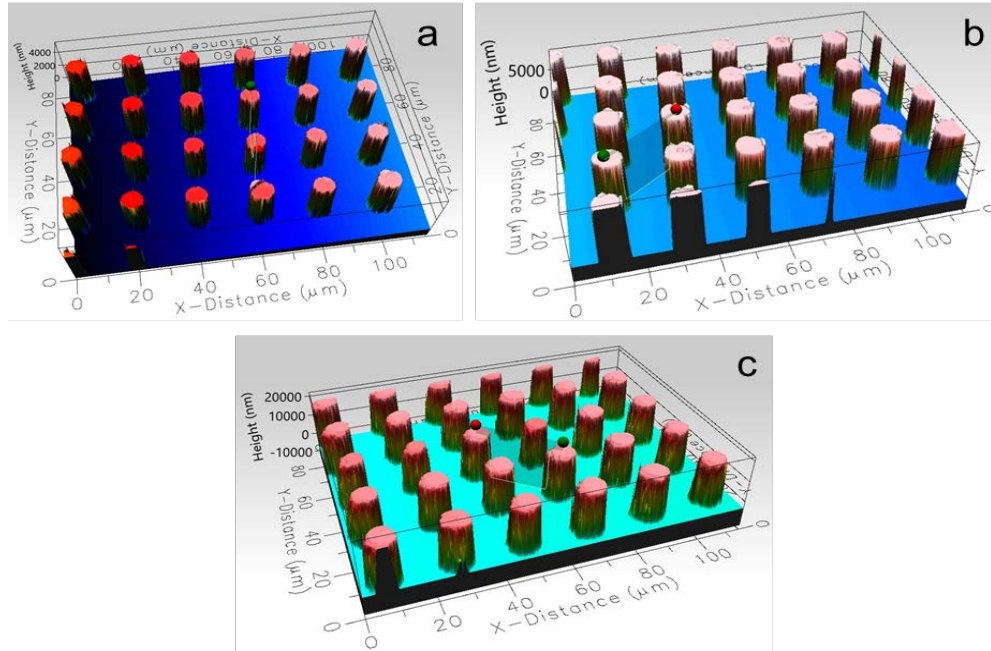
Figure 33. 3D profiles of the bare templates-Bare AR0.4 (a), Bare AR1 (b) and Bare AR2 (c).

4.4.2 FE-SEM

FE-SEM was used to characterize the morphology of the bare templates and the hybrid structures (Figure 34). Images of Bare AR0.4, Bare AR1 and Bare AR2 (**Figure 34a, 34b, and 34c respectively**) display the bare templates with vacant interstitial spaces between the micropatterns. The increasing height of the PDMS pillars (lowest for Bare AR0.4 and highest for Bare AR2) was also evident from these images. **Figure 34d, 34e, and 34f** indicate the presence of the adhesive hydrogel coating on the hybrid structures AD-AR0.4, AD-AR1 and AD-AR2, respectively. Equal volumes of precursor were used to coat bare templates with different ARs. Since the volume of interstitial spaces between the pillars was different (lowest for AR0.4 and highest for AR2), different levels of filling

114

by the adhesive hydrogel were observed. Overall, the adhesive hydrogel was present in the interstitial spaces between the bare micropillars, and also exhibits the formation of a layer coating the top and the sides of the bare templates. In case of AD-AR0.4 (**Figure 34d**), most of the bare template was obscured by the coating, and the hybrid structure appeared like a bumpy surface. For AD-AR1, an appreciable height of the pillars was still visible after the coating (**Figure 34e**). When Bare AR2 was coated with the adhesive, it settled toward the bottom of the pillars, and likely formed a web like pattern due to the relatively lower volume of precursor as compared to the volume of interstitial spaces (**Figure 34f**).
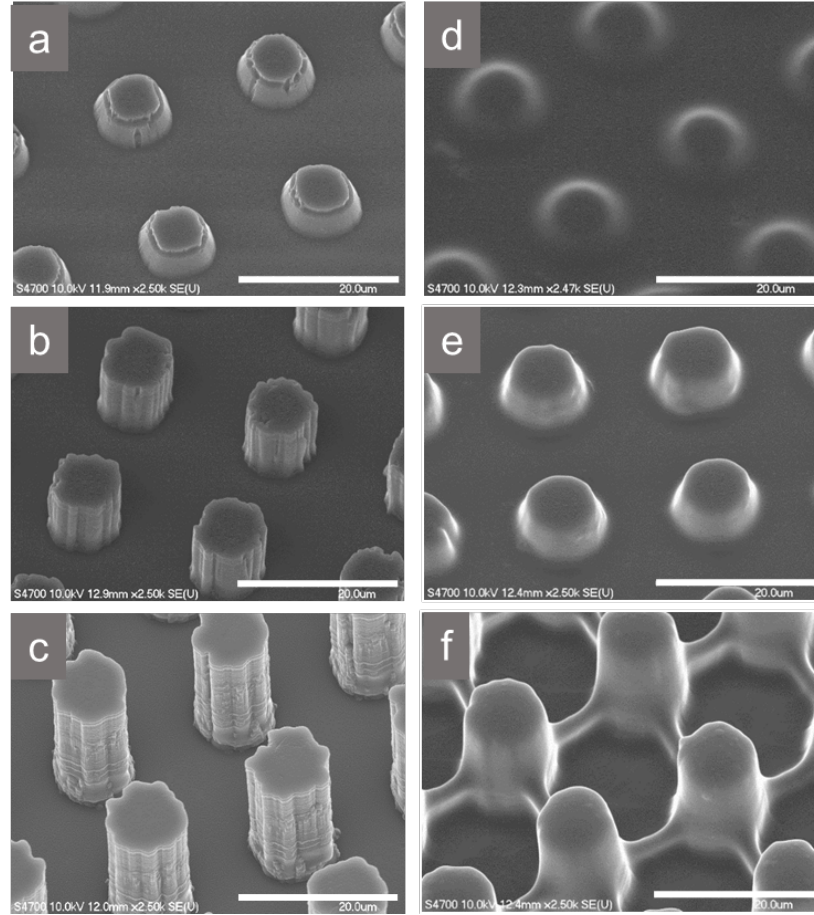
Figure 34. FE-SEM images showing bare templates Bare AR0.4 (a), Bare AR1 (b), Bare AR2 (c), and hybrid structures AD-AR0.4 (d), AD-AR1 (e), AD-AR2 (f). Scale bar = 20 µm.

4.4.3 ESEM

ESEM was used to characterize the filling of interstitial spaces by the adhesive hydrogel at pH 3 or pH 9 for the hybrid structures . For AR-AR0.4 incubated at pH 3, the top of the pillared structures was still visible (**Figure 35a**). On elevating the pH to 9, the negative charge on the catechol-boronate complex led to extensive swelling, which

116

obscured the features and **decreased the AR** (**Figure 35d**). AD-AR1 after 5 min

incubation at pH 3 displayed the existence of the adhesive coated pillared structures

(**Figure 35b**), which were similar to the patterns seen in the bare AR1 template (**Figure

34b**). Increasing the pH to 9 created a globular coating around the pillars and interstitial

spaces between the pillars appeared to be filled with the adhesive, thus dramatically

decreasing the AR (**Figure 35e**). In the case of AD-AR2, no significant differences in

morphology were seen in the samples incubated at pH 3 (**Figure 35c**) and pH 9 (**Figure

35f**). This could perhaps be attributed to the relatively lower filling of interstitial spaces.
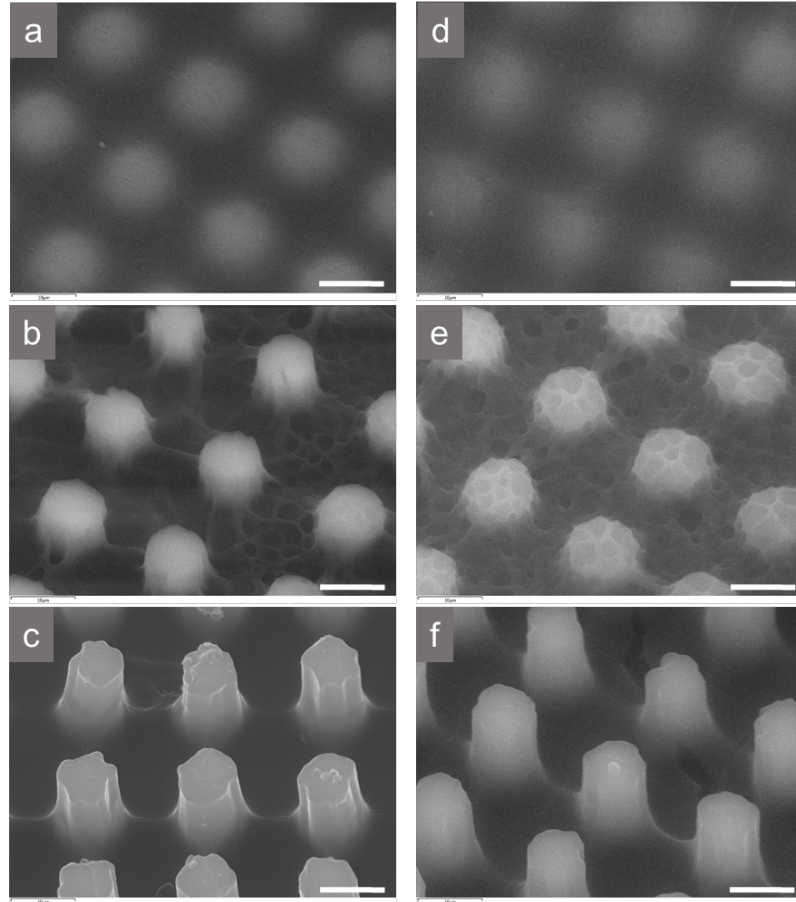
Figure 35. ESEM images showing hybrid structures AD-AR0.4 (first row) AD-AR1 (second row) and AD-AR2 (third row) incubated in pH 3 (a-c) or pH 9 (d-f) for 5 min. Scale bar = 10 µm.

4.4.4   CA Analysis

The wetting of the bare templates and the hybrid structures was evaluated by performing CA measurements. The representative contact images for the contact angles before and after coating can be seen in **Figure 36**. Overall, the CA for the bare templates was higher than the hybrid structures. Specifically, the CA for Bare AR0.4 decreased from 135.6 ±

0.7989° to 113.3 ± 6.072° for AD-AR0.4 (**Figures 36a** and **36d**, respectively). The CA for Bare AR1 decreased from 146.9 ± 1.710° to 115.29 ± 1.854° for AD-AR1 (**Figures 36b** and **36e**, respectively), while the CA for Bare AR2 decreased from 149.4 ± 0.6228° to 129.2 ± 1.461° for AD-AR2 (**Figures 36c** and **36f**, respectively). Thus, the wettability of the bare templates decreased significantly after the adhesive hydrogel coating. The higher hydrophilicity of the hybrid structures confirmed the presence of the adhesive hydrogel coating.

119
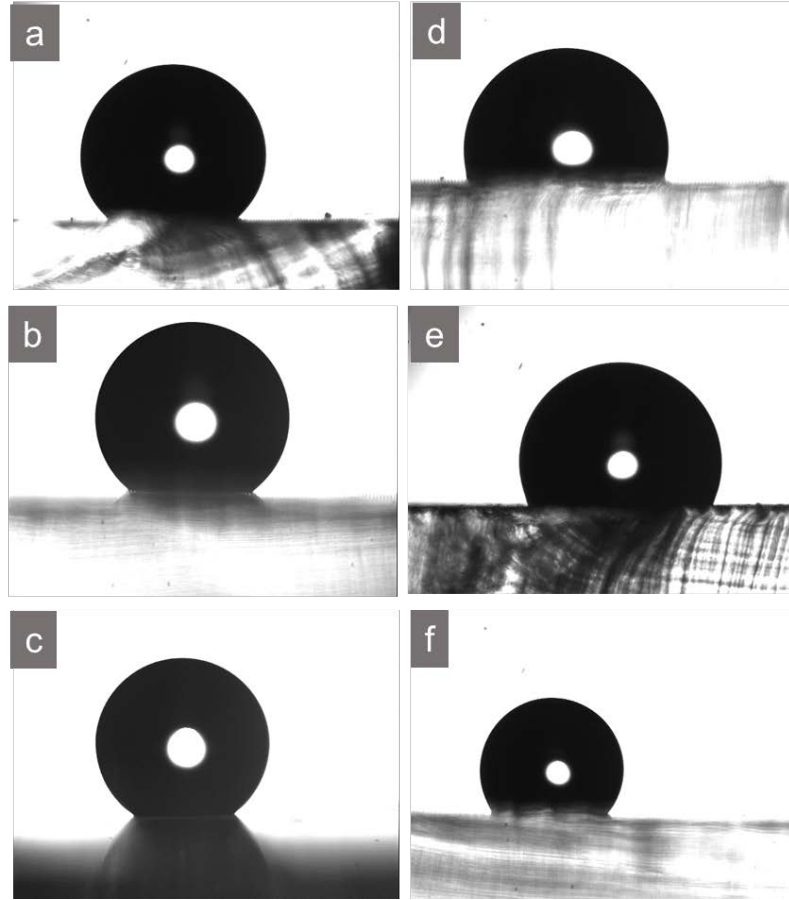
Figure 36. Contact angle images showing representative images for bare templates Bare AR0.4 (a), Bare AR1 (b), Bare AR2 (c) and hybrid structures AD-AR0.4 (d), AD-AR1 (e), AD-AR2 (f).

4.4.5　FTIR

FTIR was used for detecting the presence of the adhesive hydrogel coating on the bare template (**Figure 37**). Bare AR1 showed the typical spectrum of PDMS with Si-CH$_3$ at 2960-2950 cm^{-1}, 1260-1259 cm^{-1} and 796-789 cm^{-1}, and Si-O-Si at 1074-1020 cm^{-1}[131] When compared to the PDMS surface, the presence of the adhesive hydrogel coating on

120

AD-AR0.4, AD-AR1 and AD-AR2 was verified by presence of functional groups

hydroxyl -OH 3400-3000 cm^{-1}, secondary amide -NH 1680-1630 cm^{-1}, C=O 1600-1500

cm^{-1}, benzene groups 1500-1400, 800-700 cm^{-1}.[80]
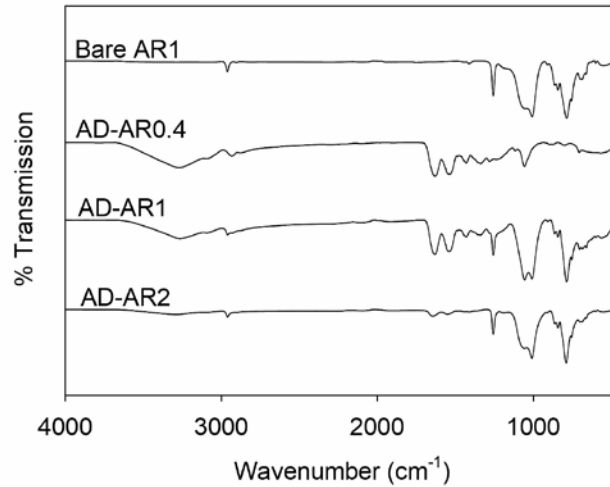
Figure 37. FTIR spectra of Bare AR1, AD-AR0.4, AD-AR1 and AD-AR2.

4.4.6 XPS

XPS was used to confirm the presence of the adhesive hydrogel coating on the bare

template (**Figure 38**). Bare AR1 showed the presence of oxygen (1s, 530.8 eV), carbon

(1s, 284.8 eV) and silicon (2s, 153 eV and 2p, 103 eV) (**Figure 38a**).[132] In addition to

silicon, the hybrid structures showed the presence of nitrogen (1s, 399 eV) and boron

(1s, ≈ 191.5 eV) (**Figure 38b-38d**), which indicated the presence of the adhesive

hydrogel.

121
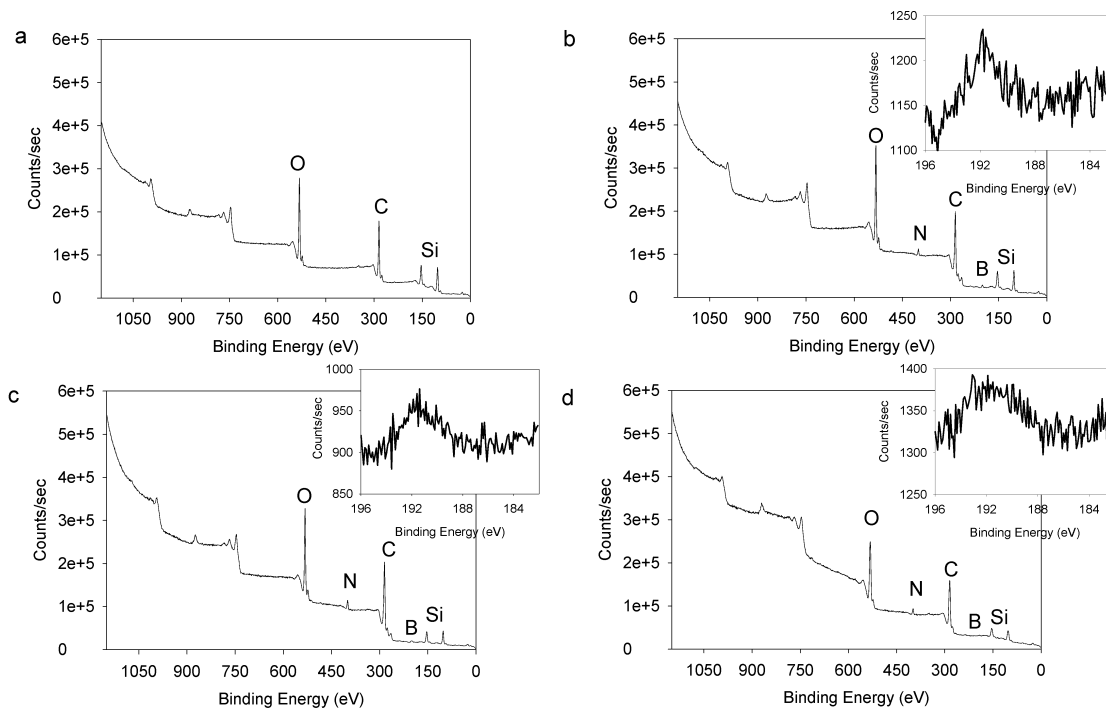
Figure 38. XPS spectra of Bare AR1 (a), AD-AR0.4 (b), AD-AR1 (c) and AD-AR2 (d). The inset images in (b-d) show the presence of boron with binding energy ≈ 191.5 eV.

4.4.7   Contact Mechanics Test

4.4.7.1   *Effect of micropatterning on adhesive properties at a fixed preload*

To assess the effect of micropatterning on the adhesive properties, AD-Flat, bare templates and hybrid structures with different ARs were analyzed at pH 3 or pH 9. Bare templates with different ARs showed negligible W_{adh} values at pH 3 (**Figure 39a**). AD-Flat demonstrated strong adhesion because of H-bonds and other electrostatic attractions offered by the catechol and boronic acid at pH 3.[80] Although AD-AR0.4 showed the presence of the adhesive hydrogel coating (**Figure 40**), its adhesion was not significantly

122

different from AD-Flat. On increasing the AR, AD-AR1 demonstrated a significant increase in W_{adh} when compared to AD-AR0.4 ($W_{adh} = 421.1 \pm 24.49$ mJ/m^2) (**Table 19**). This increase in adhesion could be corroborated by ESEM image of AD-AR1 which showed distinct pillars with adhesive coating (**Figure 35b**). Thus, contact-splitting phenomenon potentially contributed to elevated adhesion in the case of AD-AR1.[133] On the other hand, in case of AD-AR0.4, the adhesive hydrogel coating had obscured the micropillared structures (**Figure 35a**). On further increase in the AR, AD-AR2 showed poor adhesion. This can be attributed to the fact that the interstitial space was largest in Bare AR2 template and the same volume of precursor was used to coat bare templates with different ARs. Because of this, there was perhaps negligible interaction between the hemisphere and the adhesive coating which was toward the bottom of the template (**Figure 35c**). S_{adh} for all the bare templates as well as AD-AR2 was very low at pH 3 (**Figure 39b**). Even though AD-Flat demonstrated strong W_{adh} value at pH 3, the corresponding low F_{max} and high A_{max} (**Figures 41a and 41b**, respectively), led to low S_{adh}. AD-AR0.4 ($S_{adh} = 16.67 \pm 3.398$ mJ/m^2) and AD-AR1 ($S_{adh} = 17.29 \pm 2.160$ mJ/m^2) – both showed strong, statistically comparable S_{adh} values (**Table 19**).

123
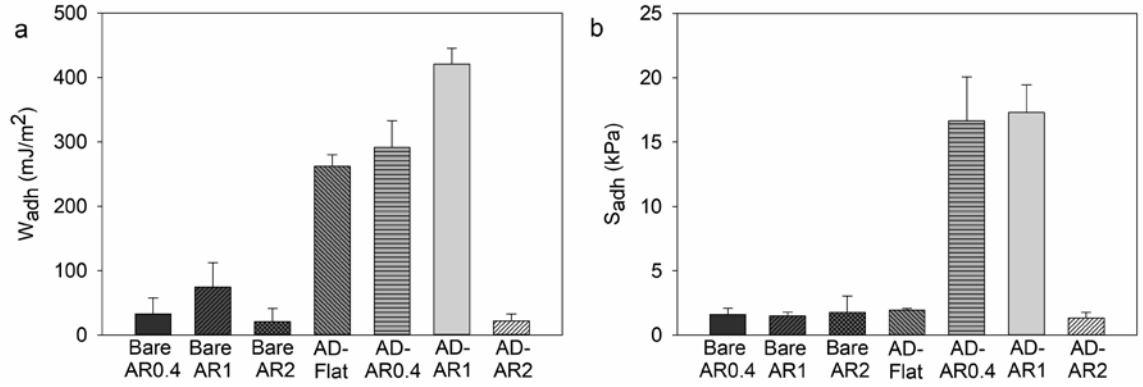
Figure 39. W_{adh} (a) and S_{adh} (b) of AD-Flat, bare templates and hybrid structures of different ARs tested at a preload of 20 mN for samples incubated at pH 3 (n = 3). Refer to Table 19 for statistical analysis.
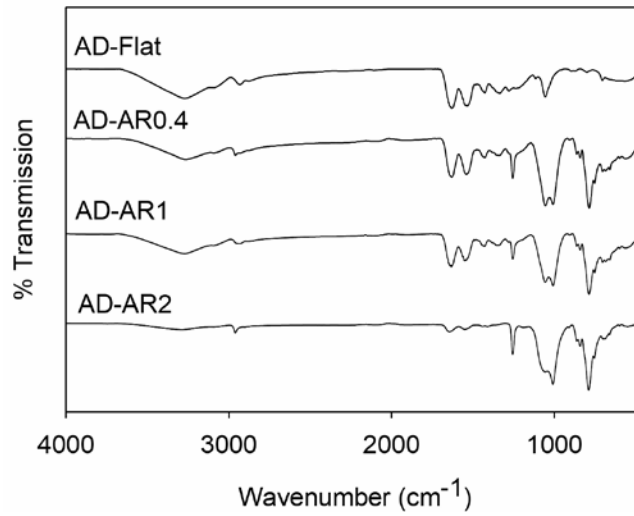
Figure 40. FTIR spectra of AD-Flat, AD-AR0.4, AD-AR1 and AD-AR2 tested at pH 3.

124

Table 19. Statistical analysis for W_{adh} (a) and S_{adh} (b) of AD-Flat, bare templates and hybrid structures of different ARs tested at a preload of 20 mN for samples incubated pH 3 (n = 3). W_{adh} or S_{adh} for compositions not connected by the same letter are significantly different.

Composition	W_{adh}	S_{adh}
Bare AR0.4	A	A
Bare AR1	A	A
Bare AR2	A	A
AD-Flat	B	A
AD-AR0.4	B	B
AD-AR1	C	B
AD-AR2	A	A
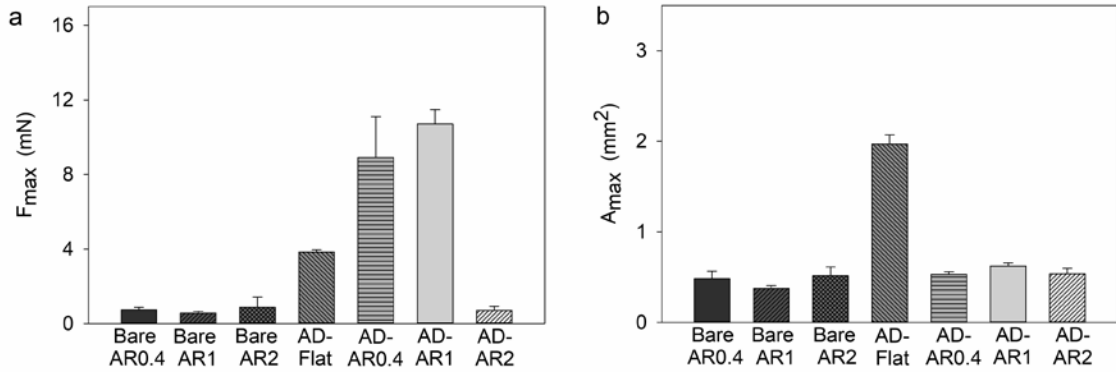
125

Figure 41. F_{max} (a) and A_{max} (b) of AD-Flat, bare templates and hybrid structures of different ARs tested at a preload of 20 mN for samples incubated at pH 3 (n = 3). Refer to Table 20 for statistical analysis.

Table 20. Statistical analysis for F_{max} (a) and A_{max} (b) of AD-Flat, bare templates and hybrid structures of different ARs tested at a preload of 20 mN for samples incubated at pH 3 (n = 3). F_{max} or A_{max} for compositions not connected by the same letter are significantly different.

Composition	F_{max}			A_{max}		
Bare AR0.4	A	B		A		C
Bare AR1	A					C
Bare AR2	A	B		A		C
AD-Flat		B			B	
AD-AR0.4			C	A		C
AD-AR1			C	A		
AD-AR2	A			A		C

126

At pH 9, the W_{adh} demonstrated by the bare templates of different ARs was still low (**Figure 42a**). The adhesion exhibited by the AD-Flat continued to remain high (**Table 21**). This was despite FTIR results which showed the formation of the catechol-boronate complex for these samples (**Figures 43 and 44**), indicating that formation of complex alone was insufficient to cause a dramatic decrease in adhesion within the short incubation period. Both AD-AR0.4 and AD-AR1 showed a significant decrease in W_{adh} when compared to pH 3. Specifically, W_{adh} for AD-AR1 ($W_{adh} = 85.27 \pm 15.34$ mJ/m^2) was around 5-fold lower than that at pH 3. The corresponding ESEM image at pH 9 (**Figure 35e**) showed that swelling of adhesive coating[80] transformed distinct pillared structures (**Figure 35b**) into globular structures which perhaps lowered the good contact formation. When combined with the decrease in adhesion caused by the formation of the complex,[80] the dual effect caused a drastic decrease in adhesion at pH 9. AD-AR2 showed weak adhesion, which could be attributed no significant difference in morphology between the pH 3 and pH 9 incubations (**Figure 35f**). S_{adh} values for all the tested compositions (**Figure 42b**) were largely in agreement with the W_{adh}, except in case of AD-Flat. S_{adh} for AD-AR0.4 ($S_{adh} = 1.127 \pm 0.3424$ mJ/m^2) and AD-AR1 ($S_{adh} = 1.240$

127

$\pm$ 0.4269 mJ/m^2) decreased by over and order of magnitude when compared to pH 3.
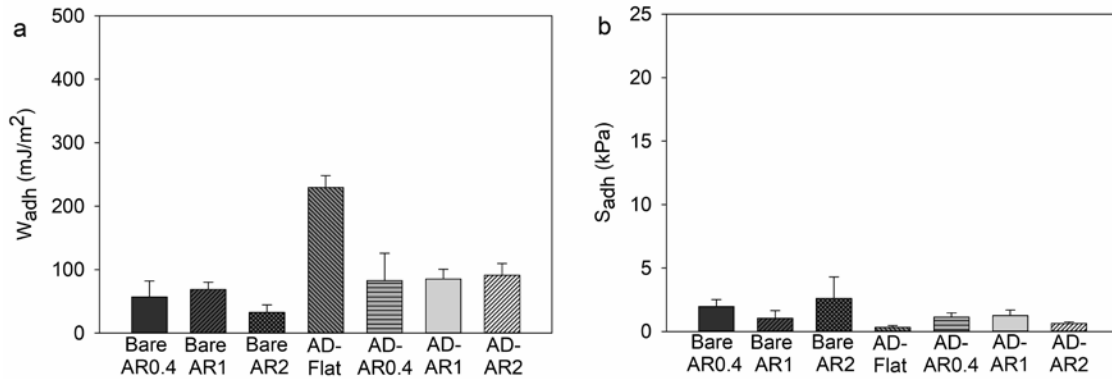
Figure 42. W$_{adh}$ (a) and S$_{adh}$ (b) of AD-Flat, bare templates and hybrid structures of different ARs tested at a preload of 20 mN for samples incubated at pH 9 (n = 3). Refer to Table 21 for statistical analysis.

Table 21. Statistical analysis for W$_{adh}$ (a) and S$_{adh}$ (b) of AD-Flat, bare templates and hybrid structures of different ARs tested at a preload of 20 mN for samples incubated at pH 9 (n = 3). W$_{adh}$ or S$_{adh}$ for compositions not connected by the same letter are significantly different.

Composition	W$_{adh}$		S$_{adh}$
Bare AR0.4	A		A
Bare AR1	A		A
Bare AR2	A		A
AD-Flat		B	A
AD-AR0.4	A		A
AD-AR1	A		A
AD-AR2	A		A

128
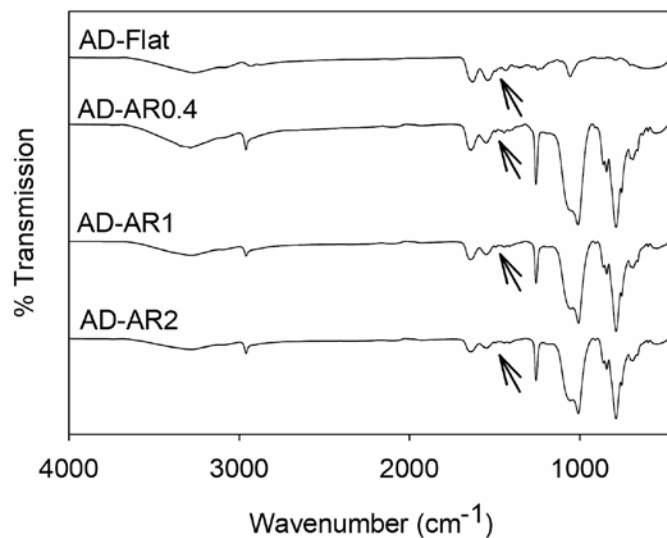
Figure 43. FTIR spectra of AD-Flat, AD-AR0.4, AD-AR1 and AD-AR2 tested at pH 9.

The arrows indicate the formation of the catechol-boronate complex at 1495 cm^{-1}.
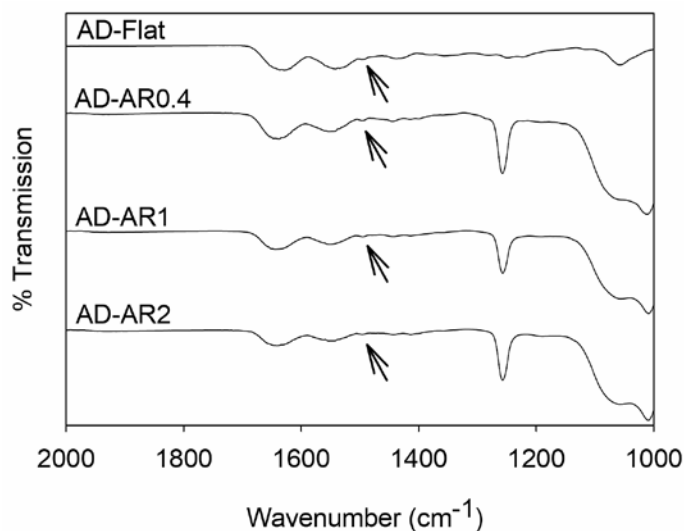
Figure 44. FTIR spectra (2000-1000 cm^{-1}) of AD-Flat, AD-AR0.4, AD-AR1 and AD-AR2 (in the smaller range of 2000-1000 cm^{-1}) tested at pH 9. The arrows indicate the formation of the catechol-boronate complex at 1495 cm^{-1}.
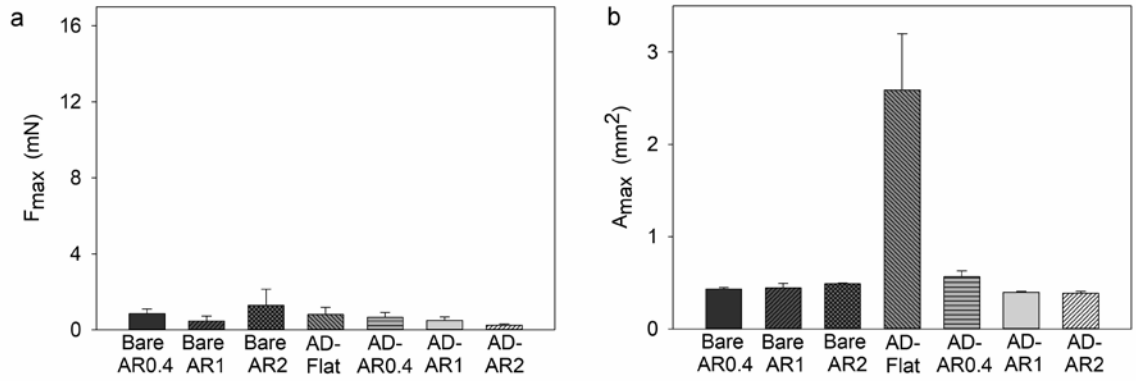
Figure 45. F_{max} (a) and A_{max} (b) of AD-Flat, bare templates and hybrid structures different ARs tested at a preload of 20 mN for samples incubated at pH 9 (n = 3). Refer to Table 22 for statistical analysis.

Table 22. Statistical analysis for F_{max} (a) and A_{max} (b) of AD-Flat, bare templates and hybrid structures of different ARs tested at a preload of 20 mN for samples incubated at pH 9 (n = 3). F_{max} or A_{max} for compositions not connected by the same letter are significantly different.

Composition	F_{max}	A_{max}
Bare AR0.4	A	A
Bare AR1	A	A
Bare AR2	A	A
AD-Flat	A	B
AD-AR0.4	A	A
AD-AR1	A	A
AD-AR2	A	A

130

To determine the effect of preload on the adhesive behavior of the hybrid structures of different ARs at pH 3 or 9, the preload was varied from 10-80 mN, and the W_{adh} and S_{adh} were calculated. At any given preload, the W_{adh} values demonstrated by AD-AR1 were higher than both AD-AR0.4 and AD-AR2 (**Figure 46a, Table 23**). For AD-AR0.4, even though the S_{adh} remained constant when the preload was increased from 10 to 20 mN, further increase in preload resulted in a decrease in the S_{adh} values (**Fig. 46b, Table 26**). This is because even though the A_{max} increased with increasing preload (**Figure 47b, Table 25**), the F_{max} values did not show a significant increase (**Figure 47a, Table 25**). This could be supported by ESEM data for AD-AR0.4 at pH 3 (**Figure 35a**) which showed that the micropillared template was covered with the adhesive, thus decreasing the effective area available for interfacial binding. This confirmed that we could not take advantage of micropatterning for adhesion in case of AD-AR0.4. For AD-AR1, statistical analysis revealed that the S_{adh} values were constant with increasing preload (**Table 24**).[134] Here, F_{max} and A_{max} – both increased with increasing preload (**Figures 47a and 47b, Table 25**), indicating that as the hemisphere made contact with increasing area of the sample, the pull-off forces also increased. This meant that AD-AR1 was the ideal sample to take advantage of the increased adhesion *via* micropatterning. This is in line with our observations from the tests conducted at a single preload which indicated that contact-splitting effects resulting in increased adhesion for AD-AR1. Meanwhile, AD-AR2 showed low adhesion across the range of preloads.

131

This is likely because the presence adhesive coating was present at the bottom of the hybrid structure (**Figure 35c** and relatively weak transmittance as seen in FTIR-**Figure 37**), indicating that the hemisphere perhaps could not form adhesive bonds even at higher preloads.
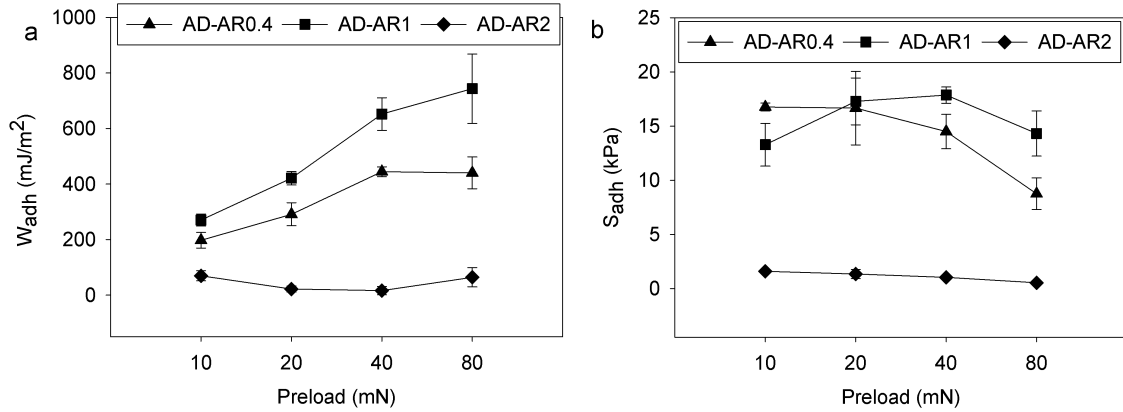
Figure 46. W_{adh} (a) and S_{adh} (b) of hybrid structures of different ARs while varying the preload from 10-80 mN at pH 3 (n = 3). Refer to Tables 23 and 24 for statistical analysis.

Table 23. Statistical analysis for W_{adh} and S_{adh} of hybrid structures of different ARs while varying the preload from 10-80 mN at pH 3 (n = 3). W_{adh} and S_{adh} for compositions at a particular preload not connected by the same letter are significantly different.

	W_{adh}				S_{adh}			
Preload	10	20	40	80	10	20	40	80
AD-AR0.4	A	A	A	A	A	A	A	A
AD-AR1	B	B	B	B	A	A	B	B
AD-AR2	C	C	C	C	B	B	C	C

133

Table 24. Statistical analysis for W_{adh} (a) and S_{adh} (b) of hybrid structures of different ARs while varying the preload from 10-80 mN at pH 3 (n = 3). W_{adh} or S_{adh} at preload values for a given composition not connected by the same letter are significantly different.

Preload	AD-AR0.4		AD-AR1		AD-AR2	
	W_{adh}	S_{adh}	W_{adh}	S_{adh}	W_{adh}	S_{adh}
10	A	A	A	A	A	A
20	A	A	A	A	A	A
40	B	A B	B	A	A	A B
80	B	B	B	A	A	B
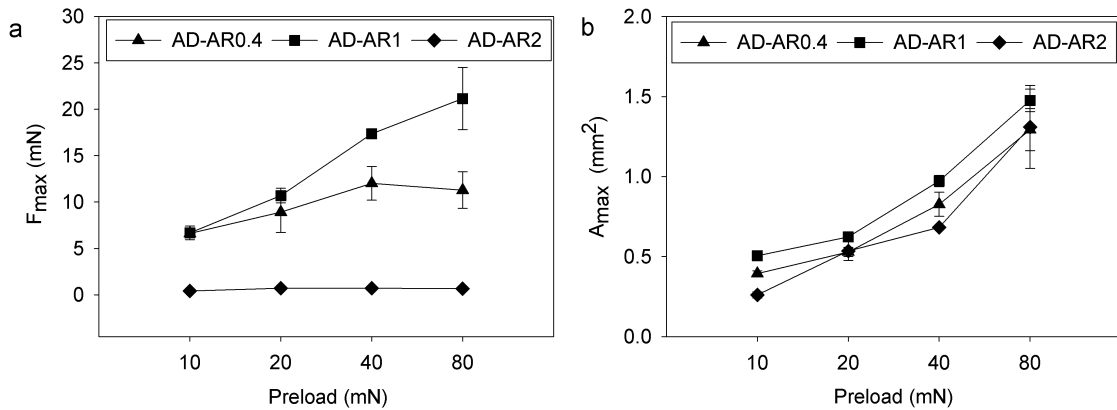
Figure 47. F_{max} (a) and A_{max} (b) of hybrid structures of different ARs while varying the preload from 10-80 mN at pH 3 (n = 3). Refer to Tables 25 and 26 for statistical analysis.

134

Table 25. Statistical analysis for F_{max} (a) and A_{max} (b) of hybrid structures of different ARs while varying the preload from 10-80 mN at pH 3 (n = 3). F_{max} or A_{max} at preload values for a given composition not connected by the same letter are significantly different.

	AD-AR0.4		AD-AR1		AD-AR2	
Preload	F_{max}	A_{max}	F_{max}	A_{max}	F_{max}	A_{max}
10	A	A	A	A	A	A
20	A	A	A	A	A	A
40	A	B	B	B	A	A
80	A	C	B	C	A	B

Table 26. Statistical analysis for F_{max} and A_{max} of hybrid structures of different ARs while varying the preload from 10-80 mN at pH 3 (n = 3). F_{max} or A_{max} for compositions at a particular preload not connected by the same letter are significantly different.

	F_{max}				A_{max}			
Preload	10	20	40	80	10	20	40	80
AD-AR0.4	A	A	A	A	A	A	A B	A
AD-AR1	A	A	B	B	B	A	A	A
AD-AR2	B	B	C	C	C	A	B	A

W_{adh} for all the hybrid structures was low across the range of tested preloads at pH 9 (**Figure 48a**). Specifically, the largest reduction (6-fold) in the average W_{adh} values was shown by AD-AR1. This is because of the dual effect resulting from the formation of the complex (**Figure 49b**), due to which catechol and boronic acid were not available for interfacial binding, and the related swelling of the adhesive network,[80] which could be corroborated by the ESEM images (**Figure 35e**). S_{adh} values were negligible for all

136

hybrid structures. The greatest decrease ($\approx$ 20-fold) in average S_{adh} values across the range of tested preloads was also seen in the case of AD-AR1 (**Figure 48b**).
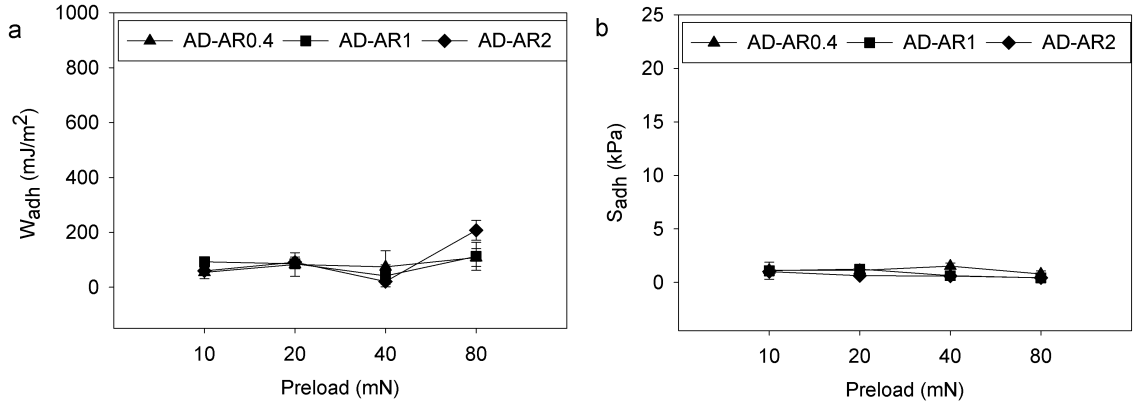
Figure 48. W_{adh} (a) and S_{adh} (b) of hybrid structures of different ARs while varying the preload from 10-80 mN at pH 9 (n = 3). Refer to Tables 27 and 28 for statistical analysis.

Table 27. Statistical analysis for W_{adh} (a) and S_{adh} (b) of hybrid structures of different ARs while varying the preload from 10-80 mN at pH 9 (n = 3). W_{adh} or S_{adh} at preload values for a given composition not connected by the same letter are significantly different.

	AD-AR0.4		AD-AR1		AD-AR2		
Preload	W_{adh}	S_{adh}	W_{adh}	S_{adh}	W_{adh}		S_{adh}
10	A	A	A	A	A	B	A
20	A	A	A	A	A		A
40	A	A	A	A		B	A
80	A	A	A	A		C	A

137

Table 28. Statistical analysis for W_{adh} and S_{adh} of hybrid structures of different ARs while varying the preload from 10-80 mN at pH 9 (n = 3). W_{adh} and S_{adh} for compositions at a particular preload not connected by the same letter are significantly different.

	W_{adh}				S_{adh}			
Preload	10	20	40	80	10	20	40	80
AD-AR0.4	A	A	A	A	A	A	A	A
AD-AR1	A	A	A	A	A	A	A	A
AD-AR2	A	A	A	A	A	A	A	A

138
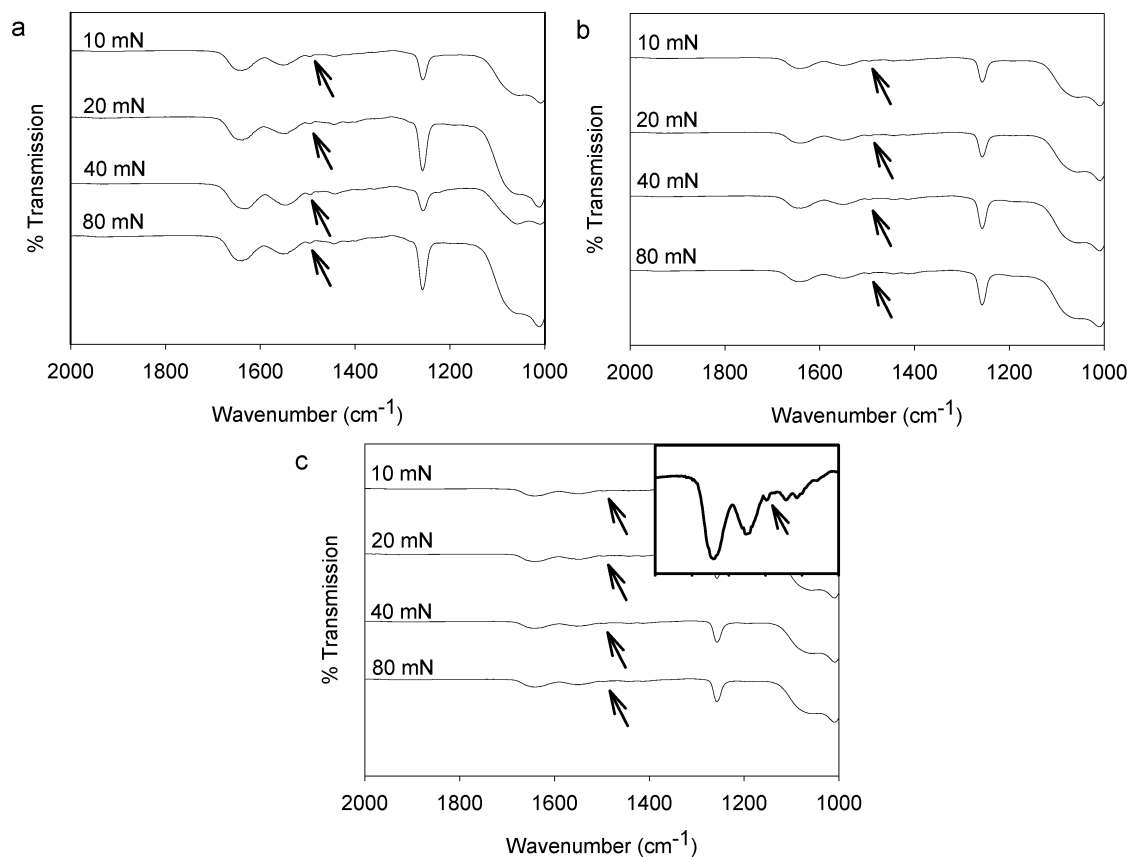
Figure 49. FTIR spectra of hybrid structures AD-AR0.4 (a), AD-AR1 (b) and AD-AR2 (c) tested while varying the preload from 10-80 mN at pH 9. The arrows indicate the formation of the catechol-boronate complex at 1495 cm^{-1}. The inset image in (c) shows the presence of the complex at a zoomed in scale.
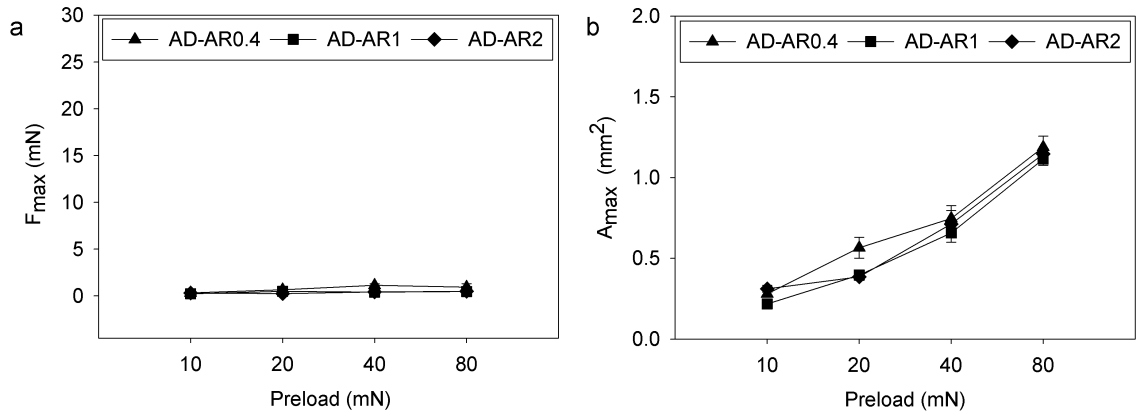
Figure 50. F_{max} (a) and A_{max} (b) of hybrid structures of different ARs while varying the preload from 10-80 mN at pH 9 (n = 3). Refer to Tables 29 and 30 for statistical analysis.

140

Table 29. Statistical analysis for F_{max} (a) and A_{max} (b) of hybrid structures of different ARs while varying the preload from 10-80 mN at pH 9 (n = 3). F_{max} or A_{max} at preload values for a given composition not connected by the same letter are significantly different.

Pre-load	AD-AR0.4		AD-AR1		AD-AR2	
	F_{max}	A_{max}	F_{max}	A_{max}	F_{max}	A_{max}
10	A	A	A	A	A	A
20	A B	B	A	B	A	A
40	B	C	A	C	A	B
80	A B	D	A	D	A	C

Table 30. Statistical analysis for F_{max} and A_{max} of hybrid structures of different ARs while varying the preload from 10-80 mN at pH 9 (n = 3). F_{max} and A_{max} for compositions at a particular preload not connected by the same letter are significantly different.

	F_{max}				A_{max}			
Preload	10	20	40	80	10	20	40	80
AD-AR0.4	A	A	A	A	A	A	A	A
AD-AR1	A	A	B	A	B	B	A	A
AD-AR2	A	A	B	A	A	B	A	A

142

4.4.7.3 *Reversibly Switching Adhesion of Hybrid Structures*

To investigate the reversible transitions of the hybrid structures between strong and weak adhesion, a SiO_2 hemisphere was repeatedly brought into contact with the samples while changing the pH value. W_{adh} for all bare templates (Bare AR0.4-2) was low and not responsive to pH (**Figure 51a**). AD-Flat demonstrated appreciable W_{adh} value during the first contact cycle at pH 3 ($W_{adh} = 262.3 \pm 17.67$ mJ/m^2) (**Figure 52a**). This could be attributed to the compliant behavior of a bulk polymer which shows greater displacement for the same value of preload (**Figure 53a**) with low E values (**Figure 54, Table 31**) when compared to the hybrid structures.[132] Moreover, the adhesion did not diminish significantly during the second contact cycle at pH 9 ($W_{adh} = 162.1 \pm 14.21$ mJ/m^2), and was not recovered during the third contact cycle at pH 3 ($W_{adh} = 196.9 \pm 66.40$ mJ/m^2) (**Table 32**). However, FTIR results showed that the catechol-boronate complex formed after the second contact cycle (pH 9) continued to exist even after the third contact cycle (pH 3) (**Figure 53e**). This not only indicated that formation of the complex alone was not sufficient to significantly reduce adhesion, but also demonstrated that the 5 min incubation period between contact cycles was insufficient to break the complex into the bulk in case of AD-Flat.

143
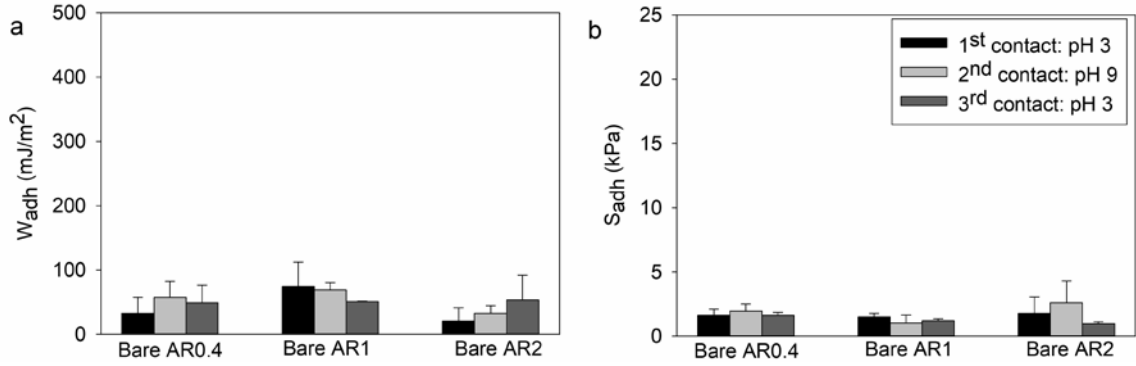
Figure 51. Averaged W_{adh} (a) and S_{adh} (b) of bare templates of different ARs tested in 3 successive contact cycles using a SiO_2 hemisphere (n = 3). Refer to Tables 32-35 for further statistical analysis.

The W_{adh} exhibited by AD-AR0.4 during the first contact cycle was not significantly different from AD-Flat (**Table 33**). Additionally, the adhesion did not decrease significantly ($\approx$ 38 %) during the second contact cycle (**Table 32**). This is because the swelling of the adhesive due to the complex obscured the micropillared features (**Figure 35d**) and AD-AR0.4 likely behaved similar to AD-Flat (i.e., comparable adhesion values during the first cycle that did not diminish significantly during the second cycle (**Table 33**)). Moreover, statistical analysis revealed that the recovery of adhesion during the third contact cycle was not significant (**Table 32**).

www.manaraa.com
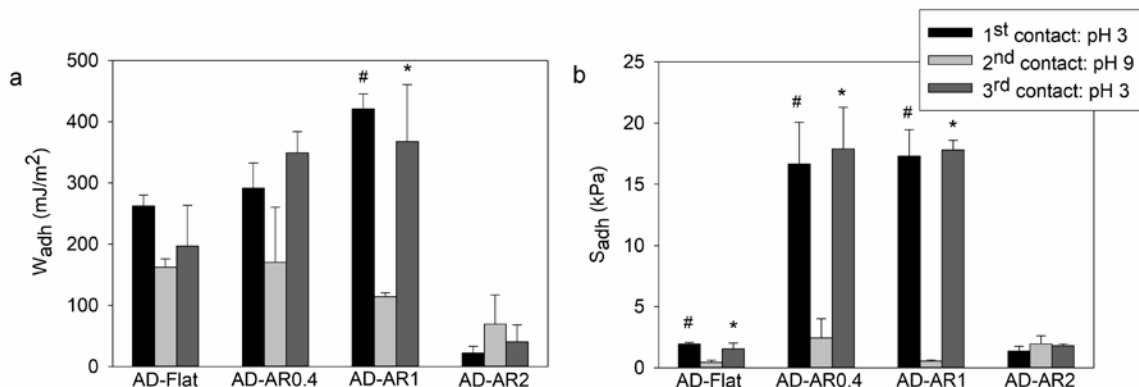
Figure 52. Averaged W_{adh} (a) and S_{adh} (b) of AD-Flat, and hybrid structures of different ARs tested in 3 successive contact cycles using a SiO_2 hemisphere (n = 3). $^{\#,*}p < 0.05$ when compared to 2nd contact cycle for a given composition. Refer to Tables 32-35 for further statistical analysis.

AD-AR1 exhibited strong W_{adh} during the first contact cycle at pH 3, which was significantly higher than both- AD-Flat as well as AD-AR0.4 (**Table 33**). Further, the adhesion decreased drastically ($\approx$ 73 %) during the second contact cycle (**Table 32**). This could be attributed to the dual effect involving obscuring of the micropillared pattern and formation of globular structures caused by the swelling of the adhesive coating (**Figure 35e**) combined with the unavailability of catechol and boronic acid for interfacial adhesion. Thus, formation of the complex (**Figure 53g**) in addition to the change in morphology caused by the swelling likely contributed to the dramatic decrease in adhesion. During the third contact cycle, the adhesion values demonstrated a significant recovery of adhesion ($\approx$ 69 %), which was $\approx$ 87 % of the value during the first contact cycle. Since the same volume of precursor was used to coat the bare templates with different ARs, the interstitial spaces filled by the adhesive hydrogel in case of AD-AR1

145

was lower than AD-AR0.4 (**Figure 35a and 35b**), making it ideal to observe reversibly switching adhesion. AD-AR2 showed negligible adhesion during the three successive contact cycles. S_{adh} for all bare templates (Bare AR0.4-2) was low and not responsive to pH (**Figure 51b**). Statistical analysis indicated that S_{adh} for AD-Flat demonstrated pH responsiveness (**Table 34**); but adhesion values were low. AD-AR0.4 exhibited high S_{adh} during the first and third contact cycles at pH 3, while demonstrating low S_{adh} during the second contact cycle at pH 9. However, since the W_{adh} values did not show a significant decrease (**Figure 52a, Table 32**), AR-AR0.4 was not suitable for switching between strong and weak adhesion. AD-AR1 demonstrated high S_{adh} values during the first contact at pH 3, which dramatically decreased by an order of magnitude during the second contact cycle at pH 9 (**Figure 52b, Table 34**). Further, we were able to recover 97 % of the adhesion during the third contact cycle at pH 3. AD-AR1 showed high W_{adh} and S_{adh} values during the first contact cycle. These values decreased significantly in the second contact cycle before showing an appreciable increase during the third contact cycle. Hence, we chose AD-AR1 to investigate rapidly switching and repeatable adhesion.

146
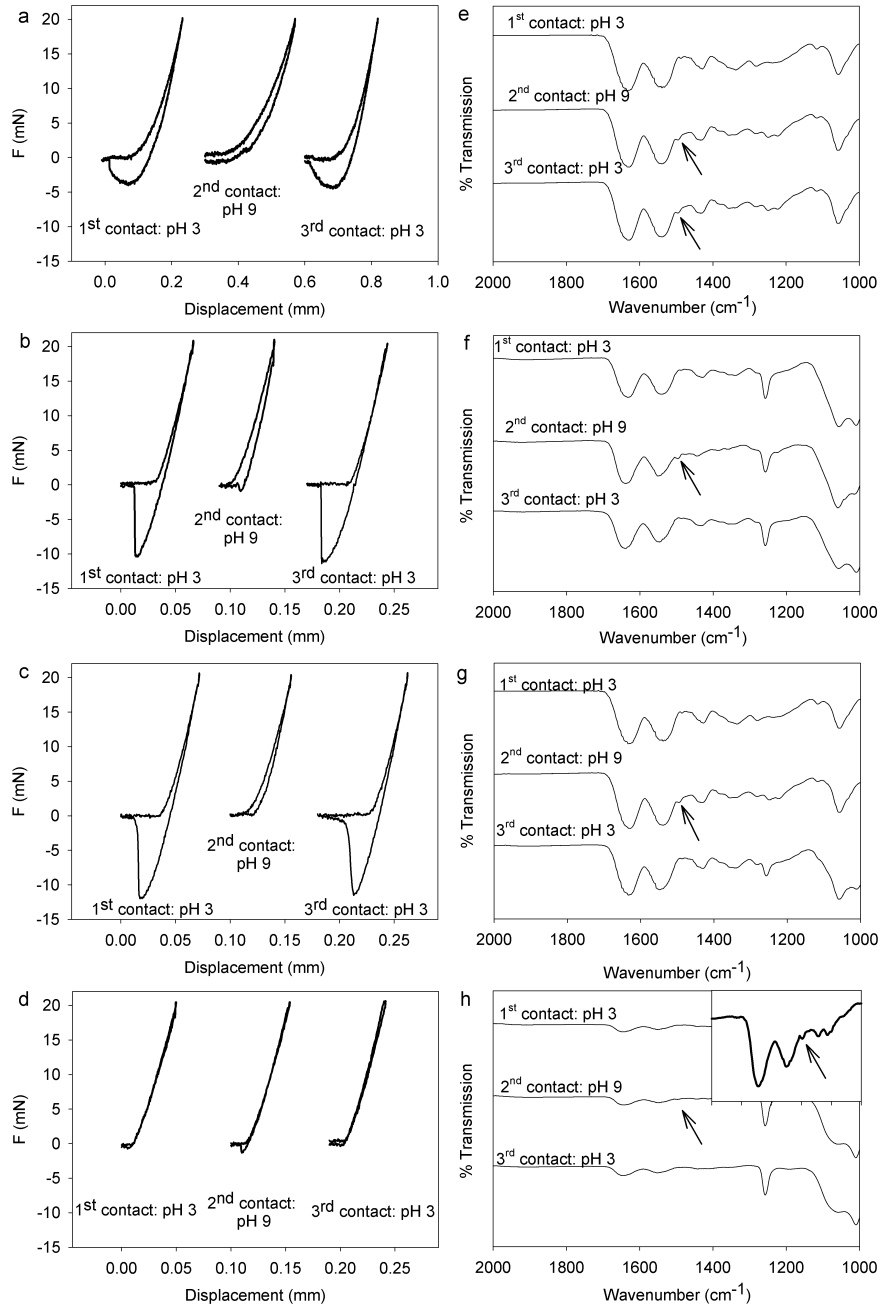
Figure 53. Three successive contact curves of the compositions (left column, a-d) and their corresponding FTIR graphs (right column, e-h) for AD-Flat (a-e), AD-AR0.4 (b-f), AD-AR1 (c-g), and AD-AR2 (d-h) tested at pH 3, pH 9 and then pH 3 using a SiO_2 hemisphere.

147
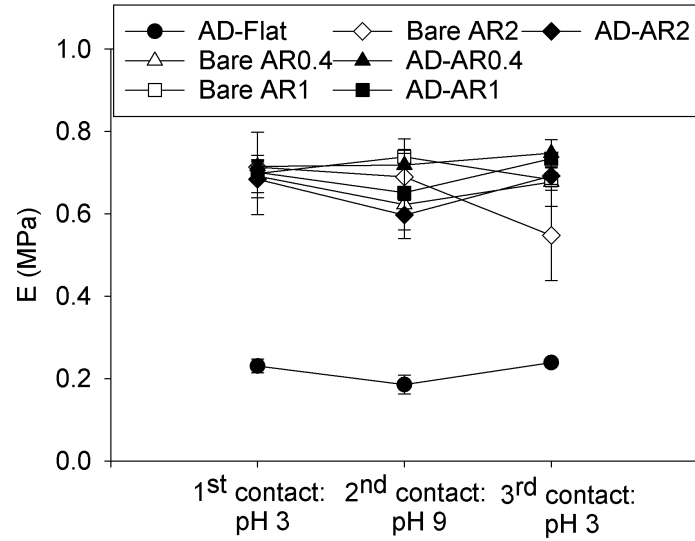
Figure 54. Young's modulus (E) of AD-Flat, bare templates and hybrid structures of different ARs tested in 3 successive contact cycles (n = 3). Refer to Table 31 for statistical analysis.

Table 31. Statistical analysis for the 'E' of AD-Flat, bare templates and hybrid structures of different ARs tested in 3 successive contact cycles using a SiO_2 hemisphere (n = 3). 'E' at contact cycle numbers for a given composition not connected by the same letter are significantly different.

E							
Cycle #	Bare AR0.4	Bare AR1	Bare AR2	AD-Flat	AD-AR0.4	AD-AR1	AD-AR2
1st contact: pH 3	A	A	A	A B	A	A	A
2nd contact: pH 9	A	A	A	B	A	A	A
3rd contact: pH 3	A	A	A	A	A	A	A

149

Table 32. Statistical analysis for the W_{adh} of AD-Flat, bare templates and hybrid structures of different ARs tested in 3 successive contact cycles using a SiO_2 hemisphere (n = 3). W_{adh} at contact cycle numbers for a given composition not connected by the same letter are significantly different.

	W_{adh}						
Cycle #	Bare AR0.4	Bare AR1	Bare AR2	AD-Flat	AD-AR0.4	AD-AR1	AD-AR2
1st contact: pH 3	A	A	A	A	A	A	A
2nd contact: pH 9	A	A	A	A	A	B	A
3rd contact: pH 3	A	A	A	A	A	A	A

150

Table 33. Statistical analysis for W_{adh} of AD-Flat, bare templates and hybrid structures of different ARs tested in 3 successive contact cycles using a SiO_2 hemisphere (n = 3). W_{adh} of compositions during a particular contact cycle not connected by the same letter are significantly different.

	W_{adh}		
Composition	1st contact: pH 3	2nd contact: pH 9	3rd contact: pH 3
Bare AR0.4	A	A	A
Bare AR1	A	A	A
Bare AR2	A	A	A
AD-Flat	B	A	B
AD-AR0.4	B	A	B C
AD-AR1	C	A	C
AD-AR2	A	A	A

151

Table 34. Statistical analysis for the S_{adh} of AD-Flat, bare templates and hybrid structures of different ARs tested in 3 successive contact cycles using a SiO_2 hemisphere (n = 3). S_{adh} at contact cycle numbers for a given composition not connected by the same letter are significantly different.

	S_{adh}						
Cycle #	Bare AR0.4	Bare AR1	Bare AR2	AD-Flat	AD-AR0.4	AD-AR1	AD-AR2
1st contact:	A	A	A	A	A	A	A
2nd contact: pH 9	A	A	A	B	B	B	A
3rd contact:	A	A	A	A	A	A	A

152

Table 35. Statistical analysis for S_{adh} of AD-Flat, bare templates and hybrid structures of different ARs tested in 3 successive contact cycles using a SiO_2 hemisphere (n = 3). S_{adh} of compositions during a particular contact cycle not connected by the same letter are significantly different.

	S_{adh}		
Composition	1st contact: pH 3	2nd contact: pH 9	3rd contact: pH 3
Bare AR0.4	A	A	A
Bare AR1	A	A	A
Bare AR2	A	A	A
AD-Flat	A	A	A
AD-AR0.4	B	A	B
AD-AR1	B	A	B
AD-AR2	A	A	A

153

4.4.7.4 Rapidly Switching, Repeatable Adhesion of AD-AR1

The adhesion tests conducted hitherto indicated that AD-AR1 had the ability to form strong interfacial bonds and reversibly switch between strong and weak adhesion while allowing an incubation time of 5 min between cycles. To further investigate the adhesion switching and capabilities of AD-AR1, the incubation time between changing the pH from 3 to 9 was decreased to 1 min, and to examine the repeatability, four-adhesion on/off cycles were conducted. When AD-AR1 was tested for multiple adhesion on/off cycles with alternate incubations at pH 3 and 9, strong W_{adh} observed during each pH 3 cycle decreased significantly during the subsequent corresponding pH 9 cycle after only 1 min of incubation (**Figure 55a**). On an average, the W_{adh} values at pH 3 were around 2-fold higher than those at pH 9. Moreover the adhesion could be repeatedly and rapidly activated by 1 min incubation at pH 3. The S_{adh} (**Figure 55b**) and F_{max} (**Figure 56a**) values were also in agreement with the W_{adh} values. Specifically, averaged S_{adh} values at pH 3 were around 4-fold higher than those at pH 9. It was interesting to note that the calculated A_{max} values at pH 3 were higher than those at pH 9 (**Figure 56b**), which further corroborated our observations that the adhesive was deswollen at pH 3 and presented a greater surface area of the hybrid adhesives for interfacial binding. On the other hand, the pH 9 incubation caused the adhesive to rapidly swell and likely obscured the large surface area. The FE-SEM images of the hybrid structures obtained at the end of these tests indicated no significant damage to them (**Figure 57**). Additionally, the FTIR spectra of samples at the end of these tests revealed the presence of the catechol-boronate complex (**Figure 58**).

154
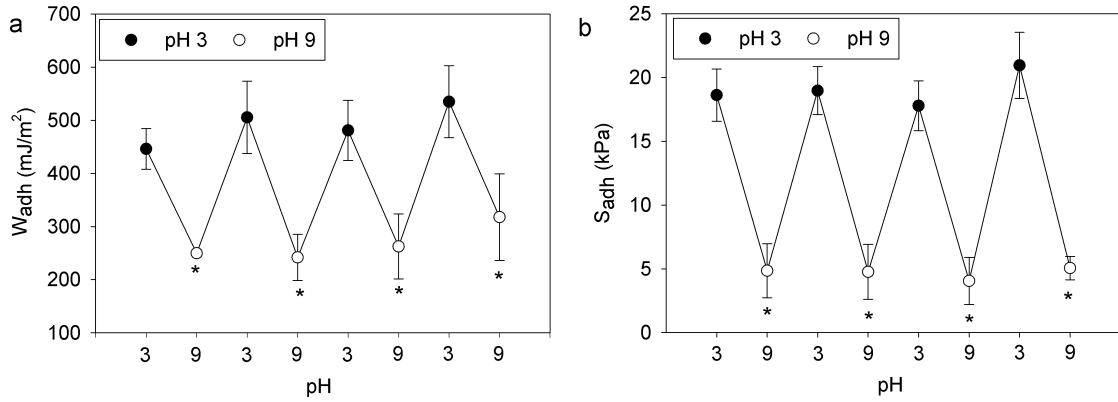
Figure 55. W_{adh} (a) and S_{adh} (b) of AD-AR1 showing multiple adhesion on/off cycles with alternate incubations at pH 3 and pH 9 (n = 3) using a SiO_2 hemisphere. *p < 0.05 when compared to the preceding pH 3 contact.
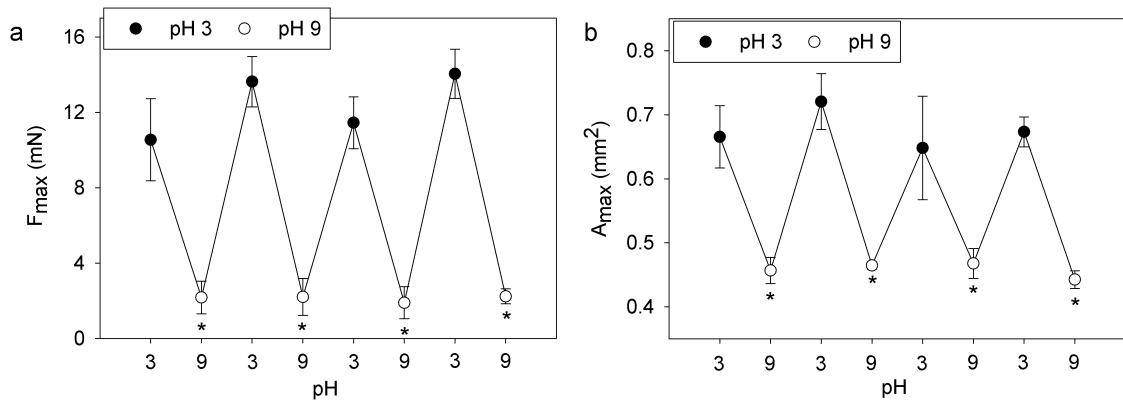
Figure 56. F_{max} (a) and A_{max} (b) of AD-AR1 showing multiple adhesion on/off cycles with alternate incubations at pH 3 and pH 9 (n = 3) using a SiO_2 hemisphere. *p < 0.05 when compared to the preceding pH 3 contact.

155
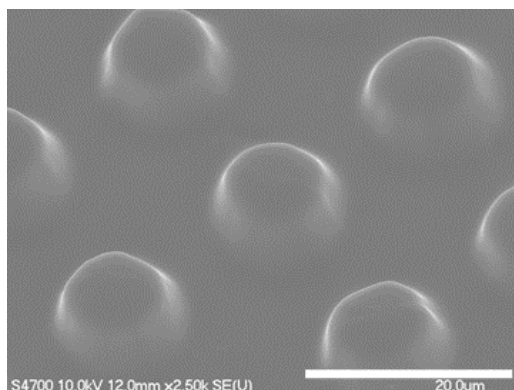
Figure 57. Representative FE-SEM image of one of the samples at the end of the rapidly switching, repeatable adhesion tests for AD-AR1. Scale bar = 20 μm.
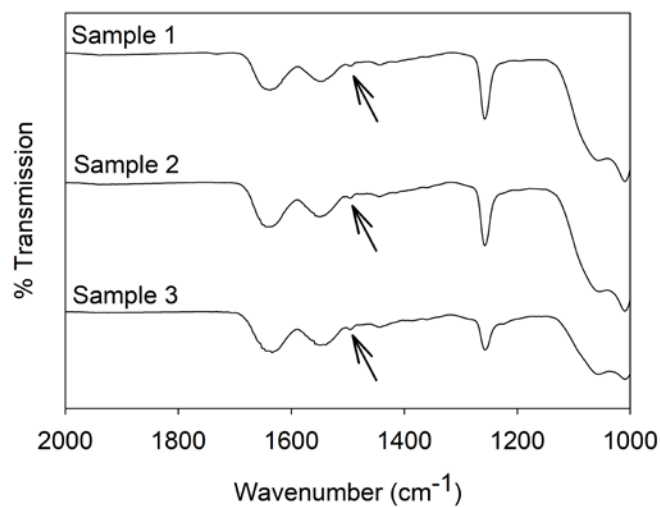
Figure 58. FTIR spectra of the samples at the end of the rapidly switching, repeatable adhesion tests for AD-AR1 (n = 3). The arrows indicate the formation of the catechol-boronate complex at 1495 cm^{-1}.

156

In summary, the bare templates were neither adhesive nor responsive to pH in wet conditions. The flat adhesive adhered strongly at acidic pH but could not quickly switch between adhesive and non-adhesive states in response to changing pH, indicating that the pH responsive switch was limited by the rate of diffusion. These results indicated that neither bare templates nor flat adhesive could not be used as rapidly switching smart adhesives. AD-AR0.4 showed promising adhesion strength due to the micropatterning. However, its work of adhesion during the reversible switching tests was comparable to the flat adhesive, i.e., it did not show pH responsiveness. This limited it from being employed for quick attachment and detachment.

For AD-AR1 under acidic conditions, the adhesive coating was deswollen, revealing the coated micropillars which took advantage of the contact-splitting phenomenon. Additionally, catechol and boronic acid were in the uncomplexed state and able to form strong interfacial bonds with the surface. This resulted in a combined effort to demonstrate strong, elevated adhesion. At a basic pH, the reduced surface area due to the swelling of the hydrogel coupled with the formation of the catechol-boronate complex led to a dramatic decrease in adhesion. The strong adhesion values could be recovered upon lowering the pH to an acidic value. Moreover, we demonstrated that AD-AR1 could rapidly and repeatedly switch between strong and weak adhesion in response to pH. Thus, we exploited the gecko-inspired design to provide large surface area for rapid diffusion of the ions from the pH solution into the adhesive network. Additionally, the large surface area combined with the pH responsive, reversible catechol-boronate complex facilitated strong wet adhesion. Taken together, we were able to incorporate

157

catechol chemistry and gecko-inspired structures into a single hybrid adhesive and demonstrate elevated adhesion and rapid responsivity. To our knowledge, this is the first report that includes the chemical and wet morphological characterization of smart adhesive coated-micropillars and the study of their wet adhesion capabilities in response to rapidly changing pH.

4.5   Conclusion

We prepared hybrid structures composed of an adhesive hydrogel coating on bare PDMS templates. The presence of the coating on the bare template was verified using FE-SEM, ESEM, CA, FTIR and XPS experiments. The enhanced adhesive property and rapidly switching repeatable adhesion was demonstrated using JKR contact mechanics test. It was found that the large contact area provided by the template along with strong adhesion of the smart adhesive at an acidic pH resulted in elevated adhesion. On the other hand, at a basic pH, the swelling of the adhesive and the unavailability of the catechol and boronic acid groups due to formation of the catechol-boronate complex drastically decreased adhesion. Thus, the micropillared templates and the smart adhesive coating were both essential for the hybrid structures to rapidly transition between strong and weak adhesion in response to changing pH.

4.6 Acknowledgements

5 Summary

This dissertation describes the progress made toward controlling the oxidation state of catechol by addition of boronic acid for reversible adhesion, introduction of acrylic acid for adhesion at neutral to mildly basic pH, and the incorporation of acrylic acid to smart adhesives for reversible adhesion at neutral to mildly basic pH. The microfabrication-oriented approach to demonstrate rapid switching between adhesive and non-adhesive states was also included.

In Chapter 1, we added phenylboronic acid to catecholic polymers. This strategy allowed us to protect catecholic groups from undergoing irreversible oxidation and crosslinking. The incorporation of boronic acid not only contributed to strong adhesion (in addition to catechol) at an acidic pH (pH 3), but also provided temporary protection against oxidation of catechol at a basic pH (pH 9) due to the formation of the catechol-boronate complex. The reversible nature of the complex allowed the catechol and boronic acid groups to interact with the surface once again after the pH was reduced. We thus demonstrated a novel wet adhesive with tunable transitions between adhesive states in response to changing pH.

Chapter 2 describes the effect of addition of ionic species on the interfacial binding ability of catechol containing polymers. Quantification of the amount of hydrogen peroxide released as a result of catechol oxidation showed that the addition of anionic species buffered the local pH environment and preserved the reduced state of catechol,

160

while cationic species accelerated the oxidation. This was further corroborated by adhesion tests which showed that presence of anionic species preserved the reduced and adhesive state of catechol at neutral to mildly basic pH, whereas presence of cationic species led to formation of cohesive crosslinking and diminished adhesion at higher basic pH. Addition of ionic species was thus a simple, yet effective strategy to manipulate the oxidation state of catechol.

Although the ideal pH for formation of the catechol boronate complex is 9, it is known that the complex readily forms at a neutral to slightly basic pH. In Chapter 3, the addition of elevated amounts of acrylic acid to smart adhesives containing catechol and boronic acid acidified the local pH and demonstrated strong adhesion at a neutral to mildly basic pH value (pH 7.5 - 8.5) and a higher pH was required for the formation of the complex. The adhesive property decreased significantly due to the formation of the complex at pH 9. While we were able to tune the reversible interfacial interactions by changing pH during successive contact cycles, pH 3 was required to break the complex and recover strong adhesion.

The ability of the bulk adhesives (reported in Chapters 1-3) to switch between strong and weak adhesion was largely limited by the process of slow diffusion of the ions from the pH medium into the hydrogel network. To address this concern, in Chapter 4, we coated our smart adhesive onto the surface of a micropillared PDMS structure, which demonstrated increased differences between adhesion strengths at acidic and basic pH.

161

Additionally, the hybrid structure enabled rapid, reversible switching between adhesive and non-adhesive adhesive states in response to pH.

6 References

1.   Heinzmann, C.; Coulibaly, S.; Roulin, A.; Fiore, G. L.; Weder, C., Light-Induced Bonding and Debonding with Supramolecular Adhesives. *ACS Appl. Mater. Interfaces* **2014,** 6, (7), 4713-4719.

2.   Northen, M. T.; Greiner, C.; Arzt, E.; Turner, K. L., A Gecko-Inspired Reversible Adhesive. *Adv. Mater.* **2008,** 20, (20), 3905-3909.

3.   Luo, X.; Lauber, K. E.; Mather, P. T., A thermally responsive, rigid, and reversible adhesive. *Polymer* **2010,** 51, (5), 1169-1175.

4.   Banea, M.; da Silva, L.; Campilho, R., An overview of the technologies for adhesive debonding on command. *The Annals of" Dunarea de Jos" University of Galati. Fascicle XII: Welding Equipment and Technology* **2013,** 24, 11.

5.   Sudre, G.; Olanier, L.; Tran, Y.; Hourdet, D.; Creton, C., Reversible adhesion between a hydrogel and a polymer brush. *Soft Matter* **2012,** 8, (31), 8184-8193.

6.   Comyn, J., The relationship between joint durability and water diffusion. In *Developments in Adhesives*, Kinloch, A. J., Ed. Applied Science Publishers: Barking, UK, 1981; Vol. 2, pp 279-313.

7.   Lee, B. P.; Messersmith, P. B.; Israelachvili, J. N.; Waite, J. H., Mussel-Inspired Adhesives and Coatings. *Annu. Rev. Mater. Res.* **2011,** 41, 99-132.

8.   Waite, J. H., Nature's underwater adhesive specialist. *Int. J. Adhes. Adhes.* **1987,** 7, (1), 9-14.

9.   Yamamoto, H., Marine adhesive proteins and some biotechnological applications. *Biotechnol. Genet. Eng. Rev.* **1996,** 13, 133-65.

10.   Meredith, H. J.; Wilker, J. J., The Interplay of Modulus, Strength, and Ductility in Adhesive Design Using Biomimetic Polymer Chemistry. *Adv. Funct. Mater.* **2015,** 25, (31), 5057-5065.

11.   Pechey, A.; Elwood, C. N.; Wignall, G. R.; Dalsin, J. L.; Lee, B. P.; Vanjecek, M.; Welch, I.; Ko, R.; Razvi, H.; Cadieux, P. A., Anti-adhesive coating and clearance of device associated uropathogenic escherichia coli cystitis. *J. Urol.* **2009,** 182, (4), 1628-1636.

12.	Liu, Y.; Meng, H.; Konst, S.; Sarmiento, R.; Rajachar, R.; Lee, B. P., Injectable Dopamine-Modified Poly(Ethylene Glycol) Nanocomposite Hydrogel with Enhanced Adhesive Property and Bioactivity. *ACS Appl. Mater. Interfaces* **2014,** 6, (19), 16982-92.

13.	Ejima, H.; Richardson, J. J.; Liang, K.; Best, J. P.; van Koeverden, M. P.; Such, G. K.; Cui, J.; Caruso, F., One-step assembly of coordination complexes for versatile film and particle engineering. *Science* **2013,** 341, (6142), 154-157.

14.	Holten-Andersen, N.; Harrington, M. J.; Birkedal, H.; Lee, B. P.; Messersmith, P. B.; Lee, K. Y. C.; Waite, J. H., pH-induced mussel metal-ligand crosslinks yield self-healing polymer networks with near-covalent elastic moduli. *Proc. Natl. Acad. Sci. USA* **2011,** 15, 2651-2655.

15.	Lee, B. P.; Konst, S., Novel hydrogel actuator inspired by reversible mussel adhesive protein chemistry. *Adv. Mat.* **2014,** 26, (21), 3415-3419.

16.	Lee, B. P.; Lin, M.-H.; Narkar, A.; Konst, S.; Wilharm, R., Modulating the Movement of Hydrogel Actuator based on Catechol-Iron Ion Coordination Chemistry. *Sens. Actuators, B* **2015,** 206, 456–462.

17.	Lee, B. P.; Narkar, A.; Wilharm, R., Effect of metal ion type on the movement of hydrogel actuator based on catechol-metal ion coordination chemistry. *Sens. Actuators, B* **2016,** 227, 248-254.

18.	Guo, J. L.; Ping, Y.; Ejima, H.; Alt, K.; Meissner, M.; Richardson, J. J.; Yan, Y.; Peter, K.; von Elverfeldt, D.; Hagemeyer, C. E.; Caruso, F., Engineering Multifunctional Capsules through the Assembly of Metal-Phenolic Networks. *Angew. Chem., Int. Ed.* **2014,** 53, (22), 5546-5551.

19.	Wilke, P.; Helfricht, N.; Mark, A.; Papastavrou, G.; Faivre, D.; Börner, H. G., A Direct Biocombinatorial Strategy toward Next Generation, Mussel-Glue Inspired Saltwater Adhesives. *J. Am. Chem. Soc.* **2014,** 136, (36), 12667-12674.

20.	Shafiq, Z.; Cui, J.; Pastor-Pérez, L.; San Miguel, V.; Gropeanu, R. A.; Serrano, C.; del Campo, A., Bioinspired Underwater Bonding and Debonding on Demand. *Angew. Chem. Int. Ed.* **2012,** 51, (18), 4332-4335.

21.	Yu, M.; Hwang, J.; Deming, T. J., Role of l-3,4-Dihydroxyphenylalanine in Mussel Adhesive Proteins. *J. Am. Chem. Soc.* **1999,** 121, (24), 5825-5826.

22.	Lee, B. P.; Chao, C.-Y.; Nunalee, F. N.; Motan, E.; Shull, K. R.; Messersmith, P. B., Rapid Gel Formation and Adhesion in Photocurable and Biodegradable Block Copolymers with High DOPA Content. *Macromolecules* **2006,** 39, (5), 1740-1748.

23.　　Yu, J.; Wei, W.; Menyo, M. S.; Masic, A.; Waite, J. H.; Israelachvili, J. N., Adhesion of Mussel Foot Protein-3 to TiO2 Surfaces: the Effect of pH. *Biomacromolecules* **2013,** 14, (4), 1072-1077.

24.　　Lee, H.; Scherer, N. F.; Messersmith, P. B., Single-molecule mechanics of mussel adhesion. *Proc. Natl. Acad. Sci. U. S. A.* **2006,** 103, (35), 12999-13003.

25.　　Yang, J.; Cohen Stuart, M. A.; Kamperman, M., Jack of all trades: versatile catechol crosslinking mechanisms. *Chem. Soc. Rev.* **2014,** 43, (24), 8271-8298.

26.　　Lee, B. P.; Dalsin, J. L.; Messersmith, P. B., Synthesis and Gelation of DOPA-Modified Poly(ethylene glycol) Hydrogels. *Biomacromolecules* **2002,** 3, (5), 1038-1047.

27.　　Pizer, R.; Babcock, L., Mechanism of Complexation of Boron Acids with Catechol and Substituted Catechols. *Inorg. Chem.* **1977,** 16, (7), 1677-1681.

28.　　He, L.; Fullenkamp, D. E.; Rivera, J. G.; Messersmith, P. B., pH responsive self-healing hydrogels formed by boronate–catechol complexation. *Chem. Commun.* **2011,** 47, 7497-7499.

29.　　Huang, K.; Lee, B. P.; Ingram, D.; Messersmith, P. B., Synthesis and Characterization of Self-Assembling Block Copolymers Containing Bioadhesive End Groups. *Biomacromol.* **2002,** 3, (2), 397-406.

30.　　Kan, Y.; Danner, E. W.; Israelachvili, J. N.; Chen, Y.; Waite, J. H., Boronate Complex Formation with Dopa Containing Mussel Adhesive Protein Retards pH-Induced Oxidation and Enables Adhesion to Mica. *PLOS ONE* **2014,** 9, (10), e108869.

31.　　Guo, J.; Sun, H.; Alt, K.; Tardy, B. L.; Richardson, J. J.; Suma, T.; Ejima, H.; Cui, J.; Hagemeyer, C. E.; Caruso, F., Boronate–Phenolic Network Capsules with Dual Response to Acidic pH and cis-Diols. *Adv. Healthcare Mater.* **2015,** 4, (12), 1796-1801.

32.　　Lee, H.; Lee, B. P.; Messersmith, P. B., A reversible wet/dry adhesive inspired by mussels and geckos. *Nature* **2007,** 448, (7151), 338-341.

33.　　Bryant, S. J.; Anseth, K. S., Hydrogel properties influence ECM production by chondrocytes photoencapsulated in poly(ethylene glycol) hydrogels. *J. Biomed. Mater. Res.* **2002,** 59, (1), 63-72.

34.　　Yang, F. K.; Zhang, W.; Han, Y.; Yoffe, S.; Cho, Y.; Zhao, B., "Contact" of Nanoscale Stiff Films. *Langmuir* **2012,** 28, (25), 9562-9572.

35.　　Flanigan, C. M.; Crosby, A. J.; Shull, K. R., Structural development and adhesion of acrylic ABA triblock copolymer gels. *Macromolecules (Washington, DC, U. S.)* **1999,** 32, (21), 7251-7262.

165

36.	Hertz, H., *On the contact of elastic solids*. J. Reine Angew. Math.: 1881; Vol. 92.

37.	Shull, K. R.; Chen, W.-L., Fracture Mechanics Studies of Adhesion in Biological Systems. *Interface Sci.* 8, (1), 95-110.

38.	Ding, X.; Vegesna, G. K.; Meng, H.; Winter, A.; Lee, B. P., Nitro-Group Functionalization of Dopamine and its Contribution to the Viscoelastic Properties of Catechol-Containing Nanocomposite Hydrogels. *Macromol. Chem. Phys.* **2015,** 216, 1109-1119.

39.	Yan, J.; Springsteen, G.; Deeter, S.; Wang, B., The relationship among pKa, pH, and binding constants in the interactions between boronic acids and diols—it is not as simple as it appears. *Tetrahedron* **2004,** 60, (49), 11205-11209.

40.	Springsteen, G.; Wang, B., A detailed examination of boronic acid–diol complexation. *Tetrahedron* **2002,** 58, (26), 5291-5300.

41.	Bull, S. D.; Davidson, M. G.; van den Elsen, J. M. H.; Fossey, J. S.; Jenkins, A. T. A.; Jiang, Y.-B.; Kubo, Y.; Marken, F.; Sakurai, K.; Zhao, J.; James, T. D., Exploiting the Reversible Covalent Bonding of Boronic Acids: Recognition, Sensing, and Assembly. *Acc. Chem. Res.* **2013,** 46, (2), 312-326.

42.	Meng, H.; Li, Y.; Faust, M.; Konst, S.; Lee, B. P. In *Hydrogen peroxide generation and cytotoxicity of hydrogel-bound mussel inspired adhesives*, Biomedical Engineering Society, San Antonio, TX, 2014; San Antonio, TX, 2014.

43.	Lee, B. P.; Dalsin, J. L.; Messersmith, P. B., Synthesis and Gelation of DOPA-Modified Poly(ethylene glycol) Hydrogels. *Biomacromol.* **2002,** 3, (5), 1038-47.

44.	Kalyanaraman, B.; Felix, C. C.; Sealy, R. C., Semiquinone anion radicals of catechol(amine)s, catechol estrogens, and their metal ion complexes. *Environ. Health Perspect.* **1985,** 64, 185-198.

45.	Kim, A.; Mujumdar, S.; Siegel, R., Swelling Properties of Hydrogels Containing Phenylboronic Acids. *Chemosensors* **2014,** 2, (1), 1-12.

46.	Sever, M. J.; Weisser, J. T.; Monahan, J.; Srinivasan, S.; Wilker, J. J., Metal-Mediated Cross-Linking in the Generation of a Marine-Mussel Adhesive. *Angewandte Chemie* **2004,** 116, (4), 454-456.

47.	Lee, B. P.; Narkar, A.; Wilharm, R., Effect of metal ion type on the movement of hydrogel actuator based on catechol-metal ion coordination chemistry. *Sens. Actuators, B* **2016,** 227, 248-254.

166

48.   Chen, G. C., Synthesis and evaluation of aminoborates derived from boric acid and diols for protecting wood against fungal and thermal degradation. *Wood Fiber Sci.* **2008,** 40, (2), 248-257.

49.   Skelton, S.; Bostwick, M.; O'Connor, K.; Konst, S.; Casey, S.; Lee, B. P., Biomimetic adhesive containing nanocomposite hydrogel with enhanced materials properties. *Soft Matter* **2013,** 9, (14), 3825-3833.

50.   Li, Y.; Meng, H.; Liu, Y.; Narkar, A.; Lee, B. P., Gelatin Microgel Incorporated Poly(ethylene glycol)-Based Bioadhesive with Enhanced Adhesive Property and Bioactivity. *ACS Appl. Mater. Interfaces* **2016,** 8, (19), 11980-11989.

51.   Chung, H.; Glass, P.; Pothen, J. M.; Sitti, M.; Washburn, N. R., Enhanced Adhesion of Dopamine Methacrylamide Elastomers via Viscoelasticity Tuning. *Biomacromolecules* **2011,** 12, (2), 342-347.

52.   Mian, S. A.; Gao, X.; Nagase, S.; Jang, J., Adsorption of catechol on a wet silica surface: density functional theory study. *Theor. Chem. Acc.* **2011,** 130, 333-339.

53.   Mian, S. A.; Saha, L. C.; Jang, J.; Wang, L.; Gao, X.; Nagase, S., Density Functional Theory Study of Catechol Adhesion on Silica Surfaces. *J. Phys. Chem. C* **2010,** 114, 20793-20800.

54.   Stewart, R. J., Protein-based underwater adhesives and the prospects for their biotechnological production. *Appl. Microbiol. Biotechnol.* **2011,** 89, (1), 27-33.

55.   Deming, T. J., Synthetic polypeptides for biomedical applications. *Prog. Polym. Sci.* **2007,** 32, (8), 858-875.

56.   Bordes, M.; Davies, P.; Cognard, J. Y.; Sohier, L.; Sauvant-Moynot, V.; Galy, J., Prediction of long term strength of adhesively bonded steel/epoxy joints in sea water. *Int. J. Adhes. Adhes.* **2009,** 29, (6), 595-608.

57.   Lee, B. P.; Messersmith, P. B.; Israelachvili, J. N.; Waite, J. H., Mussel-inspired adhesives and coatings. *Annu. Rev. Mater. Res.* **2011,** 41, 99-132.

58.   Wilker, J. J., Positive charges and underwater adhesion. *Science* **2015,** 349, (6248), 582-583.

59.   Comyn, J., *The relationship between joint durability and water diffusion*. Applied Science Publishers: London, 1981.

60.   Lu, Q.; Danner, E.; Waite, J. H.; Israelachvili, J. N.; Zeng, H.; Hwang, D. S., Adhesion of mussel foot proteins to different substrate surfaces. In *J. R. Soc., Interface*, 2013; Vol. 10, p 20120759.

61.   Yamamoto, H., Marine adhesive proteins and some biotechnological applications. *Biotechnology and Genetic Engineering Reviews* **1996,** 13, (1), 133-166.

62.   Lee, H.; Dellatore, S. M.; Miller, W. M.; Messersmith, P. B., Mussel-Inspired Surface Chemistry for Multifunctional Coatings. *Science* **2007,** 318, (5849), 426-430.

63.   Brubaker, C. E.; Messersmith, P. B., The Present and Future of Biologically Inspired Adhesive Interfaces and Materials. *Langmuir* **2012,** 28, (4), 2200-2205.

64.   Faure, E.; Falentin-Daudré, C.; Jérôme, C.; Lyskawa, J.; Fournier, D.; Woisel, P.; Detrembleur, C., Catechols as versatile platforms in polymer chemistry. *Progress in Polymer Science* **2013,** 38, (1), 236-270.

65.   Kord Forooshani, P.; Lee, B. P., Recent approaches in designing bioadhesive materials inspired by mussel adhesive protein. *J. Polym. Sci., Part A: Polym. Chem.* **2017,** 55, 9-33.

66.   Waite, J. H.; Housley, T. J.; Tanzer, M. L., Peptide repeats in a mussel glue protein: theme and variations. *Biochemistry* **1985,** 24, (19), 5010-5014.

67.   White, J. D.; Wilker, J. J., Underwater bonding with charged polymer mimics of marine mussel adhesive proteins. *Macromolecules* **2011,** 44, (13), 5085-5088.

68.   Maier, G. P.; Rapp, M. V.; Waite, J. H.; Israelachvili, J. N.; Butler, A., Adaptive synergy between catechol and lysine promotes wet adhesion by surface salt displacement. *Science* **2015,** 349, (6248), 628-632.

69.   Clancy, S. K.; Sodano, A.; Cunningham, D. J.; Huang, S. S.; Zalicki, P. J.; Shin, S.; Ahn, B. K., Marine Bioinspired Underwater Contact Adhesion. *Biomacromolecules* **2016,** 17, (5), 1869-1874.

70.   Guvendiren, M.; Messersmith, P. B.; Shull, K. R., Self-Assembly and Adhesion of DOPA-Modified Methacrylic Triblock Hydrogels. *Biomacromolecules* **2008,** 9, (1), 122-128.

71.   Lee, H.; Scherer, N. F.; Messersmith, P. B., Single-molecule mechanics of mussel adhesion. *Proc. Natl. Acad. Sci. U. S. A.* **2006,** 103, (35), 12999-13003.

72.   Yu, J.; Wei, W.; Danner, E.; Ashley, R. K.; Israelachvili, J. N.; Waite, J. H., Mussel protein adhesion depends on interprotein thiol-mediated redox modulation. *Nature chemical biology* **2011,** 7, (9), 588-590.

73.   Wei, W.; Tan, Y.; Martinez Rodriguez, N. R.; Yu, J.; Israelachvili, J. N.; Waite, J. H., A mussel-derived one component adhesive coacervate. *Acta Biomaterialia* **2014,** 10, (4), 1663-1670.

168

74.   Wei, W.; Yu, J.; Broomell, C.; Israelachvili, J. N.; Waite, J. H., Hydrophobic enhancement of dopa-mediated adhesion in a mussel foot protein. *J. Am. Chem. Soc.* **2012,** 135, (1), 377-383.

75.   Moulay, S.; Mehdaoui, R., Hydroquinone/catechol-bearing polyacrylic acid: redox polymer. *React. Funct. Polym.* **2004,** 61, (2), 265-275.

76.   Wang, W.; Xu, Y.; Li, A.; Li, T.; Liu, M.; von Klitzing, R.; Ober, C. K.; Kayitmazer, A. B.; Li, L.; Guo, X., Zinc induced polyelectrolyte coacervate bioadhesive and its transition to a self-healing hydrogel. *Rsc Advances* **2015,** 5, (82), 66871-66878.

77.   Kiernan, J., Strategies for preventing detachment of sections from glass slides. *Micros Today* **1999,** 99, (96), 22-24.

78.   Chandradoss, S. D.; Haagsma, A. C.; Lee, Y. K.; Hwang, J.-H.; Nam, J.-M.; Joo, C., Surface passivation for single-molecule protein studies. *Journal of visualized experiments: JoVE* **2014**, (86), 50549.

79.   Taglietti, A.; Arciola, C. R.; D'Agostino, A.; Dacarro, G.; Montanaro, L.; Campoccia, D.; Cucca, L.; Vercellino, M.; Poggi, A.; Pallavicini, P., Antibiofilm activity of a monolayer of silver nanoparticles anchored to an amino-silanized glass surface. *Biomaterials* **2014,** 35, (6), 1779-1788.

80.   Narkar, A. R.; Barker, B.; Clisch, M.; Jiang, J.; Lee, B. P., pH Responsive and Oxidation Resistant Wet Adhesive based on Reversible Catechol–Boronate Complexation. *Chem. Mater.* **2016,** 28, (15), 5432-5439.

81.   Lin, M.-H.; Narkar, A.; Konst, S.; Wilharm, R., Modulating the movement of hydrogel actuator based on catechol–iron ion coordination chemistry. *Sens. Actuators, B* **2015,** 206, 456-462.

82.   Meng, H.; Liu, Y.; Lee, B. P., Model polymer system for investigating the generation of hydrogen peroxide and its biological responses during the crosslinking of mussel adhesive moiety. *Acta Biomater.* **2017,** 48, 144-56.

83.   Meng, H.; Li, Y.; Faust, M.; Konst, S.; Lee, B. P., Hydrogen Peroxide Generation and Biocompatibility of Hydrogel-Bound Mussel Adhesive Moiety. *Acta biomaterialia* **2015,** 17, 160-169.

84.   Hertz, H., On the contact of elastic solids. *J. Reine Angew Math.* **1881,** 92, 156-171.

85.   Shull, K. R.; Chen, W.-L., Fracture mechanics studies of adhesion in biological systems. *Interface Sci.* **2000,** 8, (1), 95-110.

169

86.   Burkett, J. R.; Wojtas, J. L.; Cloud, J. L.; Wilker, J. J., A Method for Measuring the Adhesion Strength of Marine Mussels. *The Journal of Adhesion* **2009,** 85, (9), 601-615.

87.   Cencer, M.; Liu, Y.; Winter, A.; Murley, M.; Meng, H.; Lee, B. P., Effect of pH on the Rate of Curing and Bioadhesive Properties of Dopamine Functionalized Poly(ethylene glycol) Hydrogels. *Biomacromolecules* **2014,** 15, (8), 2861-2869.

88.   Ohman, H.; Vahlquist, A., In vivo studies concerning a pH gradient in human stratum corneum and upper epidermis. *Acta dermatovenereologica-stockholm* **1994,** 74, 375-379.

89.   Waugh, A.; Grant, A., *Ross & Wilson Anatomy and Physiology in Health and Illness E-Book*. Elsevier Health Sciences: 2010.

90.   Zhang, S.; Soller, B. R. In *In-vivo determination of myocardial pH during regional ischemia using near-infrared spectroscopy*, SPIE Proc, 1998; 1998; pp 110-117.

91.   Chester, R.; Jickells, T., *Marine Geochemistry*. Wiley-Blackwell Publishing: 2012.

92.   Min, Y.; Hammond, P. T., Catechol-modified polyions in layer-by-layer assembly to enhance stability and sustain release of biomolecules: a bioinspired approach. *Chem. Mater.* **2011,** 23, (24), 5349-5357.

93.   Jin, X.; Hsieh, Y.-L., pH-responsive swelling behavior of poly (vinyl alcohol)/poly (acrylic acid) bi-component fibrous hydrogel membranes. *Polymer* **2005,** 46, (14), 5149-5160.

94.   Hu, X.; Tong, Z.; Lyon, L. A., Synthesis and physicochemical properties of cationic microgels based on poly (N-isopropylmethacrylamide). *Colloid. Polym. Sci.* **2011,** 289, (3), 333-339.

95.   Yang, J.; Saggiomo, V.; Velders, A. H.; Stuart, M. A. C.; Kamperman, M., Reaction Pathways in Catechol/Primary Amine Mixtures: A Window on Crosslinking Chemistry. *PloS one* **2016,** 11, (12), e0166490.

96.   Yang, J.; Stuart, M. A. C.; Kamperman, M., Jack of all trades: versatile catechol crosslinking mechanisms. *Chem. Soc. Rev.* **2014,** 43, (24), 8271-8298.

97.   Bokare, A. D.; Choi, W., Singlet-oxygen generation in alkaline periodate solution. *Environmental science & technology* **2015,** 49, (24), 14392-14400.

98.   Tort, M.; Fletcher, C.; Wooster, G.; Bowser, P., Stability of hydrogen peroxide in aquaria as a fish disease treatment. *Journal of applied aquaculture* **2004,** 14, (3-4), 37-45.

170

99.   Fu, Q.; Rahaman, M. N.; Fu, H.; Liu, X., Silicate, borosilicate, and borate bioactive glass scaffolds with controllable degradation rate for bone tissue engineering applications. I. Preparation and in vitro degradation. *Journal of Biomedical Materials Research Part A* **2010,** 95, (1), 164-171.

100.   Lee, S.-B.; González-Cabezas, C.; Kim, K.-M.; Kim, K.-N.; Kuroda, K., Catechol-Functionalized Synthetic Polymer as a Dental Adhesive to Contaminated Dentin Surface for a Composite Restoration. *Biomacromolecules* **2015,** 16, (8), 2265-2275.

101.   Kaushik, N.; Kaushik, N.; Pardeshi, S.; Sharma, J.; Lee, S.; Choi, E., Biomedical and Clinical Importance of Mussel-Inspired Polymers and Materials. *Marine Drugs* **2015,** 13, (11), 6792-6817.

102.   Nesrinne, S.; Djamel, A., Synthesis, characterization and rheological behavior of pH sensitive poly (acrylamide-co-acrylic acid) hydrogels. *Arabian J. Chem.* **2017,** 10, (4), 539-547.

103.   Tombácz, E.; Szekeres, M., Colloidal behavior of aqueous montmorillonite suspensions: the specific role of pH in the presence of indifferent electrolytes. *Applied Clay Science* **2004,** 27, (1), 75-94.

104.   Wei, W.; Yu, J.; Gebbie, M. A.; Tan, Y.; Martinez Rodriguez, N. R.; Israelachvili, J. N.; Waite, J. H., Bridging Adhesion of Mussel-Inspired Peptides: Role of Charge, Chain Length, and Surface Type. *Langmuir* **2015,** 31, (3), 1105-1112.

105.   Seo, S.; Das, S.; Zalicki, P. J.; Mirshafian, R.; Eisenbach, C. D.; Israelachvili, J. N.; Waite, J. H.; Ahn, B. K., Microphase Behavior and Enhanced Wet-Cohesion of Synthetic Copolyampholytes Inspired by a Mussel Foot Protein. *J. Am. Chem. Soc.* **2015,** 137, (29), 9214-9217.

106.   Cholewinski, A.; Yang, F. K.; Zhao, B., Underwater Contact Behavior of Alginate and Catechol-Conjugated Alginate Hydrogel Beads. *Langmuir* **2017,** 33, (34), 8353-8361.

107.   Banea, M. D.; da Silva, L. F. M.; Carbas, R. J. C.; de Barros, S., Debonding on command of multi-material adhesive joints. *The Journal of Adhesion* **2017,** 93, (10), 756-770.

108.   Waite, J. H., The phylogeny and chemical diversity of quinone-tanned glues and varnishes. *Comparative Biochemistry and Physiology Part B: Comparative Biochemistry* **1990,** 97, (1), 19-29.

109.   Pechey, A.; Elwood, C. N.; Wignall, G. R.; Dalsin, J. L.; Lee, B. P.; Vanjecek, M.; Welch, I.; Ko, R.; Razvi, H.; Cadieux, P. A., Anti-adhesive coating and clearance of

device associated uropathogenic Escherichia coli cystitis. *The Journal of urology* **2009,** 182, (4), 1628-1636.

110.   Liu, Y.; Meng, H.; Konst, S.; Sarmiento, R.; Rajachar, R.; Lee, B. P., Injectable dopamine-modified poly (ethylene glycol) nanocomposite hydrogel with enhanced adhesive property and bioactivity. *ACS Appl. Mater. Interfaces* **2014,** 6, (19), 16982-16992.

111.   Zhao, Y.; Wu, Y.; Wang, L.; Zhang, M.; Chen, X.; Liu, M.; Fan, J.; Liu, J.; Zhou, F.; Wang, Z., Bio-inspired reversible underwater adhesive. *Nat. Commun.* **2017,** 8, (1), 2218.

112.   He, L.; Fullenkamp, D. E.; Rivera, J. G.; Messersmith, P. B., pH responsive self-healing hydrogels formed by boronate–catechol complexation. *Chem. Commun.* **2011,** 47, (26), 7497-7499.

113.   Narkar, A. R.; Kelley, J. D.; Pinnaratip, R.; Lee, B. P., Effect of Ionic Functional Groups on the Oxidation State and Interfacial Binding Property of Catechol-Based Adhesive. *Biomacromolecules* **2017**.

114.   Kirwan, L. J.; Fawell, P. D.; van Bronswijk, W., In Situ FTIR-ATR Examination of Poly(acrylic acid) Adsorbed onto Hematite at Low pH. *Langmuir* **2003,** 19, (14), 5802-5807.

115.   Holten-Andersen, N.; Harrington, M. J.; Birkedal, H.; Lee, B. P.; Messersmith, P. B.; Lee, K. Y. C.; Waite, J. H., pH-induced metal-ligand cross-links inspired by mussel yield self-healing polymer networks with near-covalent elastic moduli. *Proc. Natl. Acad. Sci. U. S. A.* **2011,** 108, 2651-2655.

116.   Zhao, J.; Burke, N. A.; Stöver, H. D., Preparation and study of multi-responsive polyampholyte copolymers of N-(3-aminopropyl) methacrylamide hydrochloride and acrylic acid. *RSC Adv.* **2016,** 6, (47), 41522-41531.

117.   Crosby, A. J.; Shull, K. R., Adhesive failure analysis of pressure-sensitive adhesives. *J. Polym. Sci., Part B: Polym. Phys.* **1999,** 37, (24), 3455-3472.

118.   Vaenkatesan, V.; Li, Z.; Vellinga, W.-P.; de Jeu, W. H., Adhesion and friction behaviours of polydimethylsiloxane–A fresh perspective on JKR measurements. *Polymer* **2006,** 47, (25), 8317-8325.

119.   Torres, J. R.; Jay, G. D.; Kim, K. S.; Bothun, G. D., Adhesion in hydrogel contacts. *Proceedings. Mathematical, Physical, and Engineering Sciences / The Royal Society* **2016,** 472, (2189), 20150892.

120.   Ma, Y.; Ma, S.; Wu, Y.; Pei, X.; Gorb, S. N.; Wang, Z.; Liu, W.; Zhou, F., Remote Control over Underwater Dynamic Attachment/Detachment and Locomotion. *Adv. Mater.* **2018**, 1801595.

121.   Ahn, Y.; Jang, Y.; Selvapalam, N.; Yun, G.; Kim, K., Supramolecular velcro for reversible underwater adhesion. *Angew. Chem.* **2013,** 125, (11), 3222-3226.

122.   Hansen, W. R.; Autumn, K., Evidence for self-cleaning in gecko setae. *Proceedings of the National Academy of Sciences of the United States of America* **2005,** 102, (2), 385.

123.   Huber, G.; Mantz, H.; Spolenak, R.; Mecke, K.; Jacobs, K.; Gorb, S. N.; Arzt, E., Evidence for capillarity contributions to gecko adhesion from single spatula nanomechanical measurements. *Proceedings of the National Academy of Sciences of the United States of America* **2005,** 102, (45), 16293.

124.   Reddy, S.; Arzt, E.; del Campo, A., Bioinspired surfaces with switchable adhesion. *Adv. Mater.* **2007,** 19, (22), 3833-3837.

125.   Cui, J.; Drotlef, D. M.; Larraza, I.; Fernández-Blázquez, J. P.; Boesel, L. F.; Ohm, C.; Mezger, M.; Zentel, R.; del Campo, A., Bioinspired actuated adhesive patterns of liquid crystalline elastomers. *Adv. Mater.* **2012,** 24, (34), 4601-4604.

126.   Glass, P.; Chung, H.; Washburn, N. R.; Sitti, M., Enhanced Reversible Adhesion of Dopamine Methacrylamide-Coated Elastomer Microfibrillar Structures under Wet Conditions. *Langmuir* **2009,** 25, (12), 6607-6612.

127.   Glass, P.; Chung, H.; Washburn, N. R.; Sitti, M., Enhanced Wet Adhesion and Shear of Elastomeric Micro-Fiber Arrays with Mushroom Tip Geometry and a Photopolymerized p(DMA-co-MEA) Tip Coating. *Langmuir* **2010,** 26, (22), 17357-17362.

128.   Zhang, H.; Bian, C.; Jackson, J. K.; Khademolhosseini, F.; Burt, H. M.; Chiao, M., Fabrication of Robust Hydrogel Coatings on Polydimethylsiloxane Substrates Using Micropillar Anchor Structures with Chemical Surface Modification. *ACS Appl. Mater. Interfaces* **2014,** 6, (12), 9126-9133.

129.   Narkar, A. R.; Lee, B. P., Incorporation of Anionic Monomer to Tune the Reversible Catechol–Boronate Complex for pH-Responsive, Reversible Adhesion. *Langmuir* **2018**.

130.   Cuchiara, M. P.; Allen, A. C.; Chen, T. M.; Miller, J. S.; West, J. L., Multilayer microfluidic PEGDA hydrogels. *Biomaterials* **2010,** 31, (21), 5491-5497.

173

131.   Johnson, L. M.; Gao, L.; Shields IV, C. W.; Smith, M.; Efimenko, K.; Cushing, K.; Genzer, J.; López, G. P., Elastomeric microparticles for acoustic mediated bioseparations. *Journal of nanobiotechnology* **2013,** 11, (1), 22.

132.   Shahsavan, H.; Quinn, J.; d'Eon, J.; Zhao, B., Surface modification of polydimethylsiloxane elastomer for stable hydrophilicity, optical transparency and film lubrication. *Colloids and Surfaces A: Physicochemical and Engineering Aspects* **2015,** 482, 267-275.

133.   Barreau, V.; Yu, D.; Hensel, R.; Arzt, E., Elevated temperature adhesion of bioinspired polymeric micropatterns to glass. *Journal of the mechanical behavior of biomedical materials* **2017,** 76, 110-118.

134.   Boesel, L. F.; Greiner, C.; Arzt, E.; Del Campo, A., Gecko-inspired surfaces: a path to strong and reversible dry adhesives. *Adv. Mater.* **2010,** 22, (19), 2125-2137.

A   Copyright documentation

A.1   Permission for content in chapter 1

Michigan Tech

Regarding Incident 1982423 Permission to use article in PhD dissertation
1 message

support@services.acs.org <support@services.acs.org>
To: arnarkar@mtu.edu

ACS
Chemistry for Life®

Dear Dr.Narkar,

Thank you for contacting ACS Publications Support.

Your permission request is granted and there is no fee for this reuse. In your planned reuse, you must cite the ACS article as the source, add this direct link https://pubs.acs.org/doi/abs/10.1021/acs.chemmater.6b01851 and include a notice to readers that further permissions related to the material excerpted should be directed to the ACS.

I hope this is helpful and if you need further assistance, please feel free to contact me.

Sincerely,

Ashley Gibson

ACS Publications

Customer Services & Information

Website: https://help.acs.org

www.manaraa.com

Incident Information:

Incident:	1982423
Incident Created:	2018-05-15T17:47:27
Short Description:	Permission to use article in PhD dissertation
Description:	Hi,

My name is Ameya Narkar and I would like to use the following article in entirety as a part of my dissertation. I'm currently in the process of creating my dissertation draft and am providing the current name of the dissertation which may eventually be modified.Thanks.

Link to the ACS article:

https://pubs.acs.org/doi/abs/10.1021/acs.chemmater.6b01851

Portion of content I wish to reuse:

Entire article for PhD dissertation

Description of where the content will be reused:

Dissertation name: Evaluating the Reversible Adhesion of pH Responsive, Oxidation Resistant Bullk and Micron-Scale Smart Adhesives based on Marine Mussel Chemistry

Regards,
Ameya R. Narkar

PhD Candidate

Biomimetic Materials Lab, Biomedical Engineering

323, M&M

Michigan Technological University

176

A.2   Permission for content in chapter 2

A.3   Permission for content in chapter 3

Copyright Clearance Center

RightsLink®

Home | Account Info | Help | ✉

ACS Publications
Most Trusted. Most Cited. Most Read.

Title: Incorporation of Anionic Monomer to Tune the Reversible Catechol-Boronate Complex for pH Responsive, Reversible Adhesion

Author: Ameya R. Narkar, Bruce P Lee

Publication: Langmuir

Publisher: American Chemical Society

Date: Jul 1, 2018

Copyright © 2018, American Chemical Society

Logged in as:
Ameya Narkar
Account #:
3000848098

LOGOUT

PERMISSION/LICENSE IS GRANTED FOR YOUR ORDER AT NO CHARGE

This type of permission/license, instead of the standard Terms & Conditions, is sent to you because no fee is being charged for your order. Please note the following:

- Permission is granted for your request in both print and electronic formats, and translations.
- If figures and/or tables were requested, they may be adapted or used in part.
- Please print this page for your records and send a copy of it to your publisher/graduate school.
- Appropriate credit for the requested material should be given as follows: "Reprinted (adapted) with permission from (COMPLETE REFERENCE CITATION). Copyright (YEAR) American Chemical Society." Insert appropriate information in place of the capitalized words.
- One-time permission is granted only for the use specified in your request. No additional uses are granted (such as derivative works or other editions). For any other uses, please submit a new request.

BACK | CLOSE WINDOW